



Technical Report TR4.2

TECHNICAL REPORT TR4.22  
INTERIM REPORT 2 ON HYBRID ACCESS  
TECHNOLOGIES

DECEMBER 14, 2012



## Authors List

---

**Affiliation**

CNES (contributor)

Hispasat (contributor)

iTEAM, Polytechnic University of Valencia  
(contributor)

MERCE (editor, contributor)

**Authors**

Laurence Clarac, Frédéric Lacoste, Benjamin Ros,  
Christelle Boustie

Inés Sanz, Jorge Rodriguez, Marcos Iglesias

David Gómez-Barquero, Pedro F. Gómez, Jose Llorca,  
David Gozávez

Arnaud Bouttier, Cristina Ciochină, Damien Castelain

---

## Contents

1	Introduction .....	7
2	DVB-NGH satellite Hybrid Profile .....	8
2.1	State-of-art: Mobile Services via Satellite.....	8
2.1.1	Current Issues for Mobile Devices Broadcasting .....	8
2.1.2	DVB technologies for satellite broadcasting .....	9
2.2	Satellite Role in DVB-NGH architecture .....	11
2.2.1	Introduction .....	11
2.2.2	Satellite-Only Scenario.....	12
2.2.3	Hybrid scenario.....	13
2.2.4	Network Distribution Requirements.....	16
2.3	DVB-NGH Satellite Link .....	17
2.3.1	Link Budgets Calculations.....	17
2.3.2	DVB-NGH Link Budget Considerations.....	20
2.3.3	DVB-NGH Link budgets.....	23
3	Time Interleaving in the satellite context .....	29
3.1	Long Time Interleaving .....	29
3.1.1	Introduction and Background .....	29
3.1.2	State-of-the-Art – DVB-SH.....	30
3.2	Performance analysis of time interleaving .....	37
3.2.1	Physical interleaver description.....	38
3.2.2	Link layer interleaver description.....	39
3.2.3	ESR5 criteria.....	40
3.2.4	Which interleaver is the most suitable for Satellite transmission.....	41
3.2.5	Strategies for time interleaving and interleaving solutions retained in DVB-NGH standard..	46
4	L1 Signaling in the satellite context .....	47
4.1	L1 Signaling for the Hybrid Profile.....	47
4.1.1	Introduction .....	47
4.1.2	Summary of L1 Robustness in the Sheer Terrestrial NGH Profile.....	47
4.1.3	The physical layer signaling in the Hybrid NGH Profile .....	48

4.1.4	Performance of L1 Robustness in the Hybrid NGH Profile .....	48
4.1.5	Conclusion .....	53
4.2	Robust Layer 1 Signaling schemes.....	54
4.2.1	Introduction .....	54
4.2.2	Study description: Additional Parity like .....	54
4.2.3	Simulations results.....	59
4.2.4	Comparison with NGH adopted solution .....	63
4.2.5	Conclusion and warnings.....	64
5	SC-OFDM waveform .....	65
5.1	Introduction .....	65
5.2	Combining the TDM and OFDM strengths.....	66
5.3	SC-OFDM modulation in DVB-NGH.....	69
5.3.1	System Parameters.....	69
5.3.2	Pilot Pattern .....	70
5.3.3	MIMO.....	74
5.4	Performance evaluation .....	75
5.4.1	Power amplifier characterization.....	75
5.4.2	Peak to average power ratio (PAPR).....	77
5.4.3	Instantaneous normalized power (INP) .....	78
5.4.4	Satellite Pilot Pattern (PP9) .....	80
5.4.5	Modulation error ratio (MER) .....	82
5.4.6	Bit error rate (BER) and total degradation (TD) .....	83
5.4.7	Doppler performances .....	87
5.4.8	MIMO performances .....	88
5.5	Conclusion.....	90
6	Synchronization in the satellite context – Application to the SC-OFDM waveform .....	92
6.1	SC-OFDM waveform .....	92
6.2	State of the art.....	93
6.2.1	P1 symbol .....	93
6.2.2	P1 detection .....	95
6.2.3	Fine time synchronization .....	96
6.2.4	Estimation of the integer part of the frequency error.....	97

6.2.5	First estimation of the residual frequency error.....	97
6.2.6	Estimate of the residual frequency error.....	98
6.3	Improvement of the P1 detection.....	99
6.3.1	Filtering prior to P1 detection.....	99
6.3.2	Detection threshold computation.....	99
6.3.3	Performances .....	104
6.4	Estimation of the integer part of the frequency offset .....	107
6.4.1	Description of the algorithms .....	107
6.4.2	Performance evaluation .....	109
6.5	Time synchronization .....	111
6.5.1	Algorithm description.....	111
6.5.2	Performances evaluation.....	112
6.5.3	False alarm computation.....	113
6.6	Fine frequency synchronization over pilot symbols.....	114
6.6.1	Description of the algorithm.....	114
6.6.2	Performances evaluation.....	115
6.7	Conclusion.....	119
6.8	Overall performances evaluation.....	122
6.8.1	Simulator description.....	122
6.8.2	Simulation results .....	125
6.8.3	Conclusion.....	133
7	Conclusion.....	135
8	References .....	138

*Abstract – When deploying digital TV networks, operators are often requested by the legislator to guarantee a fair access to the service to a given percentage of the population. Depending on the population density over the country and its topology, it might be technically difficult or costly to satisfy these requirements solely with a terrestrial network. The combination of a satellite component along with a terrestrial network appears as a sensible solution to cover large but sparsely populated areas. This is one of the reasons that motivated the introduction of a satellite component in the Digital Video Broadcasting-Next Generation Handheld (DVB-NGH) standardized in September 2012 [1]. Due to very long propagation distances and strong power limitations, satellite links have specific requirements when it comes to dimensioning the transmission scheme. In short, satellite links require modulations robust to saturation for operating power amplifiers with small input back-offs and very robust block and interleaving coded modulation (BICM) schemes compatible with very low signal to noise ratios. In particular, it is mandatory to interleave over several seconds. In addition to the satellite link itself, another key issue lies in the efficient and smooth integration of the terrestrial and satellite components, leading to the so-called hybrid networks.*

*This document is the second revision of the second interim report dealing with Hybrid Access Technologies in the scope of the DVB-NGH standard. This second report complements the results presented in the first and second technical reports [2], [3]. To avoid any confusion, only the new results and updated parts are presented here. The two interim reports will be consolidated altogether as part of the Deliverable D2.4 entitled “Report on novel access technologies” to be issued in December 2012.*

*The following topics are addressed in the report:*

- *Link budgets for the NGH satellite component in OFDM*
- *SC-OFDM modulation*
- *Long Time Interleaving*
- *Layer 1 (L1) signaling*
- *Synchronization with application to SC-OFDM*

# 1 INTRODUCTION

The task force “TF4-Hybrid Access Technologies” focuses on the combination of the terrestrial and satellite components to extend the capabilities of broadcasting systems in the scope of the DVB Next Generation Handled (NGH) system under standardization.

TF4 encompasses the following activities:

- Satellite and terrestrial networks;
- Radio channel model;
- Air interface technologies;

This interim report updates and complements the first report with the latest results obtained as part of the TF4 activities. The newly added content focuses on air-interface technologies with four topics:

- 1 – The link budget requirements for NGH satellite links in OFDM mode.
- 2 – The performances of long time interleaving solutions for the satellite channel.
- 3 – The definition and performances of robust layer 1 signaling schemes.
- 4 – The performances of the Single Carrier-Orthogonal Frequency Multiplexing (SC-OFDM) modulation.
- 5 – The definition and performances of synchronization algorithms with application to SC-OFDM.

## 2 DVB-NGH SATELLITE HYBRID PROFILE

### 2.1 State-of-art: Mobile Services via Satellite

#### 2.1.1 Current Issues for Mobile Devices Broadcasting

Satellites are ideal for broadcast services since they are able to cover large areas with minimal ground infrastructure deployment. Satellite communications have been widely used for mobile communications by transferring services based on voice and data. However, transmission of new multimedia content presents higher requirements in terms of bandwidth, fault tolerance, access time or delay.

DVB-S (Digital Video Broadcasting - Satellite services [4]) was standardized in 1993 for the provision of video services via satellite. Its second version [5], DVB-S2, was standardized in 2005 to achieve better performance through the use of new coding and modulation techniques. Both DVB-S and DVB-S2 were designed for transmission to fixed user stations equipped with antennas located in direct line of sight with the satellite at any time. Therefore, physical layer protection mechanisms used in these standards are designed for fixed reception with the aim to correct the errors caused by interferences and thermal noise. Mobile reception is characterized by the presence of both fast and slow signal fluctuations, known as fast fading and shadowing, respectively. These fluctuations produce bursts of errors in the received information which cannot be corrected by the physical layer protection mechanisms of DVB-S and DVB-S2.

In order to increase the protection provided by the physical layer of DVB-S and DVB-S2, and also to enable the transmission of new content in mobility conditions, it is possible to incorporate additional protection techniques in the upper layers. UL-FEC (Upper Layer - Forward Error Correction) can operate transparently over the physical layer to repair error bursts originated in mobility conditions. The main advantage of UL-FEC is that it can be incorporated into existing broadcast systems such as DVB-S and DVB-S2 reusing the already deployed infrastructure with a minimal cost for the operator, as shown in the figure below. UL-FEC also allows great configuration flexibility, enabling the possibility of applying particular protection to each service transmitted.

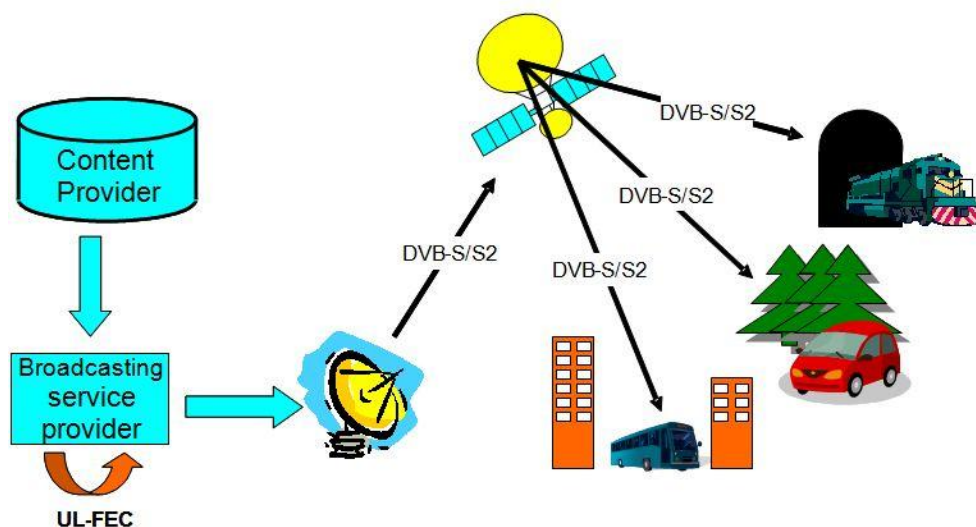


Figure 1: Mobile Satellite Network Architecture.



## 2.1.2 DVB technologies for satellite broadcasting

This section presents a review of the main DVB standards for satellite broadcasting depending on the frequency band to be used.

### 2.1.2.1 L/S Bands

Transmission in L-Band offers significant advantages over higher spectrum bands. Among these advantages, there is less vulnerability to obstructions caused by trees as well as no rain attenuation of the transmitted signal. The operation in L-band also allows the implementation of small antennas where high pointing accuracy to the satellite is not required. However, the available spectrum in this frequency band is only tens of MHz, making difficult the provision of broadband services. One clear example of service using these bands is DVB-SH [6].

## DVB<sup>®</sup> SH

DVB-SH (Digital Video Broadcasting – Satellite Handheld) derives from DVB-H (Digital Video Broadcasting - Handheld) and ETSI SDR (Satellite Digital Radio) to provide broadcasting services to various types of mobile devices.

This system provides a huge coverage through the SC (Satellite Component), which is complemented by a CGC (Complementary Ground Component) that comes from the deployment of a terrestrial network in those areas where the satellite signal is severely degraded and also in urban environments. Thus, all reception scenarios for mobile devices are supported. Figure 2 below shows the architecture of a typical DVB-SH network.

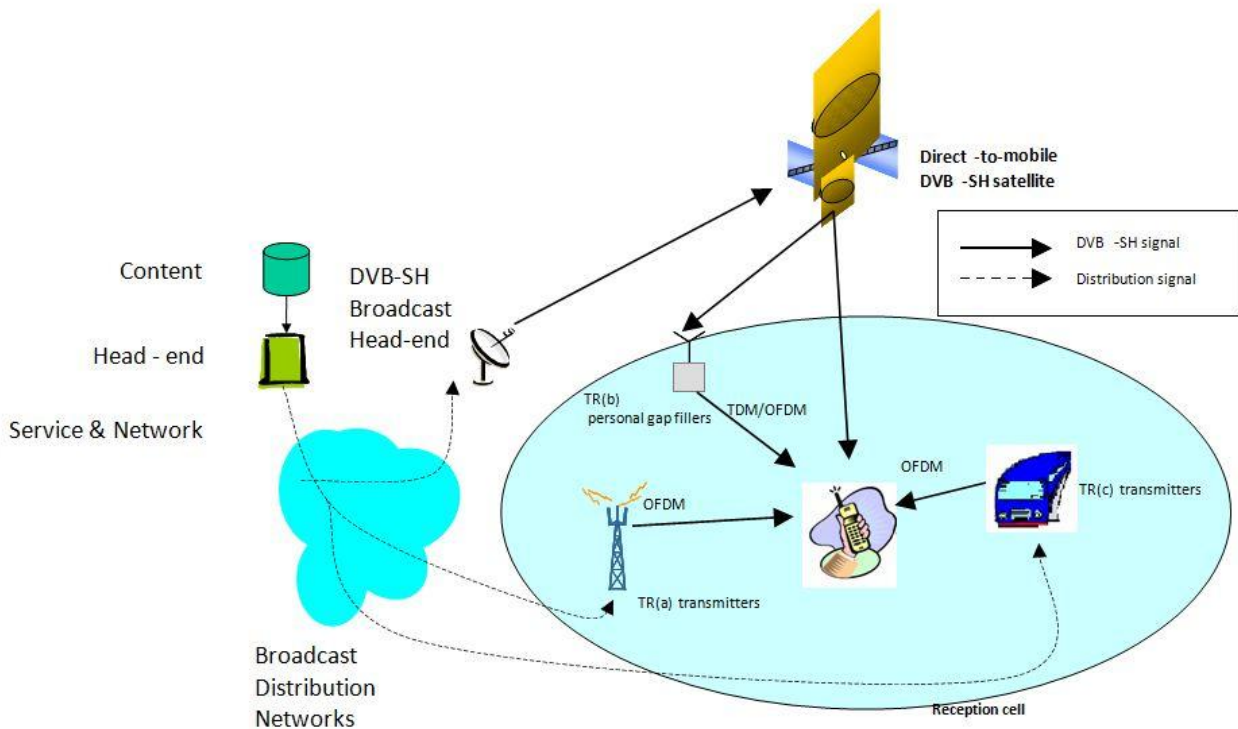


Figure 2: DVB-SH network architecture.

The standard defines two architectures:

- SH-A Architecture, where the satellite and terrestrial components use OFDM modulation (*Orthogonal Frequency Division Multiplexing*).
- SH-B Architecture, where the satellite component uses TDM (*Time Division Multiplex*), while the terrestrial component uses OFDM.

SH-A architecture enables the creation of single frequency networks (SFN) between the SC component and the CGC component, so that both components transmit the same content at the same frequency. The advantage of an SFN is spectral efficiency. However, it also presents a drawback, since it requires the signal transmitted via satellite and the signal transmitted via the terrestrial network to be exactly the same, which implies less variety in the configurations that DVB-SH provides.

Finally, one of the highlighted features incorporated in DVB-SH is the new upper layer correction system UL-FEC (Upper Layer - Forward Error Correction), called MPE-IFEC (intra-burst FEC), which is designed to be used in difficult or large shadow areas of the satellite channel.

### 2.1.2.2 C/Ku/Ka Bands

The transmission of mobile satellite services in Ku-band requires the deployment of antennas equipped with complex pointing and tracking mechanisms due to a higher directivity in this frequency range. This directivity leads to a higher vulnerability of the signal to the presence of obstacles in direct line of sight between the transmitter and the receiver. Nevertheless, today it is possible to develop antennas able to meet all the requirements associated in Ku band transmission. In the future, development of technology related with this type of antennas will allow its incorporation into all types of vehicles. Thus, it will be possible to take advantage of the wide available bandwidth in this frequency band to offer broadband services on the move.

DVB-S and DVB-S2 standards operate in the frequency range of Ku band (10.7-12.75 GHz in the downlink and 14.0-14.5 GHz in the uplink), which is used in satellite broadcasting TV and many VSAT systems.

In America, C-band (3.7-4.2 GHz in the downlink and 5.925-6.425 GHz in the uplink) is also used, and recently Ka band (17.7-21.2 GHz in the downlink and 27.5-31.0 GHz in the uplink) has started to be used in next-generation multi-spot satellites, mainly for bidirectional broadband applications.



Developed by the European Telecommunication Standard Organization, DVB-S [4] is a standard for satellite video broadcasting. It applies only to Ku-band satellites and its main purpose is to provide Direct-To-Home services through geostationary satellites.

DVB-S implements several techniques against noise and interference, as well as an efficient use of the spectrum. It uses a QPSK modulation scheme linked with powerful error correction techniques based on the concatenation of convolutional and Reed-Solomon (RS) algorithms.

DVB-S is optimized to use TDM, although it is compatible with FDM. Furthermore, the system is based on MPEG-2 coding. Depending on link characteristics, it is possible to select the appropriate coding rate (from 18.4 to 48.4 Mbit/s). This flexibility gives a compromise between spectrum efficiency (use of high-speed transmission rates) and power efficiency (low carrier-to-noise ratio).

DVB-S standard was primarily developed for one-way TV and radio broadcasting, since these are the main traditional services. However, data distribution both point-point and point-multipoint networks are also considered.



DVB-S2 (EN 302 307 [5]) is a digital satellite transmission system developed by the DVB Project. It makes use of the latest modulation and coding techniques to achieve performances that approach the theoretical limit for such systems. Satellite transmission was the first area addressed by the DVB Project in 1993, and DVB standards form the basis of most satellite DTV services around the world today, and therefore of most digital TV in general. DVB-S2 will not replace DVB-S in the short or even the medium term, but makes it possible to provide services that could never have been delivered using DVB-S.

DVB-S2 incorporates robust protection error algorithms by using two concatenated encoders (BCH – Bose Chaudhuri Hocquenghem and LDPC - Low Density Parity Check), achieving a near-Shannon limit capacity. Also, the system is more flexible and allows services with variable bit rates, modulation schemes (QPSK, 8PSK, 16APSK & 32APSK) and roll-offs ( $\alpha=0.35$ ,  $\alpha=0.25$  &  $\alpha=0.20$ ).

Thanks to the new coding and modulation techniques, DVB-S2 performance gain over DVB-S is around 30% at the same satellite transponder bandwidth and emitted signal power. DVB-S2 is compatible with current DVB-S receivers on the market.

## 2.2 Satellite Role in DVB-NGH architecture

### 2.2.1 Introduction

There are three scenarios considered in DVB-NGH:

1) *Satellite-only scenario*

For rural areas where terrestrial networks are inexistent or signal reception is poor, satellite guarantees direct reception. Gap-fillers may be used to increase coverage indoor.

2) *Hybrid scenario*

In this scenario satellite signal is received by a new network element: the Complementary Ground Component (CGC) and retransmitted to the mobile device. This new element has to be designed so that integration with existent mobile networks (2G, 3G) is easy.

3) *Terrestrial-only scenario*

Satellite coverage is poor and terrestrial infrastructure exists.

Table 1 summarizes the three scenarios considered, detailing the coverage area and a possible application.

**Table 1: DVB-NGH satellite scenarios.**

	<b>Business to consumer (Direct Service provision)</b>	<b>Business to business to consumer (Indirect service provision)</b>
<b>Satellite-Only</b>	Rural or suburban area with no terrestrial infrastructure.	Airborne, Ships
<b>Hybrid</b>	Global coverage	Railway, commercial centres. Urban communities
<b>Terrestrial-Only</b>	Suburban and urban areas with terrestrial infrastructure. Underground.	

### 2.2.2 Satellite-Only Scenario

Satellite is the best technology to cover rural or suburban areas where there are no terrestrial infrastructures. Service provision to airborne or ships are some of the most relevant examples of business to business consumers. The content distribution in this scenario uses S-band. Here we present the main characteristics.

#### S-band distribution

S band is defined by an IEEE standard for radio waves with frequencies ranging from 2 to 4 GHz, crossing the conventional boundary between UHF and SHF at 3GHz. S band coverage is typically smaller with respect to other frequency bands such as Ku. One possible solution is to use multi-spot configurations that would also allow greater frequency reuse. Obviously this solution increases satellite complexity and, therefore its associated cost.

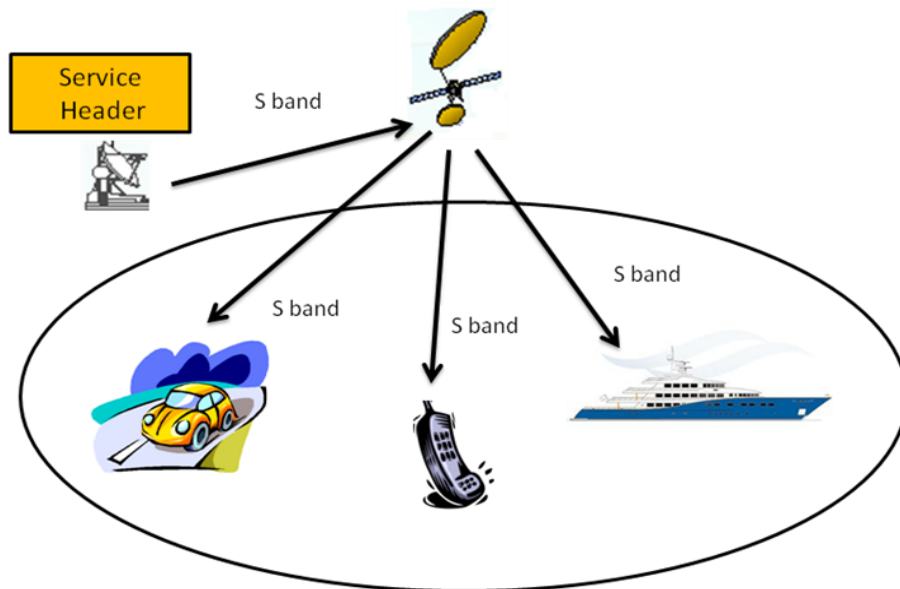


**Figure 3: Satellite only architecture.**

The main advantage of this system is that it requires a single signal to feed the end consumer terminals. The main disadvantage of this strategy is that S-band has not been widely used in satellite communications, so receivers cost is higher than the equivalent in Ku-band.

### 2.2.3 Hybrid scenario

In a normal communication operation mode, the user device is normally in line of sight with satellite. However, there are many occasions in which the receiver may lose sight of the satellite and so a signal quality degradation can be perceived, even signal reception can be totally lost. To overcome this situation, the hybrid architecture introduces a Complementary Ground Component (CGC). CGC is a network of re-transmitters that act as repeaters of the signal received from the satellite. These repeaters are also known as Gap-fillers, since they “fill” the areas where satellite signal is not received.

Gap-fillers are normally designed for frequency re-use, so that the downlink frequency and the re-transmission frequency are the same. These types of networks are called SFN (Single Frequency Network).

The application of this kind of retransmission requires the receiver to be able to apply echo-compensation techniques. Figure 4 below shows the hybrid network architecture.

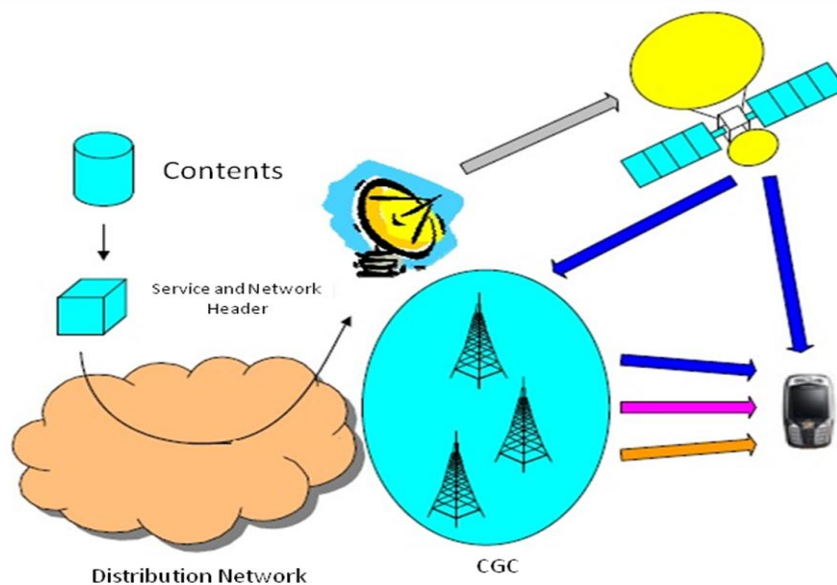


**Figure 4: DVB-NGH network architecture.**

As shown in the previous figure, CGC receives the content transmitted by the satellite and retransmits it within its coverage areas, which are the areas where satellite reception is difficult. The different elements which compose the CGC network topology are:

- **Content Generation:** Generates the contents that will be transmitted to the DVB-NGH terminals.
- **Network and Service Frontend:** It is in charge of content adaptation and encapsulation so that the transmitted signal can be interpreted by the receivers.
- **Network Distribution:** Sends the information to the transmission centres, which may be ground stations which transmit contents to the satellite, or gap-fillers.



## Technical Report TR4.2

- **Satellite/Gap-fillers:** Transmit the amplified signal received to the user terminals. In most cases, distribution to gap-fillers will be done using the downlink satellite signals aimed to user terminals.
- **DVB-NGH receivers:** receive information, de-encapsulate the signal and represent the content on the display.

### 2.2.3.1 Signal Distribution to CGC

As previously mentioned, CGC is responsible for complementing the satellite signal in areas where coverage is weak or nonexistent. In these cases, terrestrial repeaters (gap-fillers) are needed to forward the information to the end terminal. Depending on the strategy to reach this terminal, there are several possibilities:

- Use a satellite transmission in S-band.
- Use a satellite transmission at another frequency band (typically Ku).
- Getting the information through terrestrial transmitters.

Next we will go into details for the first two possibilities. The third one is widely discussed in other ENGINES deliverables, since there are significant variations in signal delay and echo canceller design is complex.

### S-band distribution

In this scenario, S-band is used for transmitting the information to shadowed areas. It presents the following characteristics:

#### **SFN (Single Frequency Network)**

Satellite and terrestrial repeaters use the same frequency band. Terminals can be simplified so that receivers with echo cancellation technology can receive information from the satellite or terrestrial broadcaster depending on the one that arrives with higher quality.

#### **Bandwidth Re-use**

Additionally to what has been said about SFN, a direct conclusion is that frequency reuse is possible for this scenario. The same frequency can be used to transmit the information to the terminals and to re-transmitters. Thus, the information source can be the same satellite in both cases and it would not require additional bandwidth rent to transmit the content, with the consequent cost saving.

#### **Limited Coverage**

S band coverage is typically smaller with respect to other frequency bands such as Ku. One possible solution is to use multi-spot configurations that would also allow greater frequency reuse. Obviously this solution increases satellite complexity and, therefore its associated cost.

The main advantage of this system is that it requires a single signal to feed both repeaters and end terminals. Processing in gap-fillers is simplified basically consists in signal acquisition and amplification. The main

disadvantage of this strategy is that S-band has not been widely used in satellite communications, so receivers cost is higher than the equivalent in Ku-band.

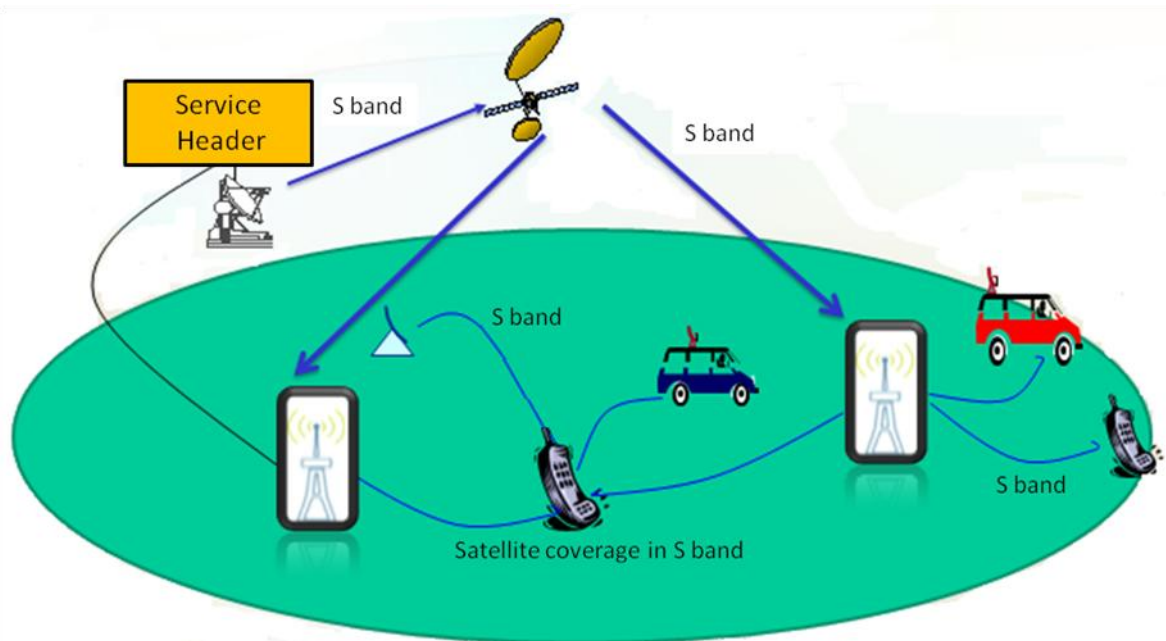


**Figure 5: S-band Architecture Contribution to the CGC.**

## Ku band Distribution

Ku band is primarily used for satellite communications, most notably for fixed and broadcast services. The use of Ku band for the distribution of content to terrestrial repeaters presents the following characteristics:

### Wide Coverage

Ku-band coverage is much larger than for S-band. This way it is possible to increase the number of potentially covered terrestrial repeaters and therefore increment the total number of costumers.

### High Available Bandwidth

Currently, existing regulations regarding Ku frequency band for satellite communications reserve 750 MHz for this type of services. In S-band the allocated bandwidth is only 30MHz.

### Consolidated Ground Segment

Ku band has been widely used in satellite communications so that its associated equipment (including ground segment) is much more developed than the S-band equivalent and so equipment costs in Ku band are also lower.

In this scenario, satellite transmits content in Ku band (14.0-14.5 GHz) to repeaters and S band is used to transmit towards the user terminals. A frequency conversion is needed in gap-fillers in order to reduce complexity in DVB-NGH terminals. Figure 6 below shows the scenario architecture.

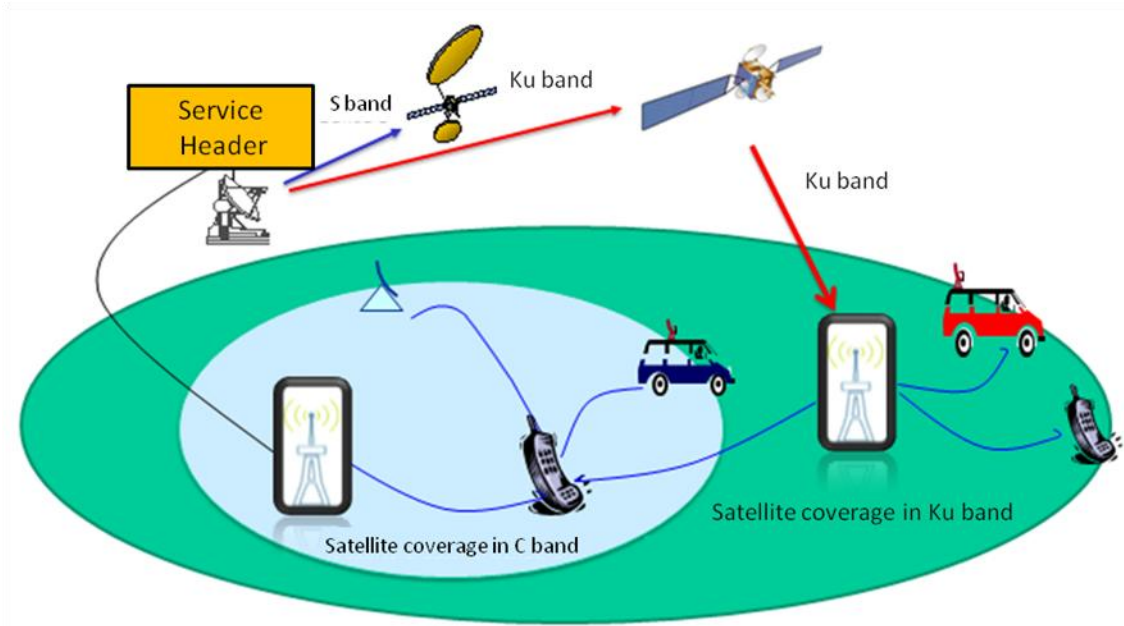


**Figure 6: CGC Architecture Contribution in Ku-band.**

The main advantage of this transmission mode is its associated technology, fully extended and cheap, the great satellite capacity and coverage. The main disadvantage is that, because there is no frequency reuse, satellite resource expenses will be greater. Additionally, since frequency conversion is required in gap-fillers, these are more complex. Processing complexity is higher than for the direct reception case, and so end user terminals will have to be able to cancel echoes with significant delays. This strategy has been analyzed in detail and results are provided in the final section of this document.

## 2.2.4 Network Distribution Requirements

The content distribution network must meet the following characteristics:

### High Availability

Most of the content sent through the network will be multimedia, so high availability must be ensured. This characteristic has to be met both for the final receivers and for the re-transmitters of the CGC. Availability depends on the propagation characteristics of the signals involved, being rain attenuation one of the most important parameters to consider. Rain attenuation causes a decrease in signal level and can be as strong as to damage completely the link. Analyzing the frequencies commonly used in satellite communications with respect to rain attenuation, Ku band more sensitive to this effect than S band. The higher the frequency the more influence of rain attenuation.

Links are designed according to statistical parameters of rainfall and additional margins are considered to ensure the required availability. This way, the higher the margins considered the higher the channel availability. A typical design objective for television signal distribution over satellite is an availability of 99.7% a.y. (average year).



## Quality of Service

In the same way as availability, high quality of service must be ensured in the link between the station which sends data to the satellite and the re-transmission elements which receive this data.

Availability and quality of service are strongly related: quality of service depends directly on the quality of the received signals. In digital communications, the parameter that determines this quality of service is usually BER (Bit Error Ratio), which refers the number of incorrect bits received with respect to the number of transmitted bits. BER depends on the ratio between the energy of the received bits and the noise energy ( $E_b/N_0$ ).

For example, for a DVB-S transmission with FEC = 3/4,  $E_b/N_0 = 5.5$  dB, the ensured BER is smaller than  $2 \times 10^{-4}$ . This is a typical design objective.

## Ground Segment Performance

To ensure quality and availability of the transmitted signal, the ground stations (both transmitters and receivers) must have the necessary equipment. Repeater stations are of vital importance since they must receive the signal, trans-modulate it and re-send it to the remote terminals with no signal degradation.

Good ground segment performance allows the system to be more robust against external interferences (such as other satellites) and internal interferences (from other carriers received from the same satellite). Performance requirements depend on satellite characteristics and equipment of the stations involved in the communications, as well as on the frequency band used.

In Ku band, for small stations a typical requirement is a radiation pattern whose envelope is lower than  $29 - 25 \times \log(\theta)$  at  $\pm 1.5^\circ$ , and a transmission isolation of 28 dB. These are desired characteristics; however, the link can always be designed to compensate possible problems in stations.

## 2.3 DVB-NGH Satellite Link

This section will examine the main satellite link parameters in the DVB-NGH architecture.

### 2.3.1 Link Budgets Calculations

First we present the methodology to be followed in order to calculate a satellite link budget. In a satellite link there are two components: the uplink or upstream and the downlink or downstream.

The uplink C/N is defined as:

$$\left[ \frac{C}{N} \right]_U = \frac{1}{kB} EIRP_{GW} \frac{1}{L_U} \left[ \frac{G}{T} \right]_{SAT}, \quad (1)$$

where:

$k$ : Boltzman constant,

$B$ : Noise BW,

$EIRP_{GW}$ : Gateway EIRP ( transmission earth station),

$L_U$ : Uplink losses,

$[G/T]_{SAT}$ : Satellite Antenna figure of merit (Gain to system noise temperature).

Furthermore:

$$EIRP_{GW} = \frac{P_{GWTX} G_{GW}}{L_T L_{FTX}}, \quad (2)$$

where  $P_{GWTX}$  is the total power transmitted by the earth station,  $G_{GW}$  is the antenna transmission gain,  $L_T$  are pointing error losses and  $L_{FTX}$  are the attenuation losses between transmitter and antenna.

$L_U = L_{FS} L_A$ , where  $L_{FS}$  are free space losses and  $L_A$ , losses related to atmospheric attenuation in the uplink.

$$L_{FS} = \left( \frac{4\pi R}{\lambda} \right)^2. \quad (3)$$

$R$  is the distance between the transmitting earth station and satellite.

For the uplink we define the following parameters:

$$\left[ \frac{C}{N} \right]_D = \frac{1}{kB} EIRP_{SAT} \frac{1}{L_D} \left[ \frac{G}{T} \right]_{ES}, \quad (4)$$

where:

$EIRP_{SAT}$ : Satellite EIRP,

$L_D$ : Downlink losses,

$\left[ \frac{G}{T} \right]_{ES}$ : Earth station figure of merit (Gain to system noise temperature).

Furthermore:

$$EIRP_{SAT} = \frac{P_{SAT} G_{SAT}}{L_T L_{FTX}}, \quad (5)$$

where  $P_{SAT}$  is the satellite transmitted power,  $G_{SAT}$  is the satellite antenna gain,  $L_T$  are pointing error losses,  $L_{FTX}$  are the attenuation losses between transmitter and antenna.

$L_D = L_{FS} L_A$  where  $L_{FS}$  are free space losses and  $L_A$ , losses related to atmospheric attenuation in the downlink.

In addition to the above mentioned formulas, it is necessary to take into account the contribution of interferences. In general, interference is considered an additional source of noise, so that:

$$\left[ \frac{C}{N+I} \right]^{-1} = \left[ \frac{C}{N} \right]^{-1} + \left[ \frac{C}{I} \right]^{-1}, \quad (6)$$

where  $I$  is the total interference (various sources): Intermodulation (IM), co-channel interference (CC) and adjacent channel interference (ACI).

$$I = I_{IM} + I_{CC} + I_{ACI}. \quad (7)$$

The link budget for transparent satellites is therefore calculated as:

$$\left[ \frac{C}{N+I} \right]^{-1} = \left[ \frac{C}{N+I} \right]_{uplink}^{-1} + \left[ \frac{C}{N+I} \right]_{downlink}^{-1}. \quad (8)$$

To have a positive margin in the link, the signal-to noise and interference should be greater than the signal to noise ratio given by the modulation-coding configuration:

$$\left[ \frac{C}{N+I} \right] \geq \left[ \frac{C}{N} \right]_{REQUIRED\ MODCOD}. \quad (9)$$

Link margin is defined as:

$$M = \left[ \frac{C}{N+I} \right] (dB) - \left[ \frac{C}{N} \right]_{REQUIRED\ MODCOD} (dB). \quad (10)$$

Considering the attenuation in the downlink, signal strength degrades and the attenuation factor  $\alpha$  appears. If the source of degradation comes from intermodulation or interference between beams of the same frequency, attenuation affects both the carrier and interference. That is:

$$\left[ \frac{C \cdot \alpha}{I \cdot \alpha} \right] = \left[ \frac{C}{I} \right] \text{ if } I = I_{IM} + I_{CC}. \quad (11)$$

Therefore, the total  $C / (N + I)$  is:

$$\left[ \frac{C}{N+I} \right]_{Faded\ downlink}^{-1} = \left[ \frac{C \alpha}{N} \right]^{-1} + \left[ \frac{C}{I} \right]^{-1}. \quad (12)$$

From this relationship, link margin is calculated as follows:

$$M_{fade} = -\alpha (dB) = \left[ \frac{C}{N} \right] (dB) + 10 \log \left[ \left[ \frac{C}{N} \right]_{REQUIRED\ MODCOD}^{-1} - \left[ \frac{C}{I} \right]^{-1} \right]. \quad (13)$$

## 2.3.2 DVB-NGH Link Budget Considerations

Work related to the satellite link technical requirements in DVB-NGH is still going on and certain parameters have to be defined or agreed. At this regard the following link budget study is based on the last draft of the ETSI EN 303 105 DVB-NGH document dated on September 2012 [1] and the information which is still applicable in the DVB-SH implementation guideline as many aspects regarding the satellite component are still the same.

### 2.3.2.1 Rx Terminal definition

The Rx terminal definition is in line with the one described for DVB-SH. There are three main categories:

- Category 1 : Car-mounted terminals (also called “vehicular”).
- Category 2 : Portable TV devices with 2 sub-categories.
  - 2a : Large screen ( $\geq 10''$ ) portable devices, battery or mains powered.
  - 2b : Pocketable (handheld) TV devices, mainly battery powered.
- Category 3 : Handheld terminal with embedded cellular telecom modem (or “convergence” terminal).

### 2.3.2.2 Rx Terminal G/T considerations

This section presents the G/T hypothesis for each of the terminals under consideration.

Hypothesis:

- Vehicular receiver (category 1) : NF=2dB (LNA 0.8 dB, filter 2.5 dB, tuner 3 dB)
- Handheld receiver (category 2b and 3) : NF=4.5 dB (filter 1.5 dB, tuner 3 dB)

**Table 2: Receiver typical G/T versus terminal category.**

Usage	Handheld	Handheld	Portable	Vehicular
Classification	category 3	category 2b	category 2a	category 1
Antenna polarization	L or C	L or C	L or C	C
Tuner	DVB-NGH	DVB-NGH	DVB-NGH	DVB-NGH
Antenna gain (dBi) or (dBic)	-3	0	2	4
Total Gain (dB)	-3	0	2	4
Antenna Temperature (K)	290	290	200	150
Active antenna	No	No	Yes	Yes
Noise Figure (dB) max	4.5	4.5	3	2
Total Noise temperature (°K)	817	817	489	320
G/T (dB/K)	<b>-32.1</b>	<b>-29.1</b>	<b>-24.9</b>	<b>-21.0</b>

Polarization losses are defined in the respective satellite and terrestrial link budgets. Table 1 gives typical figures of basic receivers (without diversity consideration) related to the terminal categories. Active antenna corresponds to an antenna with an attached LNA.

### 2.3.2.3 Minimum C/N requirements

This section presents the minimum C/N requirements for the transmission in AWGN channel. The next two tables presents the theoretical performance for OFDM and TDM configurations.

**Table 3: Theoretical C/N (dB) in AWGN channel for OFDM @ BER = 10<sup>-5</sup>.**

Code rate	QPSK	16QAM
1/5	-3.6	0.7
2/9	-3.1	1.3
1/4	-2.5	1.9
2/7	-1.8	2.8
1/3	-0.9	3.7
2/5	0.1	5.0
1/2	1.4	6.8
2/3	3.5	9.7

**Table 4: Theoretical C/N (dB) in AWGN channel for TDM @ BER = 10<sup>-5</sup>.**

Code rate	QPSK	8PSK	16APSK
1/5	-3.9	-1.3	0.4
2/9	-3.4	-0.7	1.0
1/4	-2.8	-0.1	1.6
2/7	-2.1	0.7	2.5
1/3	-1.2	1.6	3.4
2/5	-0.2	2.7	4.7
1/2	1.1	4.4	6.5
2/3	3.2	6.9	9.4

For AWGN, the following implementation losses to the C/N values are considered.

**Table 5: Implementation losses in AWGN.**

Modulation	Implementation loss (dB)
TDM- QPSK	0.5
TDM- 8PSK	1.0
TDM- 16APSK	1.5
OFDM- QPSK	1.1
OFDM- 16QAM	1.5

### 2.3.2.4 Allowed parameter settings for the DVB-NGH hybrid profile

The next table presents the parameters allowed for the hybrid profile in DVB-NGH.

**Table 6: Allowed parameter settings for the hybrid profile in DVB-NGH.**

Parameters		Hybrid waveform	
Modulation		OFDM	SC-OFDM
Bandwidth (MHz)	1.7	<input checked="" type="checkbox"/>	<input checked="" type="checkbox"/>
	2.5	<input checked="" type="checkbox"/>	<input checked="" type="checkbox"/>
	5	<input checked="" type="checkbox"/>	<input checked="" type="checkbox"/>
Constellation	QPSK	<input checked="" type="checkbox"/>	<input checked="" type="checkbox"/>
	16-QAM	<input checked="" type="checkbox"/>	<input checked="" type="checkbox"/>
FTT Size	0.5k		<input checked="" type="checkbox"/>
	1k	<input checked="" type="checkbox"/>	<input checked="" type="checkbox"/>
	2k	<input checked="" type="checkbox"/>	<input checked="" type="checkbox"/>
Guard Interval	1/32	<input checked="" type="checkbox"/>	<input checked="" type="checkbox"/>
	1/16	<input checked="" type="checkbox"/>	<input checked="" type="checkbox"/>
	1/8	<input checked="" type="checkbox"/>	
	1/4	<input checked="" type="checkbox"/>	
Preamble	P1 + aP1	<input checked="" type="checkbox"/>	<input checked="" type="checkbox"/>
Pilot Pattern	Continuous pilot symbols	<input checked="" type="checkbox"/>	
	PP1	<input checked="" type="checkbox"/>	
	PP2	<input checked="" type="checkbox"/>	
	PP3	<input checked="" type="checkbox"/>	
	PP4	<input checked="" type="checkbox"/>	
	PP5	<input checked="" type="checkbox"/>	
	PP9		<input checked="" type="checkbox"/>
FEC code rate	1/5 (=3/15)	<input checked="" type="checkbox"/>	<input checked="" type="checkbox"/>

## Technical Report TR4.2

	4/15	☑	☑
	1/3 (=5/15)	☑	☑
	2/5 (=6/15)	☑	☑
	7/15	☑	☑
	8/15	☑	☑
	3/5 (=9/15)	☑	☑
	2/3 (=10/15)	☑	☑
	11/15	☑	☑
	3/4	☑	☑

### 2.3.3 DVB-NGH Link budgets

This section presents several satellite link budget analysis for the DVB-NGH service in OFDM mode. The study considers a channalization of 1.7MHz, the use of different MODCODS and two satellite EIRP effective beam levels as to characterize both low and medium power satellites.

#### 2.3.3.1 Low power satellite link budgets

The next table shows the main considerations for the link budget analysis using a low power satellite system. These satellites are characterized by an EIRP effective beam level of 63dBW over the region of interest.

**Table 7: DVB-NGH link budget analysis for 1.7MHz channel and 63dBW EIRP.**

<b>LINK BUDGET DVB-NGH</b>				
<b>1,7MHz Channel OFDM-QPSK</b>				
<b>63dBW Satellite EIRP Effective beam</b>				
Modulation	OFDM - QPSK	OFDM - QPSK	OFDM - QPSK	OFDM - QPSK
Example Code Rates	1/5 1/3 2/3	1/5 1/3 2/3	1/5 1/3 2/3	1/5 1/3 2/3
OFDM noise bandwidth (MHz)	1,52	1,52	1,52	1,52
<b>UPLINK</b>				
C/(N+I) uplink (dB)	19,5	19,5	19,5	19,5
<b>DOWNLINK</b>				
Rx Terminal ID	Handheld Cat. 3	Portable Cat. 2b	Portable Cat. 2a	Vehicular Cat. 1
Downlink Frequency (GHz)	2,0	2,0	2,0	2,0
Satellite EIRP @ location (dBW)	63,0	63,0	63,0	63,0
Athmospheric atenuation (dB)	0,5	0,5	0,5	0,5
Polarisation losses (dB)	3,0	3,0	3,0	0,0
Free space loss (dB)	190,7	190,7	190,7	190,7
<b>G/T E/T Rx. (dB/K)</b>	<b>-32,1</b>	<b>-29,1</b>	<b>-24,9</b>	<b>-21,0</b>
C/N downlink (dB)	-1,8	1,2	5,4	12,3
C/I downlink total (dB)	14,0	14,0	14,0	14,0
C/(N+I) downlink (dB)	-1,9	1,0	4,8	10,1
<b>GLOBAL RESULTS</b>				
C/(N+I) Total (dB)	-1,9	0,9	4,7	9,6

2.3.3.1.1 OFDM-QPSK

Three example MODCODs are considered: OFDM-QPSK 1/5, 1/3 and 2/3.

**Table 8: DVB-NGH link budget closure for OFDM-QPSK 1/5 at physical layer and 63dBW EIRP.**

<b>GLOBAL RESULTS</b> <b>OFDM-QPSK 1/5</b> <b>1,7 MHz Channel</b> <b>63dBW Satellite EIRP Effective beam</b>				
Useful bit rate at physical layer (Mbps)	0,46	0,46	0,46	0,46
Modulation	OFDM - QPSK	OFDM - QPSK	OFDM - QPSK	OFDM - QPSK
Code Rate	1/5	1/5	1/5	1/5
C/(N+I) Total (dB)	-1,9	0,9	4,7	9,6
Required C/N at physical layer at BER 10 <sup>-5</sup> (dB)	-3,6	-3,6	-3,6	-3,6
Implementation loss in AWGN (dB)	1,1	1,1	1,1	1,1
LOS Margin at Physical Layer wrt AWGN (dB)	0,6	3,4	7,2	12,1

**Table 9: DVB-NGH link budget closure for OFDM-QPSK 1/3 at physical layer and 63dBW EIRP.**

<b>GLOBAL RESULTS</b> <b>OFDM-QPSK 1/3</b> <b>1,7 MHz Channel</b> <b>63dBW Satellite EIRP Effective beam</b>				
Useful bit rate at physical layer (Mbps)	0,77	0,77	0,77	0,77
Modulation	OFDM - QPSK	OFDM - QPSK	OFDM - QPSK	OFDM - QPSK
Code Rate	1/3	1/3	1/3	1/3
C/(N+I) Total (dB)	-1,9	0,9	4,7	9,6
Required C/N at physical layer at BER 10 <sup>-5</sup> (dB)	-0,9	-0,9	-0,9	-0,9
Implementation loss in AWGN (dB)	1,1	1,1	1,1	1,1
LOS Margin at Physical Layer wrt AWGN (dB)	-2,1	0,7	4,5	9,4

**Table 10: DVB-NGH link budget closure for OFDM-QPSK 2/3 at physical layer and 63dBW EIRP.**

<b>GLOBAL RESULTS</b> <b>OFDM-QPSK 2/3</b> <b>1,7 MHz Channel</b> <b>63dBW Satellite EIRP Effective beam</b>				
Useful bit rate at physical layer (Mbps)	1,53	1,53	1,53	1,53
Modulation	OFDM - QPSK	OFDM - QPSK	OFDM - QPSK	OFDM - QPSK
Code Rate	2/3	2/3	2/3	2/3
C/(N+I) Total (dB)	-1,9	0,9	4,7	9,6
Required C/N at physical layer at BER 10 <sup>-5</sup> (dB)	3,5	3,5	3,5	3,5
Implementation loss in AWGN (dB)	1,1	1,1	1,1	1,1
LOS Margin at Physical Layer wrt AWGN (dB)	-6,5	-3,7	0,1	5,0



## 2.3.3.1.2 OFDM-16QAM

Three example MODCODs are considered: OFDM-16QAM 1/5, 1/3 and 2/3.

**Table 11: DVB-NGH link budget closure for OFDM-16QAM 1/5 at physical layer and 63dBW EIRP.**

GLOBAL RESULTS OFDM-16QAM 1/5 1,7 MHz Channel 63dBW Satellite EIRP Effective beam				
Useful bit rate at physical layer (Mbps)	2,66	2,66	2,66	2,66
Modulation	OFDM - 16QAM	OFDM - 16QAM	OFDM - 16QAM	OFDM - 16QAM
Code Rate	1/5	1/5	1/5	1/5
C/(N+I) Total (dB)	-1,9	0,9	4,7	9,6
Required C/N at physical layer at BER 10 <sup>-5</sup> (dB)	0,7	0,7	0,7	0,7
Implementation loss in AWGN (dB)	1,5	1,5	1,5	1,5
LOS Margin at Physical Layer wrt AWGN (dB)	-4,1	-1,3	2,5	7,4

**Table 12: DVB-NGH link budget closure for OFDM-16QAM 1/3 at physical layer and 63dBW EIRP.**

GLOBAL RESULTS OFDM-16QAM 1/3 1,7 MHz Channel 63dBW Satellite EIRP Effective beam				
Useful bit rate at physical layer (Mbps)	4,43	4,43	4,43	4,43
Modulation	OFDM - 16QAM	OFDM - 16QAM	OFDM - 16QAM	OFDM - 16QAM
Code Rate	1/3	1/3	1/3	1/3
C/(N+I) Total (dB)	-1,9	0,9	4,7	9,6
Required C/N at physical layer at BER 10 <sup>-5</sup> (dB)	3,7	3,7	3,7	3,7
Implementation loss in AWGN (dB)	1,5	1,5	1,5	1,5
LOS Margin at Physical Layer wrt AWGN (dB)	-7,1	-4,3	-0,5	4,4

**Table 13: DVB-NGH link budget closure for OFDM-16QAM 2/3 at physical layer and 63dBW EIRP.**

GLOBAL RESULTS OFDM-16QAM 2/3 1,7 MHz Channel 63dBW Satellite EIRP Effective beam				
Useful bit rate at physical layer (Mbps)	8,87	8,87	8,87	8,87
Modulation	OFDM - 16QAM	OFDM - 16QAM	OFDM - 16QAM	OFDM - 16QAM
Code Rate	2/3	2/3	2/3	2/3
C/(N+I) Total (dB)	-1,9	0,9	4,7	9,6
Required C/N at physical layer at BER 10 <sup>-5</sup> (dB)	9,7	9,7	9,7	9,7
Implementation loss in AWGN (dB)	1,5	1,5	1,5	1,5
LOS Margin at Physical Layer wrt AWGN (dB)	-13,1	-10,3	-6,5	-1,6

### 2.3.3.2 Medium power satellite link budgets

The next table shows the main considerations for the link budget analysis using a medium power satellite system. These satellites are characterized by an EIRP effective beam level of 68dBW over the region of interest.

**Table 14: DVB-NGH link budget analysis for 1.7MHz channel and 68dBW EIRP.**

LINK BUDGET DVB-NGH 1,7MHz Channel OFDM-QPSK 68dBW Satellite EIRP Effective beam				
Modulation	OFDM - QPSK	OFDM - QPSK	OFDM - QPSK	OFDM - QPSK
Example Code Rates	1/5 1/3 2/3	1/5 1/3 2/3	1/5 1/3 2/3	1/5 1/3 2/3
OFDM noise bandwidth (MHz)	1,52	1,52	1,52	1,52
<b>UPLINK</b>				
C/(N+I) uplink (dB)	19,5	19,5	19,5	19,5
<b>DOWNLINK</b>				
Rx Terminal ID	Handheld Cat. 3	Portable Cat. 2b	Portable Cat. 2a	Vehicular Cat. 1
Downlink Frequency (GHz)	2,0	2,0	2,0	2,0
Satellite EIRP @ location (dBW)	68,0	68,0	68,0	68,0
Atmospheric attenuation (dB)	0,5	0,5	0,5	0,5
Polarisation losses (dB)	3,0	3,0	3,0	0,0
Free space loss (dB)	190,7	190,7	190,7	190,7
<b>G/T E/T Rx. (dB/K)</b>	<b>-32,1</b>	<b>-29,1</b>	<b>-24,9</b>	<b>-21,0</b>
C/N downlink (dB)	3,2	6,2	10,4	17,3
C/I downlink total (dB)	14,0	14,0	14,0	14,0
C/(N+I) downlink (dB)	2,9	5,5	8,8	12,3
<b>GLOBAL RESULTS</b>				
C/(N+I) Total (dB)	2,8	5,4	8,5	11,6

## 2.3.3.2.1 OFDM-QPSK

Three example MODCODs are considered: OFDM-QPSK 1/5, 1/3 and 2/3.

**Table 15: DVB-NGH link budget closure for OFDM-QPSK 1/5 at physical layer and 68dBW EIRP.**

GLOBAL RESULTS OFDM-QPSK 1/5 1,7 MHz Channel 63dBW Satellite EIRP Effective beam				
Useful bit rate at physical layer (Mbps)	0,46	0,46	0,46	0,46
Modulation	OFDM - QPSK	OFDM - QPSK	OFDM - QPSK	OFDM - QPSK
Code Rate	1/5	1/5	1/5	1/5
C/(N+I) Total (dB)	2,8	5,4	8,5	11,6
Required C/N at physical layer at BER 10 <sup>-5</sup> (dB)	-3,6	-3,6	-3,6	-3,6
Implementation loss in AWGN (dB)	1,1	1,1	1,1	1,1
LOS Margin at Physical Layer wrt AWGN (dB)	5,3	7,9	11,0	14,1

**Table 16: DVB-NGH link budget closure for OFDM-QPSK 1/3 at physical layer and 68dBW EIRP.**

GLOBAL RESULTS OFDM-QPSK 1/3 1,7 MHz Channel 63dBW Satellite EIRP Effective beam				
Useful bit rate at physical layer (Mbps)	0,77	0,77	0,77	0,77
Modulation	OFDM - QPSK	OFDM - QPSK	OFDM - QPSK	OFDM - QPSK
Code Rate	1/3	1/3	1/3	1/3
C/(N+I) Total (dB)	2,8	5,4	8,5	11,6
Required C/N at physical layer at BER 10 <sup>-5</sup> (dB)	-0,9	-0,9	-0,9	-0,9
Implementation loss in AWGN (dB)	1,1	1,1	1,1	1,1
LOS Margin at Physical Layer wrt AWGN (dB)	2,6	5,2	8,3	11,4

**Table 17: DVB-NGH link budget closure for OFDM-QPSK 2/3 at physical layer and 68dBW EIRP.**

GLOBAL RESULTS OFDM-QPSK 2/3 1,7 MHz Channel 63dBW Satellite EIRP Effective beam				
Useful bit rate at physical layer (Mbps)	1,53	1,53	1,53	1,53
Modulation	OFDM - QPSK	OFDM - QPSK	OFDM - QPSK	OFDM - QPSK
Code Rate	2/3	2/3	2/3	2/3
C/(N+I) Total (dB)	2,8	5,4	8,5	11,6
Required C/N at physical layer at BER 10 <sup>-5</sup> (dB)	3,5	3,5	3,5	3,5
Implementation loss in AWGN (dB)	1,1	1,1	1,1	1,1
LOS Margin at Physical Layer wrt AWGN (dB)	-1,8	0,8	3,9	7,0

2.3.3.2.2 OFDM-16QAM

Three example MODCODs are considered: OFDM-16QAM 1/5, 1/3 and 2/3.

**Table 18: DVB-NGH link budget closure for OFDM-16QAM 1/5 at physical layer and 68dBW EIRP.**

<b>GLOBAL RESULTS</b> <b>OFDM-16QAM 1/5</b> <b>1,7 MHz Channel</b> <b>63dBW Satellite EIRP Effective beam</b>				
Useful bit rate at physical layer (Mbps)	2,66	2,66	2,66	2,66
Modulation	OFDM - 16QAM	OFDM - 16QAM	OFDM - 16QAM	OFDM - 16QAM
Code Rate	1/5	1/5	1/5	1/5
C/(N+I) Total (dB)	2,8	5,4	8,5	11,6
Required C/N at physical layer at BER 10 <sup>-5</sup> (dB)	0,7	0,7	0,7	0,7
Implementation loss in AWGN (dB)	1,5	1,5	1,5	1,5
LOS Margin at Physical Layer wrt AWGN (dB)	0,6	3,2	6,3	9,4

**Table 19: DVB-NGH link budget closure for OFDM-16QAM 1/3 at physical layer and 68dBW EIRP.**

<b>GLOBAL RESULTS</b> <b>OFDM-16QAM 1/3</b> <b>1,7 MHz Channel</b> <b>63dBW Satellite EIRP Effective beam</b>				
Useful bit rate at physical layer (Mbps)	4,43	4,43	4,43	4,43
Modulation	OFDM - 16QAM	OFDM - 16QAM	OFDM - 16QAM	OFDM - 16QAM
Code Rate	1/3	1/3	1/3	1/3
C/(N+I) Total (dB)	2,8	5,4	8,5	11,6
Required C/N at physical layer at BER 10 <sup>-5</sup> (dB)	3,7	3,7	3,7	3,7
Implementation loss in AWGN (dB)	1,5	1,5	1,5	1,5
LOS Margin at Physical Layer wrt AWGN (dB)	-2,4	0,2	3,3	6,4

**Table 20: DVB-NGH link budget closure for OFDM-16QAM 2/3 at physical layer and 68dBW EIRP.**

<b>GLOBAL RESULTS</b> <b>OFDM-16QAM 2/3</b> <b>1,7 MHz Channel</b> <b>63dBW Satellite EIRP Effective beam</b>				
Useful bit rate at physical layer (Mbps)	8,87	8,87	8,87	8,87
Modulation	OFDM - 16QAM	OFDM - 16QAM	OFDM - 16QAM	OFDM - 16QAM
Code Rate	2/3	2/3	2/3	2/3
C/(N+I) Total (dB)	2,8	5,4	8,5	11,6
Required C/N at physical layer at BER 10 <sup>-5</sup> (dB)	9,7	9,7	9,7	9,7
Implementation loss in AWGN (dB)	1,5	1,5	1,5	1,5
LOS Margin at Physical Layer wrt AWGN (dB)	-8,4	-5,8	-2,7	0,4

## 3 TIME INTERLEAVING IN THE SATELLITE CONTEXT

### 3.1 Long Time Interleaving

#### 3.1.1 Introduction and Background

Mobile satellite reception is characterized by long and deep fades in the received signal [8] (Figure 7). Fades are occasioned when terminals pass through shadowed areas where the signal from the satellite is blocked by trees or buildings. This signal blocking causes error bursts in which all the information received is erroneous. Because of this, in a satellite reception environment, interleaver mechanisms aimed to spread the errors along a large portion of time are of most importance. An interleaver rearranges the information to be transmitted so that portions of information that are close to each other end up being transmitted separated in time.

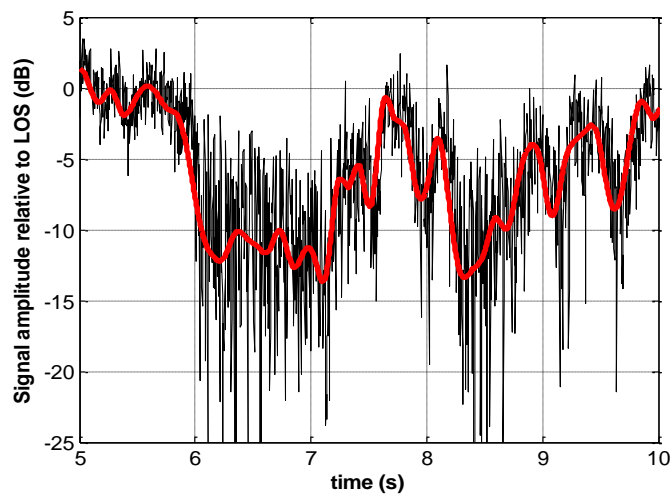


**Figure 7: LMS Suburban Channel: Elevation angle= 40°,  $f_{RF}$ =2.2 GHz, velocity=60 km/h.**

The signal fading duration depends on the reception environment and the user velocity. The blockage derived from trees causes shorter fading durations than the blockage caused by large obstacles such as buildings. On the other hand, if the user is moving at high velocities, he will go faster through shadowed areas and the fades will be shorter than if he is moving at low velocities. The interleaving time needed to guarantee a correct reception of the information is directly related to the length of the erroneous bursts and therefore is also related to the length of the fades. Durations of about 10 seconds have been estimated to be long enough to mitigate the shadowing effects caused by trees, as long as the velocity is not inferior to 10 km/h. The same duration is also long enough to mitigate the shadowing effects caused by large obstacles such as buildings, as long as the velocity is not inferior to 60 km/h [7]. In case reception is taking place at inferior velocities, as in the typical pedestrian velocity of 3 km/h, is advisable to assure service continuity by means of a larger deployment of the terrestrial component instead of increasing the interleaving duration. As the interleaving duration increases, also does the protection against long fades. However, long interleaving durations require more memory available in the terminal and bring along an increase in the delay of the information, which increments the zapping time and might degrade the user experience.

The portion of time between the moment when one user switches to one service and the moment when the information of this service is being displayed is referred to as zapping time. In the case of streaming services,

when the user switches from one stream to another, the terminal must wait until the arrival of all the interleaved information before it can display any content. As a consequence, the user will have to stand in front of a black display without any feedback during the time required to switch between services. File delivery services are not affected by zapping time; the user has to wait until the file has been completely downloaded. File delivery services are usually background services because of the fact that the user is not aware of the service until it has been completed. However, streaming services are consumed by the user during its transmission, and it is important that the user has a fast feedback of the service. Because of this, long zapping times can seriously degrade the quality perceived by the user.

### 3.1.2 State-of-the-Art – DVB-SH

#### 3.1.2.1 DVB-SH Overview

DVB-SH (Digital Video Broadcast – Satellite to Handheld), published in 2007 [6], is the European standard for the provision of video, audio and data services to handheld terminals such as mobile phones and portable receivers. The key feature of DVB-SH is that it is a hybrid satellite/terrestrial system that allows the use of a satellite to achieve wide area coverage. Satellite is probably the ideal medium for distributing a TV signal to large audiences covering large areas because the cost of network infrastructure is fixed and independent to the number of users. Whenever a line of sight between terminal and satellite does not exist, for example urban or indoor scenarios, terrestrial repeaters are employed to provide the missing coverage, but also can be used to transmit additional content particularized to each region. This capability increases the offer that is available to the users. DVB-SH hybrid architecture (see Figure 8) is able to combine the advantages of both philosophies supposing a highly efficient method for the provision of mass multimedia mobile services.

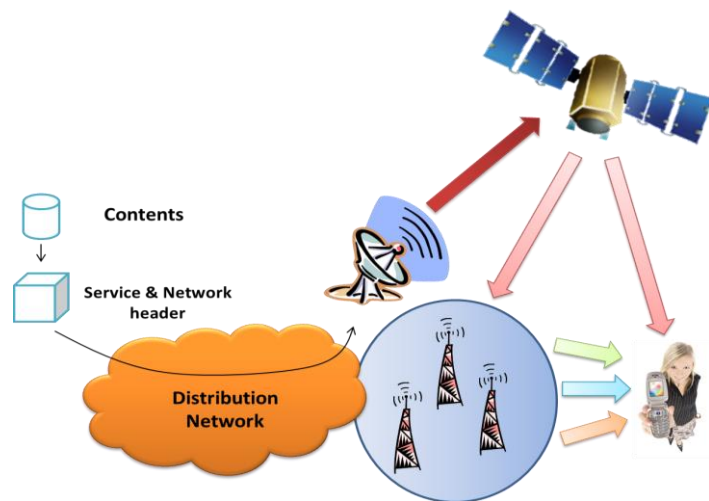


**Figure 8: DVB-SH hybrid architecture.**

DVB-SH employs an OFDM (Orthogonal Frequency Division Multiplexing) waveform in the complementary terrestrial network and an OFDM or a TDM (Time Division Multiplexing) waveform in satellite transmissions. OFDM waveform allows the deployment of Single Frequency Networks (SFN) in which receivers can combine the signals incoming from all the transmitters, satellite included, as long as the delay between signals does not overcome the guard interval of the OFDM signal. DVB-SH also allows for

the TDM waveform in the satellite component, which is capable of supporting higher satellite transmission power. This is due to the fact that multicarrier signals as OFDM are characterized by a high peak power, forcing the on-board high power amplifiers to work far from the saturation point (for which the transmitted power is maximized) in order to avoid nonlinear distortions. TDM waveform allows the on-board transmitters to work closer to the saturation point, which represents a power advantage with respect to OFDM that involves an increase in the coverage provided by the satellite component.

The DVB-SH system has been designed for frequencies below 3 GHz, typically in the S-band around 2.2 GHz adjacent to the 3G terrestrial frequencies. The S-Band is very demanding in terms of signal coverage. Its short wavelength requires a quite dense terrestrial repeater network in towns and cities. Naturally the cost of this network can be reduced if the signal-to-noise ratio (SNR) required for stable reception is low. For that, DVB-SH includes features such as turbo coding for forward error correction (FEC) that enhance the signal robustness and a highly flexible channel interleaver that provides time diversity from about one hundred milliseconds up to 30 seconds [7] that helps to counteract the effects of signal fading on the transmission channel. DVB-SH incorporates on one hand, a physical layer interleaver of long duration, and on the other hand, a link layer multi burst protection mechanism. Both approaches are aimed to cope with the long errors bursts caused by shadowing.

The physical layer of DVB-SH incorporates new protection mechanisms with respect to its predecessor DVB-H (Digital Video Broadcast – Handheld) [9] such as a long duration interleaver and a turbocoder that replaces the convolutional coder found in DVB-H. The interleaver is introduced in order to mitigate the effects of the shadowing present in satellite reception. On the other hand, the turbocoder increases the robustness of the transmission thanks to its proven effectiveness in mobile environments.

Similarly to DVB-H, DVB-SH is based on the transmission of MPEG2 transport streams (TS) carrying information bursts compatible with the time slicing technique of DVB-H. An MPEG2 TS consists of MPEG2 packets of 188 bytes that are transmitted one after another. A CRC-16 is added to each one of these packets, so the receiver can know if any of these packets is erroneous. An MPEG2 TS can follow two different paths before its radio transmission according to the waveform is going to be transmitted. The two possible waveforms, OFDM and TDM, share common subsystems that process the information no matter what the waveform is. These subsystems are the turbocoder and the physical layer interleaver. The turbocoder incorporated in DVB-SH is the one standardized by the 3GPP2 and also employed by 3G systems. However, the turbocoder implementation in DVB-SH features new code rates in order to increase the flexibility in the level of protection.

### **3.1.2.2 Convolutional Interleaver (CI)**

The channel interleaver incorporated in DVB-SH is situated right after the turbocoder output and is made of two cascade interleavers, a bit interleaver and a time interleaver. The bit interleaver is in charge of rearranging the bits inside each block word that comes from the turbocoder. After this, a rate adaptation process punctures the block words so they can be multiples of 126 bits, which is the size of one interleaving unit (IU). Following the rate adaptation process, the time interleaver takes as input the sequence of IUs of 126 bits cells and spread them over many distinct time instants by means of a convolutional interleaver. In the receiver, these IUs are again collected, reordered and forwarded to the turbo decoder. There are two

different physical layer interleaving durations defined in DVB-SH: one of about 200 ms that can work with a number of IUs up to 6528, and other one of about 10 s that can work with a number of IUs up to 417792. This possibility brings out two different terminal classes: a class 1 terminal, with short physical layer interleaving (200 ms), and a class 2 terminal with long physical layer interleaving (10 s). In order to store and process the interleaved information, class 1 terminals need at least 4 Mb of memory resources whereas class 2 terminals need at least 256 Mb [7].

### 3.1.2.3 MPE-iFEC

The implementation of long interleaving depths at the physical layer involves an increase in the memory requirements, which has an important impact in the hardware complexity and cost of user terminals. On the other hand, the implementation of interleaving at upper layers requires between 10 and 30 times less memory. Moreover, upper layer FEC mechanisms can use the general purpose memory of the user terminals for interleaving purposes. Because of this, it is possible to implement long interleaving depths at upper layers without the need of additional hardware.

DVB-SH introduces a new inter burst protection technique at the link layer called MPE-iFEC (Multi Protocol Encapsulation – Inter burst Forward Error Correction) MPE-iFEC is a *multi-burst* sliding mechanism that performs an interleaving able to repair fading typical of mobile satellite reception. However, another scheme based in Raptor codes is referred in the standard as optional. The RS sliding mechanism can benefit from the reuse of a well-known code such as the RS (255,191), whereas the Raptor based mechanism can benefit from a full software implementation of a fountain code, but are under the protection of the intellectual property. In a multi-burst codification, several bursts are coded together to generate the parity information. Later, this parity is spread over time. This *multi-burst* coding, in contrast to *intra-burst* coding, can recover burst completely lost.

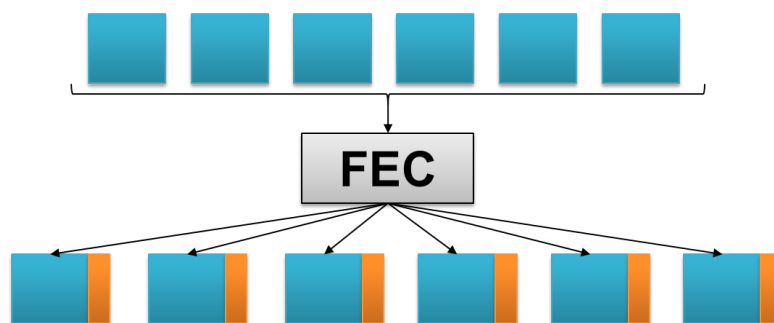


Figure 9: MPE-iFEC Encoding process.

### 3.1.2.4 Convolutional interleaving for the Long TI Feature of DVB-NGH

DVB-NGH has adopted for the sheer terrestrial profile (i.e., terminals without external TDI memory), a convolutional interleaver for inter-frame time interleaving, keeping the block interleaving only for intra-frame interleaving. This way, longer TI durations can be achieved for a given memory. In the BICM module



at the transmitter side, the CI is introduced before the BI. This allows combining the BI and CI into one single interleaver, such that each interleaver does not need dedicated memory.

Since the CI is adopted for the sheer terrestrial profile, and it is used in DVB-SH, it was considered as the reference point for the hybrid terrestrial-satellite profile of DVB-NGH. The CI can provide fast zapping with long time interleaving using a uniform-late profile or a uniform-early profile. The uniform-late profile has the advantage that full protection is progressively and smoothly achieved with time, and that the end-to-end latency is constant. The robustness after zapping is given by the amount of parity data transmitted in the late/early part. The size of the early/late part represents a trade-off between overall performance in mobile channels and performance after zapping. In DVB-SH, it is recommended to employ a code rate 4/5 [7] such that users in good reception conditions (e.g., in line-of-sight with the satellite), can benefit of fast zapping. In DVB-SH, the uniform-late profile of the CI provides good zapping performance at the expense of reducing the overall performance in the LMS channel with respect to the uniform profile (between 2 to 4 dB [7]). However, the use of CI with a single FEC is cumbersome in DVB-NGH because, unlike turbo-codes, LDPCs exhibit very poor performance with heavy puncturing (erasures).

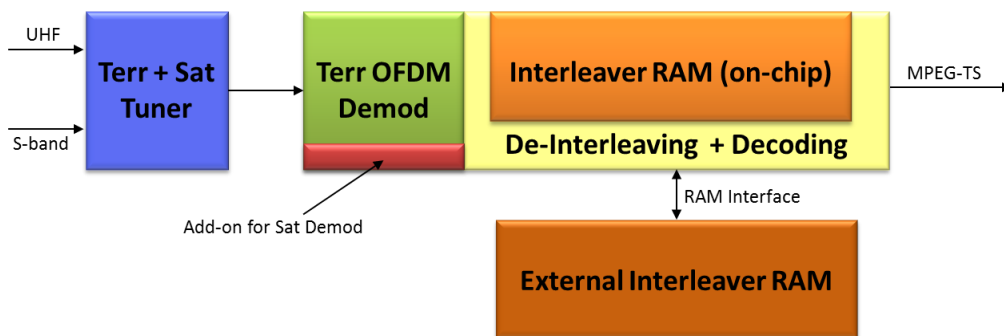


**Figure 10: Functional overview of a NGH hybrid terminal.**

Hybrid terminals have two TDI memories. On-chip and external RAM. On-chip is same memory as sheer terrestrial terminals. This memory is used only for intra-frame interleaving. DVB-NGH has the same on-chip memory size than DVB-T2 (i.e.,  $2^{19} + 2^{15}$  cells). On the other hand, external RAM is dedicated for long TI providing. The size of external TDI memory has been set by the standard to  $2^{22}$  cells.

### 3.1.2.5 Simulation Results

This section deals with the performance of convolutional interleaving with single FEC for the following channels: the AWGN (Additive White Gaussian Noise), the TU6 (Typical Urban 6-path) mobile, and the SU LMS sub-urban (SU) [8]. Table 21 shows the simulation parameters used for the simulations.

**Table 21: Simulation parameters for time interleaving performance evaluation.**

<b>Bandwidth</b>	8 MHz (AWGN/ TU6)	$f_{RF}$	600 MHz (TU6)
	5 MHz (LMS)		2.2 GHz (LMS)
<b>FFT Size</b>	8K (AWGN/TU6)	<b>FEC Codeword</b>	16200
	2K (LMS)		
<b>Antenna Conf.</b>	SISO	<b>Velocity</b>	60 km/h
<b>Guard Interval</b>	1/4	<b>Overall Code Rate</b>	1/3
<b>Frame Duration</b>	200 ms	<b>Sub-slicing</b>	Maximum
<b>Cycle Time</b>	1 s.	<b>Time interleaving</b>	10 s.
<b>Constellation</b>	QPSK	<b>Simulation time</b>	1 hour
<b>Rotated</b>	Disabled	<b>Service Rate*</b>	250 kbits/s
<b>Ch. Estimation</b>	Ideal	<b>QoS Criterion</b>	ESR5(20) 90%

\*Assumptions: 6 bytes BB frame header, 168 bits BCH

### 3.1.2.6 Fast zapping results

As previously mentioned, the TI can be configured to provide fast zapping using Uniform-Late (UL) profiles. The UL profile ensures that a big part of the encoded code word is available already with the first frame. In case of good reception conditions this part is already sufficient for successful decoding. In the worst case, when all of the transmitted redundancy is required to receive the data the zapping time may be up to the full TI length. The UL profile is recommended, if a short zapping time is important. However using UL profile involves a performance penalization in comparison to using uniform profile.

Figure 11 compares performance of single FEC with a code rate 1/3 with two sizes of the late part (40% and 50%) in AWGN channel. The early decoding performance of single FEC depends on the size of the late part, which determines the effective code rate after zapping.

Single FEC suffers performance degradation because, unlike turbo-codes, LDPCs exhibit very poor performance with heavy puncturing (erasures). It should be noted that this puncturing in DVB-NGH is at cell level, and it cannot be optimized like the one performed for layer 1 signaling in DVB-T2 [7]. When the late part of the CI profile is 50%, there is an effective puncturing after zapping of 50% of the codeword (effective code rate after zapping is 2/3). In this case, the degradation at frame error rate  $10^{-3}$  is around 0.5 dB. The performance degradation increases for lower sizes of the late part, because the puncturing is higher. If the late part is 40%, there is an effective puncturing after zapping of 60% of the codeword (effective code rate after zapping is 5/6). In this case, the degradation at frame error rate  $10^{-3}$  is around 4 dB.

Figure 12 shows the performance over time of single FEC with CI in the TU6 channel model at 10 Hz Doppler with two CI profiles configuration: Uniform and Uniform-Late 50% in comparison with Single FEC 2/3 without time interleaving. In the figure, it can be observed that single FEC with a uniform CI profile is not capable of providing fast zapping. We can also see that the performance degradation of single FEC after

zapping is significantly larger in fading channels than in AWGN. If in Figure 11 the degradation for a 50% uniform-late CI was just 0.5 dB, in Figure 12 the degradation is 4 dB.

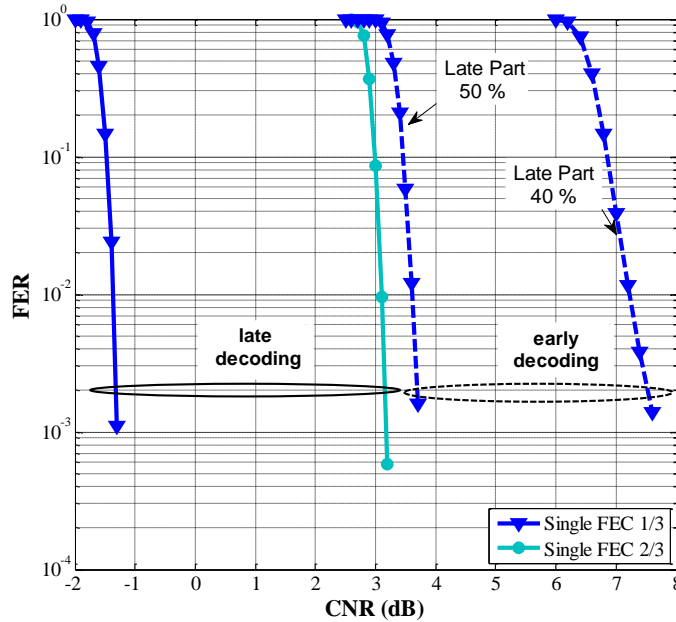


Figure 11: Performance comparison in AWGN channel of different CI profiles configuration.

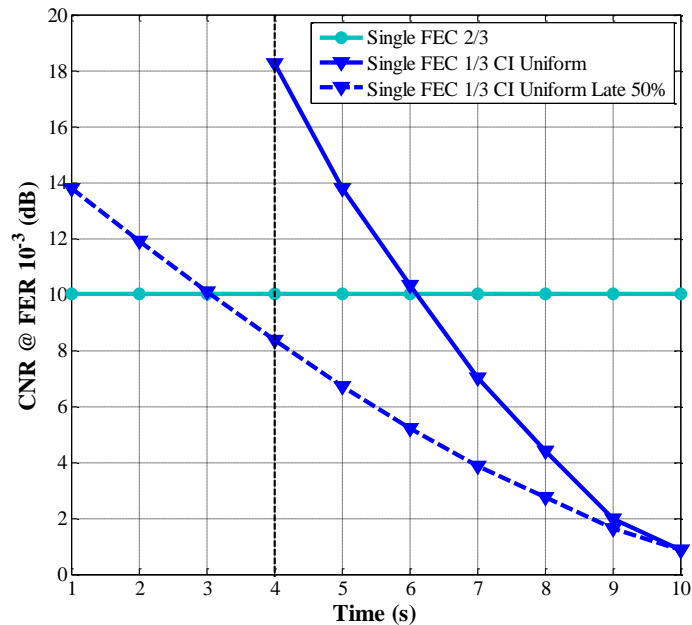
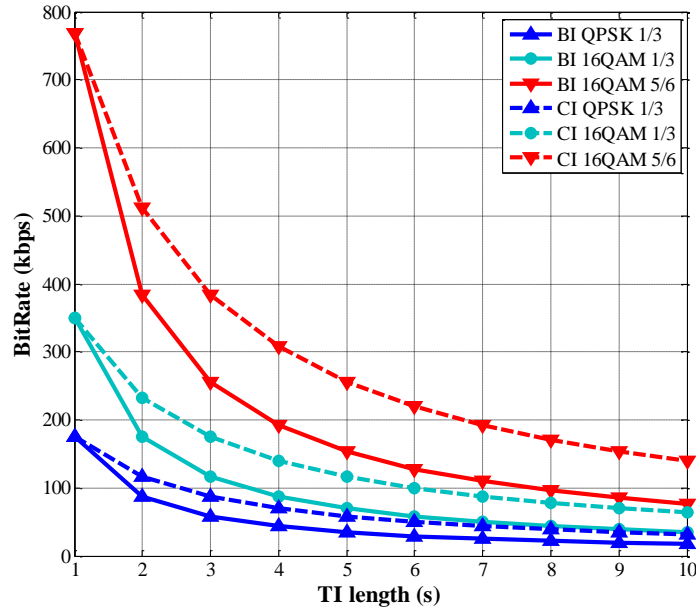


Figure 12: Performance comparison between CI Uniform and CI Uniform Late 50% for an overall code rate CR 1/3 in the TU6 channel at 10 Hz Doppler. Modulation is QPSK.

### 3.1.2.7 Time interleaving length

The maximum TI length depends on the data rate of the PLP, the amount of TDI memory available in the receivers, the FEC code rate, the constellation order and the TI profile selected. For a fixed TI length, the

memory required by a CI is always less than half of the memory required by a BI. This involves that for a certain TDI memory - set by the standard – the maximum TI length provided by a BI could be increased or even doubled using a CI.



**Figure 13: Maximum PLP data rate supported in NGH (CI) in comparison with T2-Lite (BI) with respect to the interleaving duration for different constellations and code rates. TDI memory is fixed to 218 cells.**

### 3.1.2.8 Long Time Interleaving Results

Land Mobile Satellite (LMS) channel is characterized by long signal outages (e.g., due to the blockage of the line of sight with the satellite caused by tunnels, buildings, trees, etc.), which can only be compensated with a long time interleaving duration. Figure 14 shows simulation results in the LMS Sub-Urban (SU) channel of the late decoding performance for single FEC with two different configurations of the CI for providing inter-frame interleaving: uniform and uniform-late with 50% late part (TI length of 10 s.) in comparison with using only intra-frame interleaving (TI length of 200ms). The ESR5(20) quality of service (QoS) criteria represents the percentage of intervals of twenty seconds which contain at most one second with errors. The best performance is achieved by single FEC with a uniform CI profile, as expected. The performance of single FEC with the CI uniform-late profile is reduced about 2 dB compared to the CI uniform profile. CI with TI length of 10 s. achieves gains between 6-8 dBs.

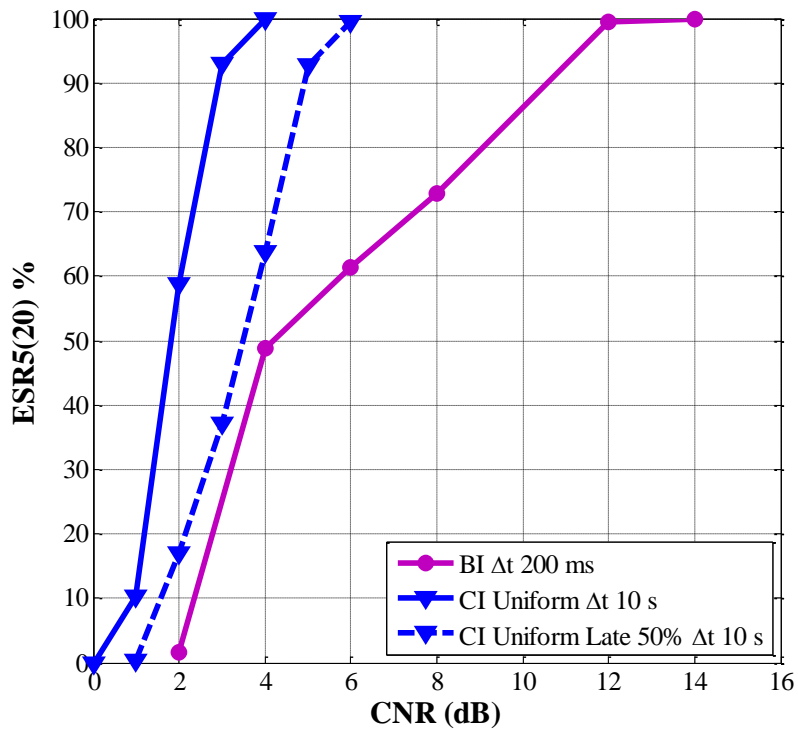


**Figure 14: Performance comparison in LMS channel of the different CI profiles (Uniform and Uniform-Late 50%) for providing long time interleaving (10s.) and BI providing only intra-frame interleaving (200ms.). Overall code rate is 1/3.**

### 3.2 Performance analysis of time interleaving

For a satellite part, a long interleaver is needed to cope with the fluctuation of the shadowing effect seen by the mobile receivers while the code-rate is tightly tuned to the optimization of the satellite link budget and the compromise with data throughput. Two solutions have been introduced in DVB-SH: one solely on the physical layer with the class 2 physical time interleaver, and the other one on the link layer with the class 1 physical time interleaver. The class 2 interleaver must be implemented at the physical layer. This solution obtains the best performance in terms of decoding capability but it has zapping and service access times higher than those expected with NGH standards. The class 2 interleaver is a good compromise between robustness and zapping time. The interleaver added with MPE-IFEC on top of class 1 physical interleaver is less performing but it allows lower zapping and service access time. The class 1 interleaver is a good compromise between zapping time and implementation easiness. The use of a return channel may improve the performance of this solution as well in a compromise to be done with the additional use of the forward link it will trigger.

### 3.2.1 Physical interleaver description

On the physical layer, four families of time interleavers have been analyzed in DVB-SH standard: the short uniform, the long uniform, the long uniform late and the long early late.

- The short uniform: the SH frame is not divided, it is sent in one time.
- The long uniform: the SH frame is divided as much as possible and sent during a long time.
- The long uniform late: the SH frame is divided in 2, the first half is sent and the other one is re-divided in small piece and sent during the rest of the time.
- The long early late is only divided in two parts and sent in a long time.

Figure 16 below illustrates their typical behavior on a satellite transmission channel.

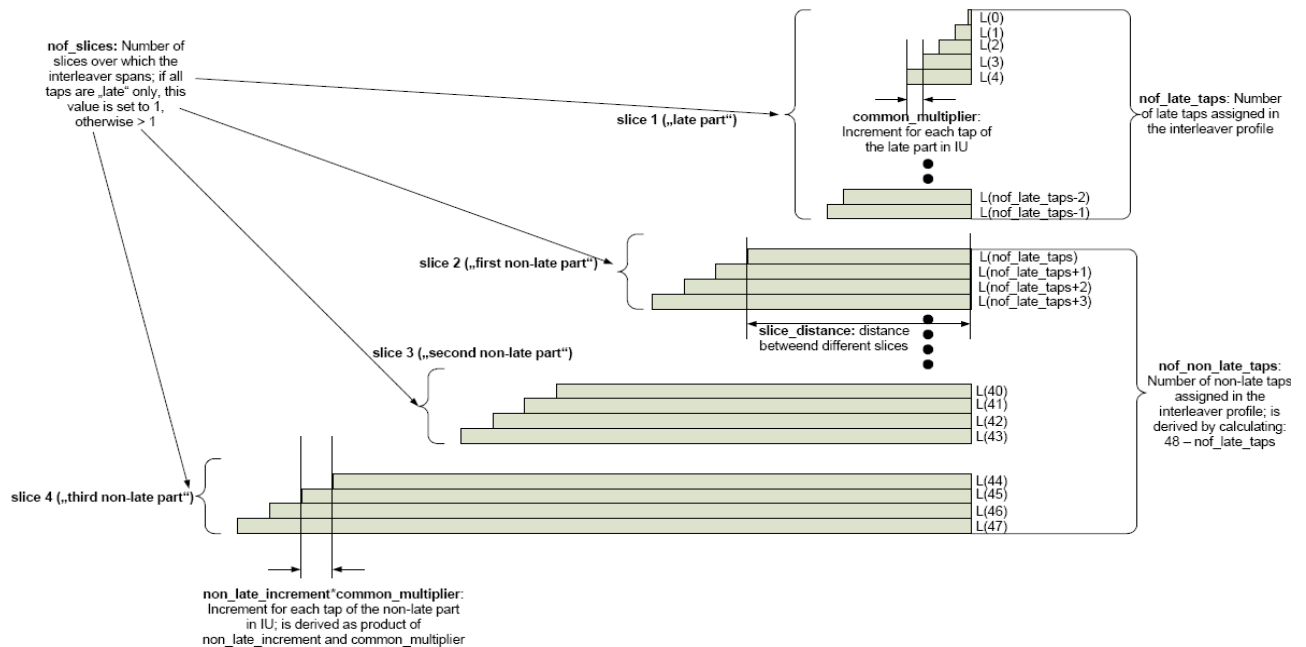


Figure 15: All the parameters for the time interleaver (from DVB-SH standard).

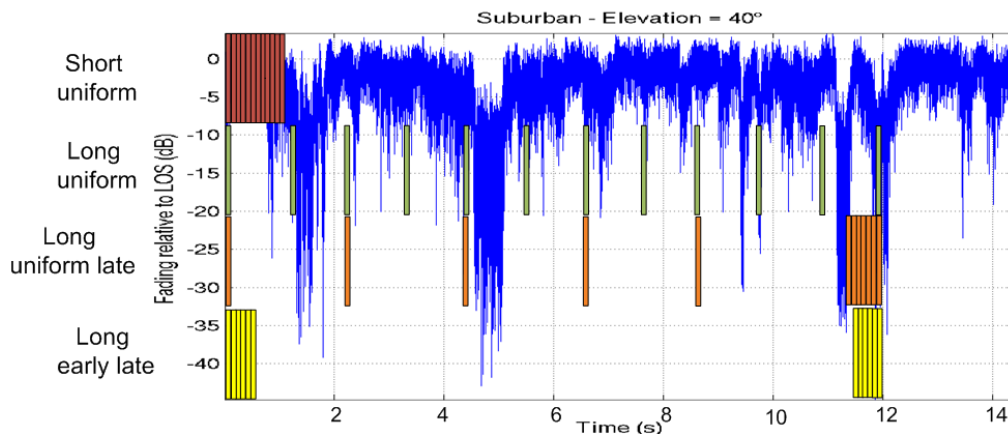


Figure 16: The 4 different families of time interleaver.

The short uniform is the best one for the zapping time. In fact, the receivers will capture faster a big amount of information than for the other temporal interleavers. The long uniform is the best against the shadowing effect. The long uniform late is the best compromise for a good zapping time and against long shadowing.

### 3.2.2 Link layer interleaver description

On the link layer, the MPE-IFEC (Multi Protocol Encapsulation- Inter Burst FEC) framework was defined to implement both erasure coding and interleaving on the link layer and is used to improve the reception when the protection level of the physical layer is not sufficient. This mechanism is described in the DVB-SH implementation guidelines [7], in Section 6.2. The principle is to use several coding windows (called ADT: Application Data Table) filled with several parts of different data bursts to build redundancy packets which are sent along with the data.

For MPE-IFEC, a datagram burst is made of one or several consecutives datagrams of the network layer (for example IP packets). The number of datagram in a burst can vary on burst by burst basis. Indeed, the principle is that the datagram burst has to contain the data corresponding to a constant duration of the video and the video can have a variable data rate. The MPE-IFEC burst is build by the addition of the redundancy created by the MPE-IFEC mechanism and the datagram burst. When MPE-IFEC is not used, the datagram burst is directly transmitted to the physical layer and the data of a link layer burst are sent during a physical layer burst.

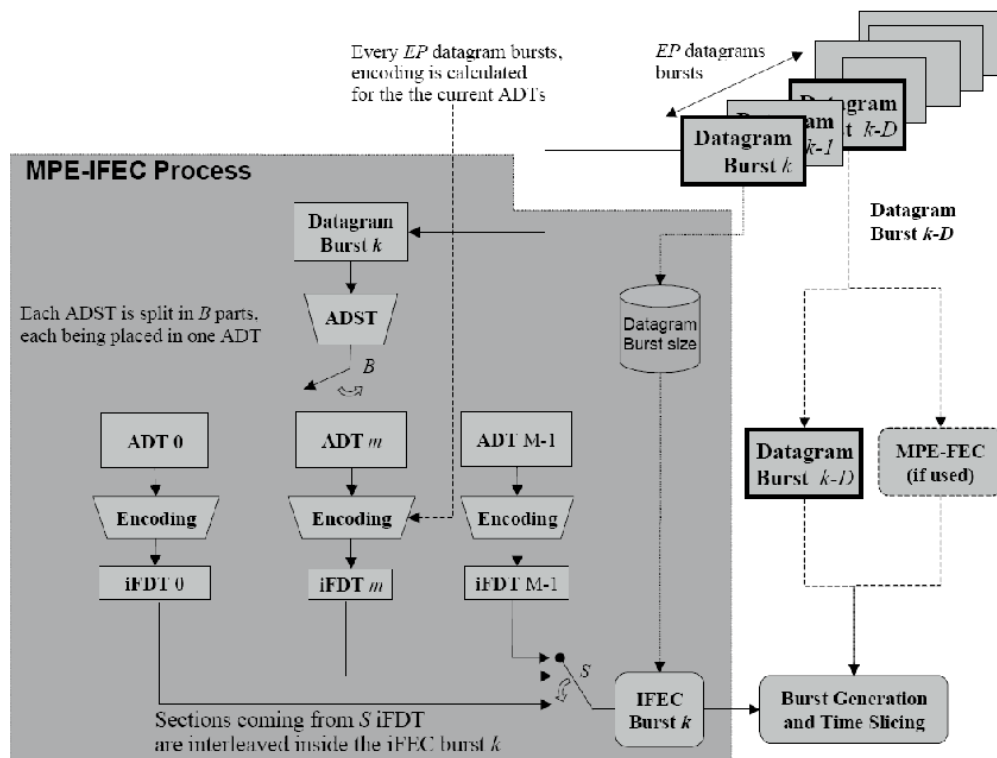


Figure 17: Overview of the MPE-IFEC process.

The different parameters of the MPE-IFEC mechanisms are:

- $B$  is the number of ADT to spread the data burst
- $M$  is the number of ADT in the system
- $S$  is the number of iFDT used to build a redundancy burst (a redundancy burst is build by the collection of the redundancy packet sent in a complete MPE-IFEC burst)
- $D$  is the delay introduced on the data packet transmission
- $EP$  is the encoding period

The MPE-IFEC mechanism will perform the following operations for each burst reception:

- The burst is spread over the  $B$  active ADT packet by packet,
- The encoding operation is performed when the ADT is completed,
- The redundancy packet are stored in the iFDT table corresponding to the active ADT,
- The redundancy burst is build using the redundancy packets from the previous  $S$  iFDT packet by packet,
- The MPE-IFEC is then composed by the data burst and the redundancy burst and the ADT are shifted.

Finally the decoding process is made as soon as possible (early decoding); it is needed to receive a sufficient number of redundancy packets to compensate the data packets losses.

### 3.2.3 ESR5 criteria

Definition is taken for DVB-SH implementation guidelines [7], in Annex A. It is important to distinguish the ESR5 criterion from the ESR5(20) ratio. Literal and mathematic definitions are given hereafter.

- ESR5(20) is the ratio of time windows for which ESR5 is fulfilled, over the total number of time windows.
- ESR5 criterion is fulfilled when in a time interval of 20 seconds there is at most one second in error.

The exact formulation of the ERS5(20) ratio is:

$$ESR5(20) = 1 - \frac{\sum_{w=1}^{N_w} \text{ceil} \left\{ \frac{\max[0; n\_of\_erroneous\_seconds(w) - 1]}{20} \right\}}{N_w},$$

where we assumed an individual observation window size of 20 seconds.

- $N_w$  represents the number of observation windows,
- $n\_of\_erroneous\_seconds(w)$  is the number of erroneous seconds in the window  $w$ ,
- The ceil function round the specified number up, and return the smallest number that is greater than or equal to the specified number.



The previous formula needs to be adapted to the type of measurements possible within the receiver:

- It is very important that ESR5(20) statistics are obtained over a long enough measurement time in particular at low mobile speed,
  - The  $N_w$  20 s windows used for the measurement may be disjoint or overlapped.
- When a burst is sent every second, ESR5(20) will be computed with 20s delay window:

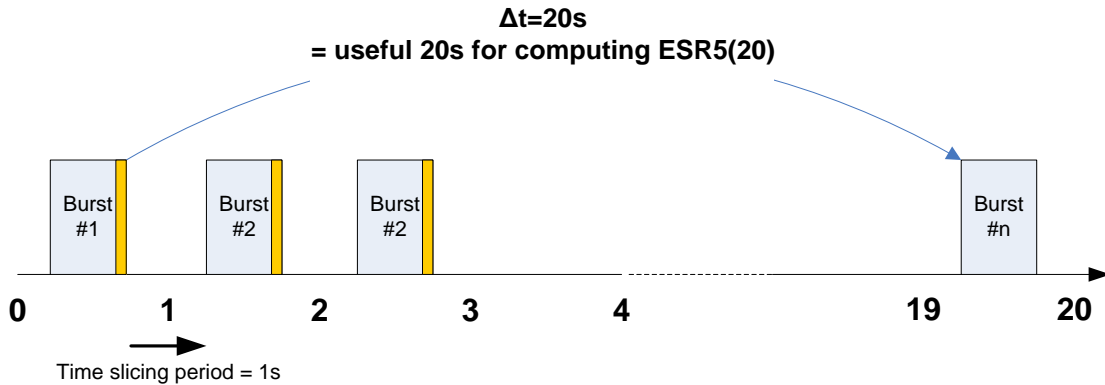


Figure 18: Computation of ESR5(20) for a 1s time slicing.

- When a burst is sent every 2 seconds, ESR5(20) will be computed with real time 40s delay window (but useful 20s window):

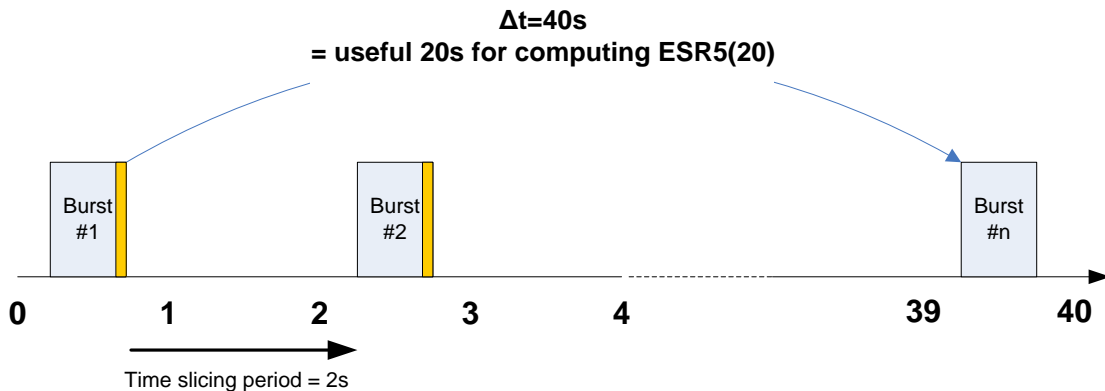


Figure 19: Computation of ESR5(20) for a 2s time slicing.

### 3.2.4 Which interleaver is the most suitable for Satellite transmission

Three main criteria can be considered to choose the most suitable interleaver for satellite transmission:

- performances,
- zapping time,
- Memory requirements on the receiver side.

In this paragraph, we present the results of the comparison of the first criteria “Performances”. Simulations have been done in the DVB-SH framework in order to compare the performance of the different solutions. Simulations are done with short uniform (identified as S), long uniform (identified as U) and uniform late (identified as UL).

The characteristics of the physical layer are: OFDM, Mode of 2K, Guard Interval of  $\frac{1}{4}$  and Bandwidth of 5 MHz. The modulation used is QPSK and Coding rate of  $\frac{1}{3}$ . The channel model is Land Mobile Satellite (LMS) channel at a speed of 50km/h. Different Interleaver lengths are simulated:

- - For the long Uniform: 11 s, (40, 0, 12 4, 2)
- - For the Uniform Late: 10 s, (10, 24, 9, 5, 12)
- - For the Short Uniform: 211 ms, (5, 48, 1, 0, 0)
- - For another Short Uniform: 86 ms, (2, 48, 1, 0, 0)

The different interleaving schemes are compared according to the ESR5 criterion.

### 3.2.4.1 Uniform and Uniform Late vs. Short interleavers in ITS LMS channel

The environment is Intermediate Tree Shadowing and the speed is of 50 km/h.

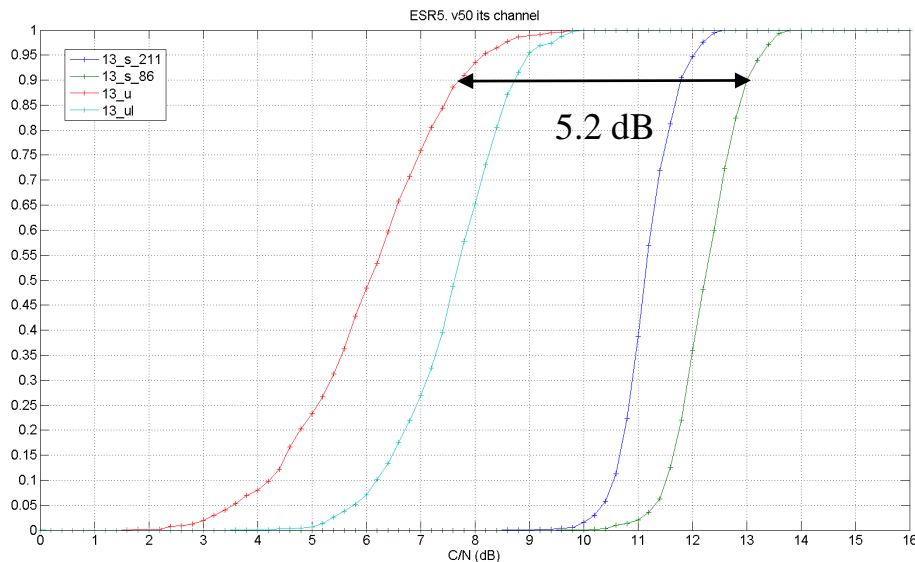


**Figure 20: Physical interleaver performance in ITS environment.**

These simulations results enable to verify the gain brought by the use of long interleaving: Long Uniform interleaver (U) outperforms Short interleaver (s\_211ms) as about 4 dB and the difference can reach 5.2 dB between the Long Uniform interleaver (U) of 11s and the Short interleaver of 86ms. Moreover, the Long Uniform interleaver (U) outperforms the Uniform Late interleaver (UL), but will have less zapping time performance.

### 3.2.4.2 Uniform and Uniform Late vs. Short interleavers in SUBURBAN LMS channel

The environment is Suburban and the speed is of 50 km/h. The satellite reception in suburban environment is easier than in the LMS-ITS environment.

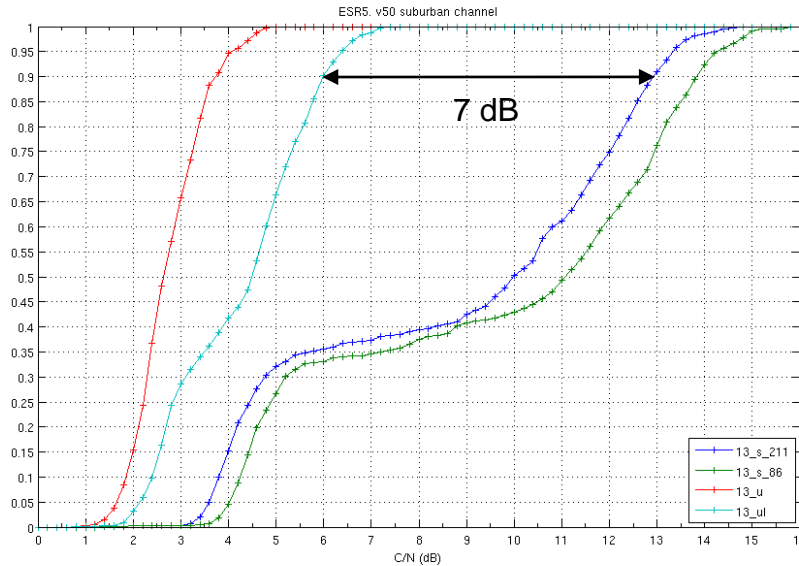


**Figure 21: Physical interleaver performance in suburban environment.**

Uniform Late interleaver (UL) outperforms Short interleaver (s\_211ms) as about 7 dB. The landing of the curves for short interleavers is due to the LMS channel in Suburban environment.

### 3.2.4.3 Short interleaving combined with upper Layer FEC in ITS environment

For link layer interleaver, the simulations are run using MPE-IFEC with the following characteristics:

- ⇒  $EP=1$ : Encoding process occurs at every burst,
- ⇒  $B=5$ : Encoding parallelization; the burst is split into  $B$  parts distributed over  $B$  parallel encoding matrices,
- ⇒  $S=5$ : Depth of the FEC spreading factor,
- ⇒  $B+S=10$ : give the number of bursts required to have complete information for the decoding of one given burst.
- ⇒ Code Rate is  $2/3$

In the simulations, one burst of the considered data stream is received every second.

The environment is the Intermediate Tree Shadowing for a speed of 50 km/h.

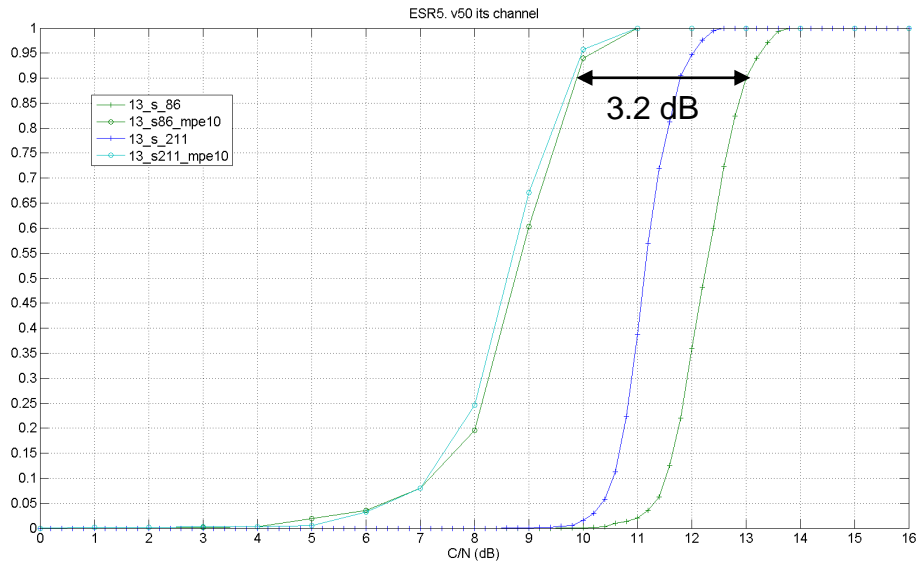


**Figure 22: MPE-iFEC added to short physical interleaver.**

The impact between the length of 86 ms or 211 ms of the short interleaver combined with the upper Layer FEC is reduced.

The upper layer FEC improves the performance of about 3.2dB of the short interleaver at the expense of spectrum efficiency.

### 3.2.4.4 Upper Layer FEC vs. Long time interleaver in ITS environment

The environment is Intermediate Tree Shadowing and the speed is of 50 km/h.

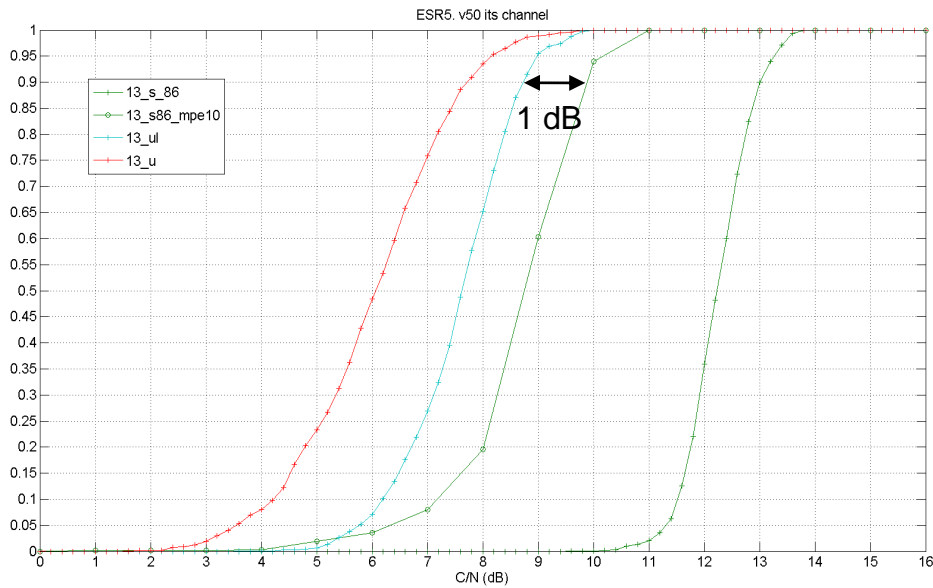


**Figure 23: Performance comparison between physical and link layer interleavers.**

In LMS-ITS channel, Upper layer FEC performance is close to Uniform Late time interleaver performance at the expense of spectrum efficiency.  $B+S$  can also be increased to improved MPE-IFEC performance.

### 3.2.4.5 Upper Layer FEC with higher $B+S$ value in ITS environment

For link layer interleaver, the simulations are run using MPE-IFEC with the following characteristics:

- ⇒  $EP=1$ : Encoding process occurs at every burst,
- ⇒  $B=5$ : Encoding parallelization ; the burst is split into B parts distributed over B parallel encoding matrices,
- ⇒  $S=5$ : Depth of the FEC spreading factor,
- ⇒  $B+S=20$ : give the number of bursts required to have complete information for the decoding of one given burst.
- ⇒ Code Rate is 2/3 for “13\_s211\_mpe20” and 1/2 for “12\_s211\_mpe20”.

In the simulations, one burst of the considered data stream is received every second.

The environment is Intermediate Tree Shadowing and the speed is of 50 km/h.

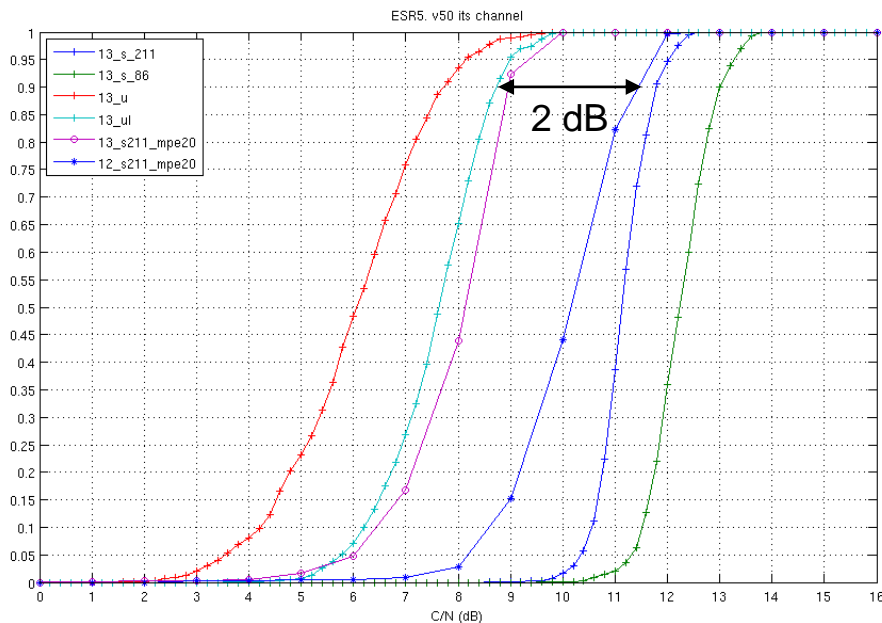


**Figure 24: Performance comparison between physical and link layer (with higher value of  $B+S$ ) interleavers.**

Uniform Late interleaver (“13\_ul”) outperforms MPE-IFEC (“12\_s211\_mpe20” curve) by only 2 dB with the same spectrum efficiency (overall code rate of 1/3).

The two solutions achieve the same performance at the cost of spectrum efficiency. Overall code rate is 2/9 for solution with FEC solution (“13\_s211\_mpe20” curve) and 1/3 for solution without FEC (“13\_ul” curve).

### 3.2.4.6 Analysis of the DVB-SH solutions

The simulations performed on the DVB-SH waveform, shows the interest of long interleaving by showing the important gain brought by this technology, and also its superiority in terms of performance in comparison to link layer solution MPE-IFEC.

Nevertheless, other criteria have to be taken into account for the selection, i.e. the zapping time performance of each solution and the constraints in term of complexity and memory.

### **3.2.5 Strategies for time interleaving and interleaving solutions retained in DVB-NGH standard**

In the DVB-NGH standard, the work has been focused on the physical layer solutions. The satellite profile includes the time interleaver options retained for the terrestrial profile, i.e. the concept of a combination of block and convolutional interleaver for inter frame interleaving. Block interleaver only can be used for intra frame interleaving. The working assumption is that the interleaver unit size is in this case equals to the FEC Frame divided by the number of the interleaved frame. Moreover, the need for long time interleaving is required in certain scenarios for the satellite; Convolution Interleaving with a Uniform Late profile is available for those contexts.

## 4 L1 SIGNALING IN THE SATELLITE CONTEXT

### 4.1 L1 Signaling for the Hybrid Profile

#### 4.1.1 Introduction

The sheer terrestrial profile in DVB-NGH has adopted three new mechanisms in order to enhance the robustness of the layer 1 (L1) signaling: 4K LDPC codes (mini-codes), Additional Parity (AP), and Incremental Redundancy (IR). These mechanisms are used in conjunction with the L1 repetition scheme from DVB-T2, being the use of In Band signaling optional in DVB-NGH.

The hybrid satellite-terrestrial profile of DVB-NGH is more robust than the sheer terrestrial profile, because it includes a more robust code rate for the data (i.e., 1/5 instead of 1/3), and the long-time interleaving feature.

The goal of this section is to investigate the feasibility of the new techniques for L1 signaling robustness for the hybrid profile. A summary of L1 signaling robustness in the sheer terrestrial is provided first. Then, the simulation performances and results are given.

#### 4.1.2 Summary of L1 Robustness in the Sheer Terrestrial NGH Profile

The physical layer signaling of DVB-T2 was designed such that it can always be made more robust than the data path. The transmission and detection of the preamble P1 symbol is very robust, and it can be correctly received even at negative signal-to-noise ratios (SNR) under mobility conditions. The transmission of the rest of the physical layer signaling in the P2 symbol(s) can be configured sufficiently robust in rather static reception conditions. However, in mobile reception conditions the robustness of the L1 signaling, in particular the L1-post field, may not be high enough due to the lack of time diversity.

DVB-NGH has enhanced the physical layer signaling of DVB-T2 in three different aspects:

- Improved transmission robustness.
- Reduced signaling overhead.
- Higher signaling capacity.

The improvement in the signaling robustness is especially relevant, because DVB-NGH adopts for the data path code rates more robust than in DVB-T2 (i.e., 1/3 for the sheer terrestrial profile, and 1/5 for the hybrid satellite-terrestrial profile). DVB-NGH adopts for L1 signaling new mini LDPC codes of size 4320 bits (4K) with a code rate 1/2. Although 4K LDPC codes have a worse performance than the 16K LDPC codes of size 16200 bits used in DVB-T2 for L1 signaling, the reduced size of the 4K LDPC codes is more suitable for the L1 signaling because it reduces the amount of shortening and puncturing. In DVB-T2, LDPC codewords with L1 are shortened (i.e., padded with zeros to fulfill the LDPC information codeword) and punctured (i.e., not all the generated parity bits are transmitted), which decreases the LDPC decoding performance.

The adopted 4K LDPC codes have the same parity check matrix structure than the 16K LDPC codes used for data protection. This allows for efficient implementations at the transmitter and receiver side efficiently

sharing the same logic. On the other hand, two mechanisms have been adopted in DVB-NGH to improve the robustness of the L1 signaling known as Incremental Redundancy (IR) and Additional Parity (AP). These two mechanisms are used as a complement of L1 repetition. The additional parity mechanism transmits punctured bits in the following frame. In case there is need for more parity bits, the incremental redundancy mechanism extends the original 4K LDPC code into an 8K LDPC code of 8640 bits. The overall code rate is thus reduced from 1/2 down to 1/4. L1 repetition can be used to further improve the robustness of the L1 signaling as a complement of AP and IR.

The robustness improvement of the L1 signaling in DVB-NGH can be translated into a reduction of the signaling overhead for the same coverage. But DVB-NGH has restructured the L1 signaling structure of DVB-T2 in order to further reduce the signaling overhead. Instead of signaling the configuration of each PLP (MODCOD, TI, modulation, code rate, and time interleaving configuration), PLPs are associated in groups with the same settings, reducing the required L1 signaling information. Furthermore, it is possible to split in several frames signaling parameters which are in practice static, and which are transmitted in DVB-T2 in every frame.

DVB-NGH has also increased the signaling capacity. A new signaling L1 PLP has been defined for the L1-post information. The signaling L1 PLP is transmitted at the beginning of the frame and can be transmitted outside the P2 symbols in data OFDM symbols.

### **4.1.3 The physical layer signaling in the Hybrid NGH Profile**

The satellite component of DVB-NGH is optional. The satellite profile of DVB-NGH has been designed with the goal of keeping the maximal commonality with the terrestrial component to ease its implementation at the receiver side.

For the hybrid profile of DVB-NGH, an additional preamble P1 (aP1) symbol has been introduced in order to increase the signaling capacity of the P1 symbol. The P1 symbol signals the presence of the aP1 symbol. The aP1 symbol is only transmitted for hybrid terrestrial-satellite DVB-NGH networks, such that it is not transmitted if it is not needed.

In the Hybrid profile study, the main objective of the study was to check if there was any issue to solve concerning the robustness of L1 signaling in the Satellite path and to suggest the extra tools needed to be added. The studies showed that the available L1 signaling robustness tools in the Terrestrial profile were sufficient to meet the requirements in the Satellite path, but with some configuration of Additional Parity (AP2) L1-dyn repetition is needed. In addition, with AP3 configuration the robustness of L1 signaling is enough to get better performance than data. As a conclusion, the tools assumed for the Terrestrial profile (4k, AP/IR and Fabric decoding) in conjunction with L1-dyn repetition are enough sufficient to meet the requirements in the Satellite path.

### **4.1.4 Performance of L1 Robustness in the Hybrid NGH Profile**

The following results were presented by Samsung at the DVB-Forum [21] and [22]. Samsung assessed the performance shown in these results with the tools adopted for the Terrestrial profile in the LMS channel.

In the Terrestrial profile, 4k PF72 codes were adopted for the NGH baseline after an exhaustive performance assessment with AP/IR over TU 6 channel [23], where the L1 signaling coding with AP was demonstrated to provide better performance than data performance (16k; 1/3, 100ms TI) and, therefore, solved the robustness issue of L1 signaling.



In the Hybrid profile study, the main objective of the study was to check if there was any issue to solve concerning the robustness of L1 signaling in the Satellite path and to suggest the extra tools needed to be added.

Samsung evidenced that the tools assumed for the Terrestrial profile (4k, AP/IR and Fabrice decoding) were not enough. The L1 signaling in the Hybrid profile with the Terrestrial tools lacked of robustness if compared to data (CR1/5, QPSK). In order to overcome this lack of robustness, Samsung suggested using the L1-dyn repetition strategy from DVB-T2 with some combinations of Additional Parity (AP2) and without L1-dynamic repetition AP3.

Finally, Samsung’s report showed that the available L1 signaling robustness tools in the Terrestrial profile were sufficient to meet the requirements in the Satellite path. Therefore, no extra tools were found necessary to be added.

Next results were presented in [22] by Samsung. The following tables summarize the simulation conditions used:

Parameter	Value
LMS Channel Model	Perez-Fontan3 state statistical model
Center Frequency	2.2 GHz
Elevation	40 degree
Receiver Speed	60 km/h
Receiver Environment	SU (Sub-Urban)

	Parameter	Value
<b>OFDM</b>	FFT Size	2048
	BW	8MHz
	GI	¼
	PP	PP1
	FEF + T2 frame	300ms
<b>Data</b> (for reference point)	MODCOD	QPSK, CR =1/5, 1/3
	Time Interleaver	100ms, Type 1 PLP
	QEF FER	10 <sup>-5</sup>
	Decoding	50 iterations, LLR : MAX_LOG

	Parameter		Value	
<b>L1 Signaling</b>	Number of PLPs, N		1, 4, 8,16, 32	
	L1 Post (Config+Dyn)	QEF FER		10 <sup>-4</sup>
		Length	Joint Encoding	136 + 89N + 79 + 48N + 32 (CRC)

MODCOD	Constellation	BPSK
	Coding	4K CR=1/2 with IR (BCH parity= 60, t=5)
	Decoding	50 iterations, LLR: MAX_LOG w/or w/o Fabrice's proposal if possible w/o repetition

Code rate achieved with Additional Parity:

PLP	FEC Block	Ksig bits	BCH bits	AP0		AP1		AP2		AP3	
				Par. bits	L1 Post Eff_Rate	Par. bits	L1 Post Eff_Rate	Par. bits	L1 Post Eff_Rate	Par. bits	L1 Post Eff_Rate
1	1	384	60	894	0.287	1206	0.232	1518	0.2	1830	0.17
4	1	795	60	1427	0.287	1926	0.232	2425	0.21	2925	0.18
8	1	1343	60	2139	0.287	2887	0.232	3636	0.27	4384	0.19
16	2	1220	60	1979	0.287	2671	0.232	3364	0.26	4056	0.19
32	3	1544	60	2410	0.287	3253	0.232	4097	0.27	4940	0.2

Eight PLPs have been taken into account as an example of the L1 signaling in the Satellite path. As it can be seen on Figure 25 and Figure 26, there is a lack of robustness compared to the most robust data method (CR1/5, QPSK). It is observed that Fabrice Decoder gives a gain of 2-3.0dB.

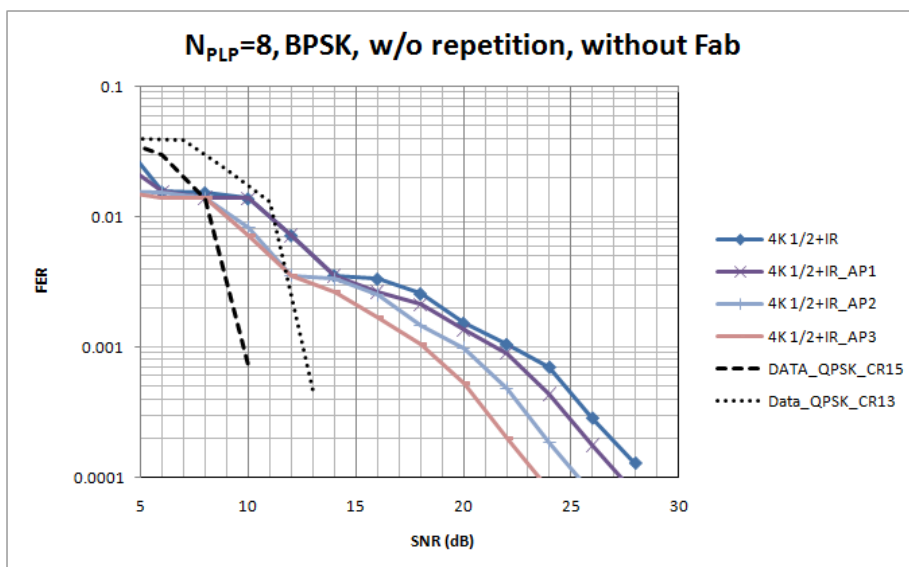
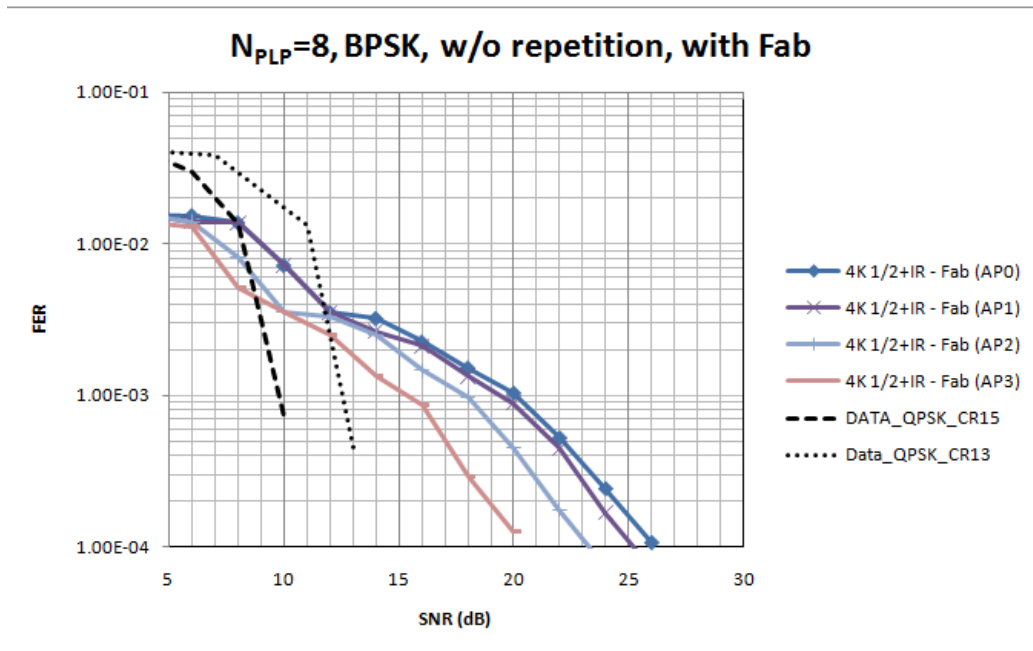


Figure 25: L1 signaling Performance over LMS Channel (NPLP = 8, without Rep and Fabrice Decoding).



**Figure 26: L1 signaling Performance over LMS Channel (NPLP = 8, without Rep and with Fabrice Decoding).**

Figure 25 shows the L1 signaling performance with 8 PLPs without using Fabrice decoding. The most robust mode AP3 has a gain of 2.0dB. Figure 26 shows the L1 signaling performance in case of using Fabrice decoding. AP1 has a gain of 3.0dB. The results considered the FER metric (vs. SNR) and show that FER performance of L1 signaling with AP does not meet the requirement to ensure better performance than data in the Satellite path.

The following results were presented in [21] by Samsung, where they suggested using the L1-dyn repetition from DVB-T2 to overcome this lack of robustness. Using of ESR5 metric instead of FER as the former was more relevant to assess the robustness in the Satellite path. The simulation conditions used throughout these results were the same used at [22].

L1 Signaling Performance over LMS (@ ESR5(20) = 90%)			
	Repetition, Additional Parity Gain	Robustness Compared to Data (R1/5, TI=200ms)	
AP0	L1-dyn gains of 2.7~3.2 dB	w/o Rep:	Not sufficient
	-	w/ Rep	Not sufficient
AP1	L1-dyn gains of 2.7~3.2 dB	w/o Rep:	Not sufficient
	AP1 gain compared to AP0 is 0.7~2.1 dB	w/ Rep	Not sufficient
AP2	L1-dyn gains of 2.7~3.2 dB	w/o Rep:	Not sufficient
	AP2 gain compared to AP0 is 1.5~4.2 dB	w/ Rep	<b>Sufficient</b>
AP3	L1-dyn gains of 2.7~3.2 dB	w/o Rep:	<b>Sufficient</b>
	AP3 gain compared to AP0 is 2.5~4.7 dB	w/ Rep	<b>Sufficient</b>

The following figures show the L1 signaling outperformance using ESR5(20) metric over LMS channel for the Satellite path. These figures are those which its combination of L1-dyn rep and AP are enough to get better performance than data.

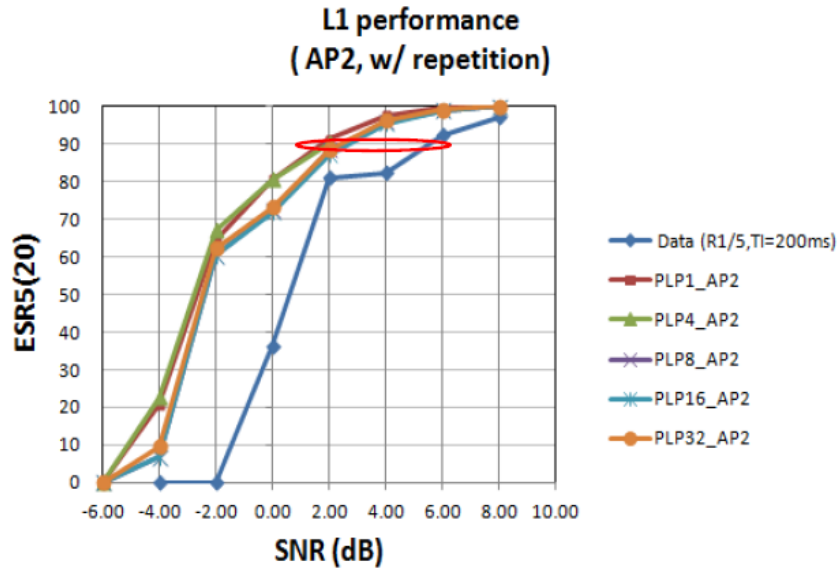


Figure 27: L1 signaling Performance over LMS Channel (AP2 with Rep and with Fabrice Decoding).

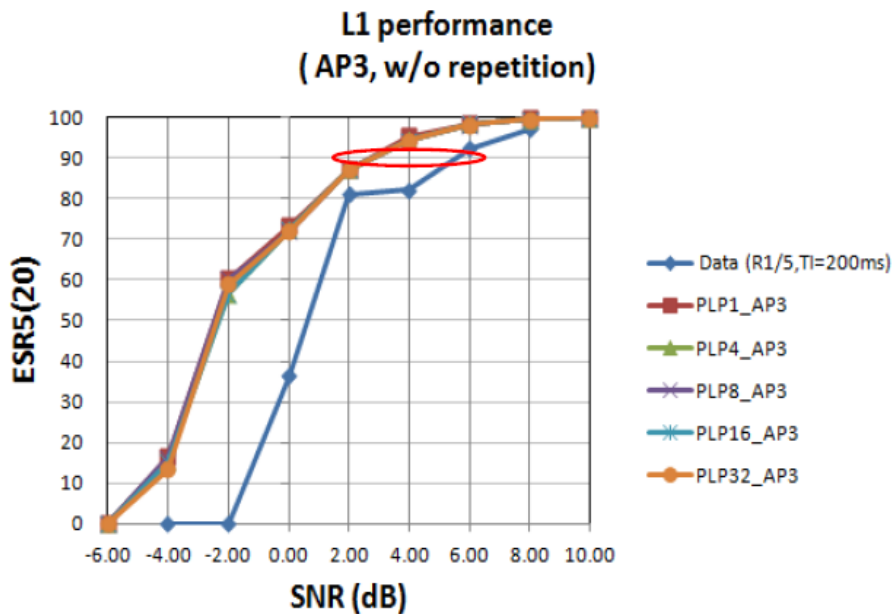
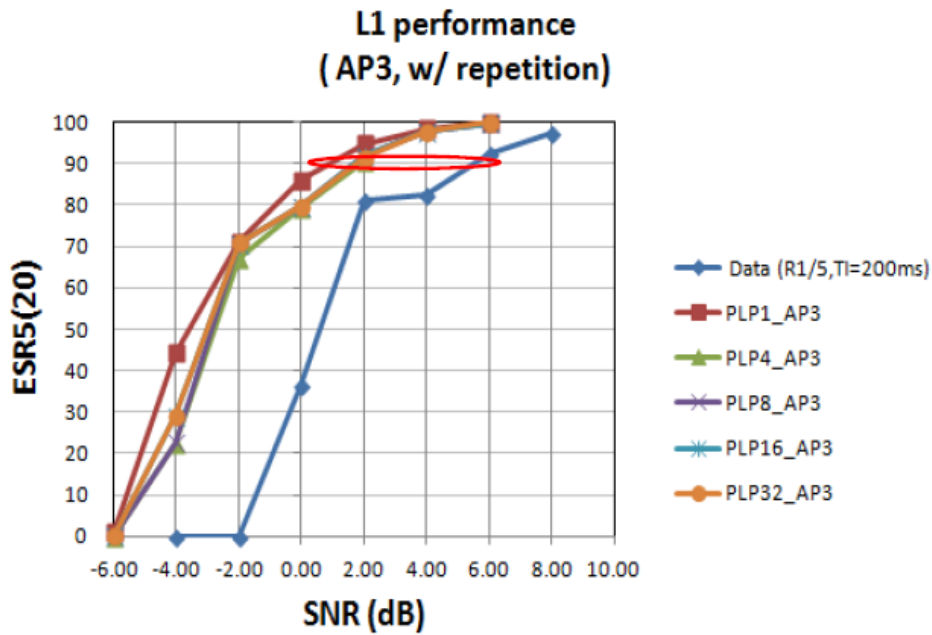


Figure 28: L1 signaling Performance over LMS Channel (AP3 without Rep and with Fabrice Decoding).



**Figure 29: L1 signaling Performance over LMS Channel  
(AP3 with Rep and with Fabrice Decoding).**

### 4.1.5 Conclusion

This section shows that the mechanisms devised in the Terrestrial profile to improve for L1 signaling robustness are sufficient to meet the requirements of the Satellite path, but with some configurations of Additional Parity (AP2) L1-dyn repetition is needed. In addition, with AP3 configuration, the robustness of L1 signaling is enough to get better performance than data. As a conclusion, the mechanisms assumed for the Terrestrial profile (4k, AP/IR and Fabrice decoding) in conjunction with L1-dyn repetition meet the requirements of the Satellite path.

## 4.2 Robust Layer 1 Signaling schemes

### 4.2.1 Introduction

#### *Focusing study on L1-post field:*

From 2010 to end of year 2011, the NGH standardization process has shown that L1-post signaling detection was a critical problem especially for mobile channels. Indeed, detection of L1-post enables localizing PLPs into the NGH frame; that is to say if the L1 post field is not correctly decoded, all PLP data will be lost. Reader shall note that information included in L1-pre fields, while being mandatory for correct reception of PLPs, may not usually change, except in case of network reassignment. Besides, the location of PLPs, included in L1 post field, may change (for a worst case) each frame. This is the reason why this section focuses only on L1 post detection field.

#### *Positioning work into standardization process:*

During the standardization process, some contributors of the NGH standard have proposed different solutions to deal with L1 post detection problems. CNES has particularly focalized on the evolution of the dealings, because discussions about the need to improve L1 might not have taken into account the specificity of the Land Mobile Satellite (LMS) channel. One Samsung contribution (NGH 755) has particularly caught the attention, offering both better robustness of the single decoding process and adjustable time diversity. By the time refinements and dealings with the NGH standardization group have lead to a slightly less robust solution (NGH 1319), while being close to the first contribution.

Because robustness of the highly punctured LDPC code was strongly decreased, especially in case of few PLP, it has been decided to work during summer 2011 on a solution closed to NGH 755 contribution. Main difference was about the amount of additional parity which would become a fix part, preventing from LDPC code capacity-nil correction. This solution aimed not to become the definitive solution, but to demonstrate that there were some configurations allowing L1 post detection in a satellite mobile environment. Thus, the conducted analysis consisted on running simulations to verify if additional parity solution was robust enough in the context of the LMS channel environment.

### 4.2.2 Study description: Additional Parity like

This section details the studied L1 post encoding improvement solution.

#### 4.2.2.1 L1 field

In DVB-T2, L1 signalization field is located in the P2 symbols of T2 frame.

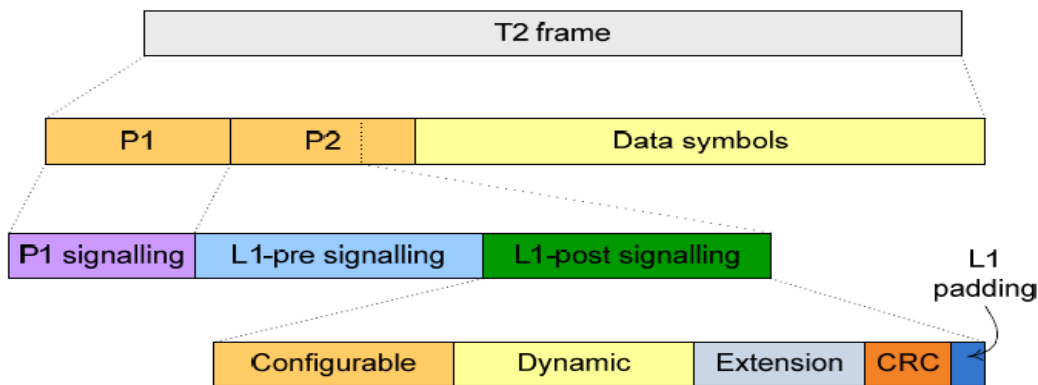


**Figure 30: DVB-T2 L1-post signaling framing.**

From an OFDM waveform point of view, L1 post cells are mapped as seen in the below figure.

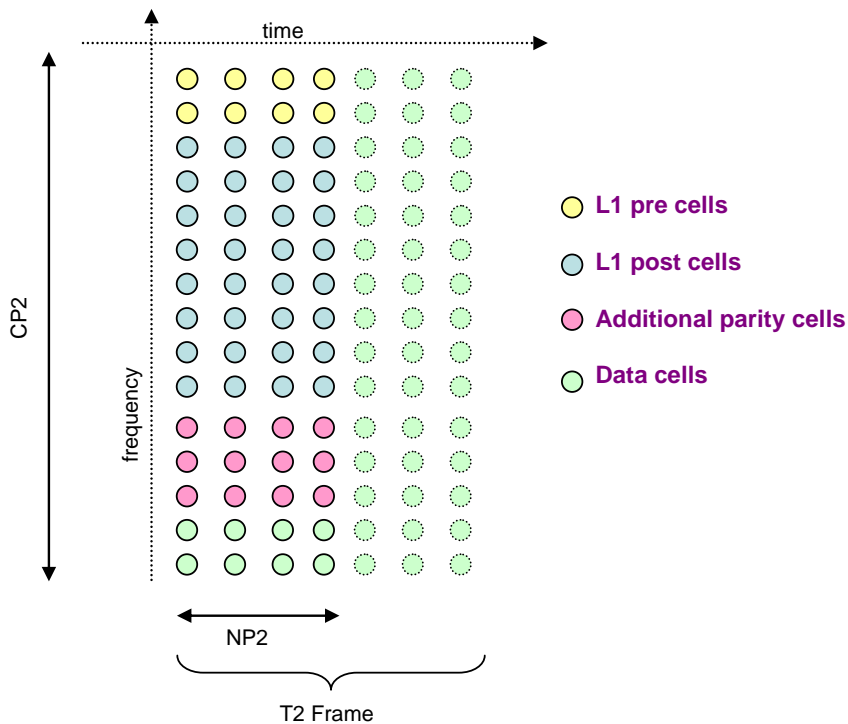


**Figure 31: L1 cells disposition in the OFDM stream. Additional parity cells are an additional feature of NGH standard.**

Size of L1 field is PLP number dependant. Here is briefly reminded the L1 size computation in DVB-T2.

- L1 pre number of bits :  $168 + 32 \text{ (CRC)} = 200$  bits
- L1 post :  $213 + 137 \times \text{Num\_PLP}$  bits
  - o L1 post config :  $102 + 89 \times \text{Num\_PLP}$  bits
  - o L1 post dynamic :  $79 + 48 \times \text{NumPLP}$  bits
  - o 32 CRC bits

To implement additional parity scheme, new fields have to be defined in order to localize and quantize new additional parity bits. Besides, new fields are taken from Samsung NGH 755 contribution. Taking into account these new fields, L1 post size calculation with new robustness solution becomes:

- Having a look only on new fields :
  - o  $(L1\_AP\_Start + L1\_NUM\_AP\_blocks) + (L1\_AP\_lenght + L1\_AP\_Frame\_pointer + L1\_AP\_RSV) \times NumPLP$
  - o 20 + 12 × NumPLP
- Total L1 post size calculation
  - o 233 + 149 × Num\_PLP bits

**Table 22: L1 post size in DVB-T2 and NGH standard.**

PLP number	DVB-T2	NGH with AP
1	350	382
2	487	531
10	1583	1723
16	2405	2617
32	4597	5001

The table above, which summarizes the L1 field size, let us understand that for a same coding rate, fulfillment of the DVB-T2 LDPC would be totally non equal, depending on the number of PLPs.

#### 4.2.2.2 L1 encoding solution with additional parity

L1 basic encoding process is strictly taken from DVB-T2 specifications. At the date of this chapter drafting, LDPC 4K codes have been approved. Nevertheless, the study has been done considering 16K codes to assess the effect of the fulfillment of the code and additional parity (4K codes were not definitely approved when the study began).

Steps of the L1 post encoding:

- (1) BCH block code is zero padded in complement to L1 post to fulfill BCH input.
- (2) Zero padded data + BCH parity bits are encoded with LDPC.
- (3) LDPC parity is punctured according to the size of L1 post.
- (4) In DVB-T2, only L1 post, BCH\_FEC and remaining LDPC parity bits are sent.

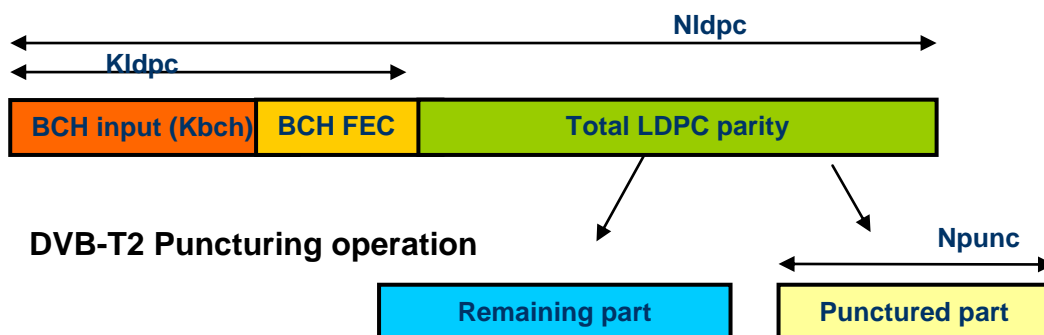


**Figure 32: Puncturing of the LDPC.**



From step (4), additional parity is then applied. Total LDPC parity is sorted in a circular buffer starting with punctured bits, and then Additional Parity vector is built by parsing circular buffer. By this, robustness is first reached by taking better performance of the LDPC code before sending parity bits sent yet.

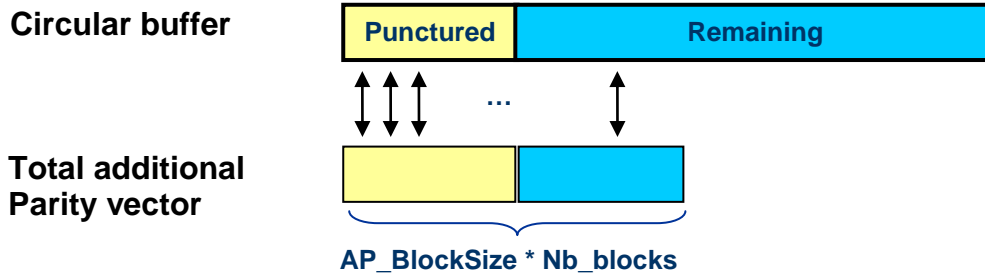


**Figure 33: Additional parity vector building.**

Total size of Additional parity vector is arbitrary called  $AP\_BlockSize \times Nb\_blocks$ , names being directly linked to the additional parity mapping scheme (as seen later in the section).

Independently from the number of PLPs, keeping additional parity size as a fixed value was chosen. This solution may provide:

- Very low Coding Rates with few PLP when there is a need to make more robust the LDPC code,
- Higher Coding Rates when there is just a time diversity need.

Additional parity size is then fixed to the total LDPC parity size ( $N_{LDPC} - K_{LDPC}$ ). Equivalent Coding Rate is computed as:

$$CR = \frac{L1_{post}(Nb\_PLP)}{L1_{post}(Nb\_PLP) + BCH\_parity + LDPC\_remaining\_bits(Nb\_PLP) + Total\_AP\_bits}$$

- L1post: size of the field to encode (including CRC)
- BCH parity: 168 bits
- LDPC remaining bits: LDPC parity bits which are sent
- Total AP bits: total amount of Additional parity bits, equal in our case to total parity size (before puncturing) ~ 9000 bits

To bring time diversity, it may be suitable to spread the total Additional Parity in several blocks, as depicted below. The new fields defined by NGH standard for signaling additional Parity are consequently explained: Additional parity blocks have to be localized.

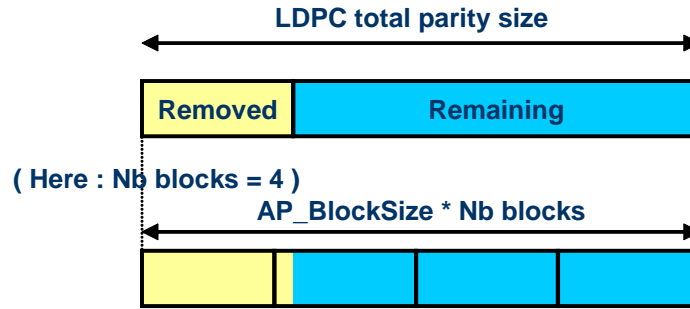
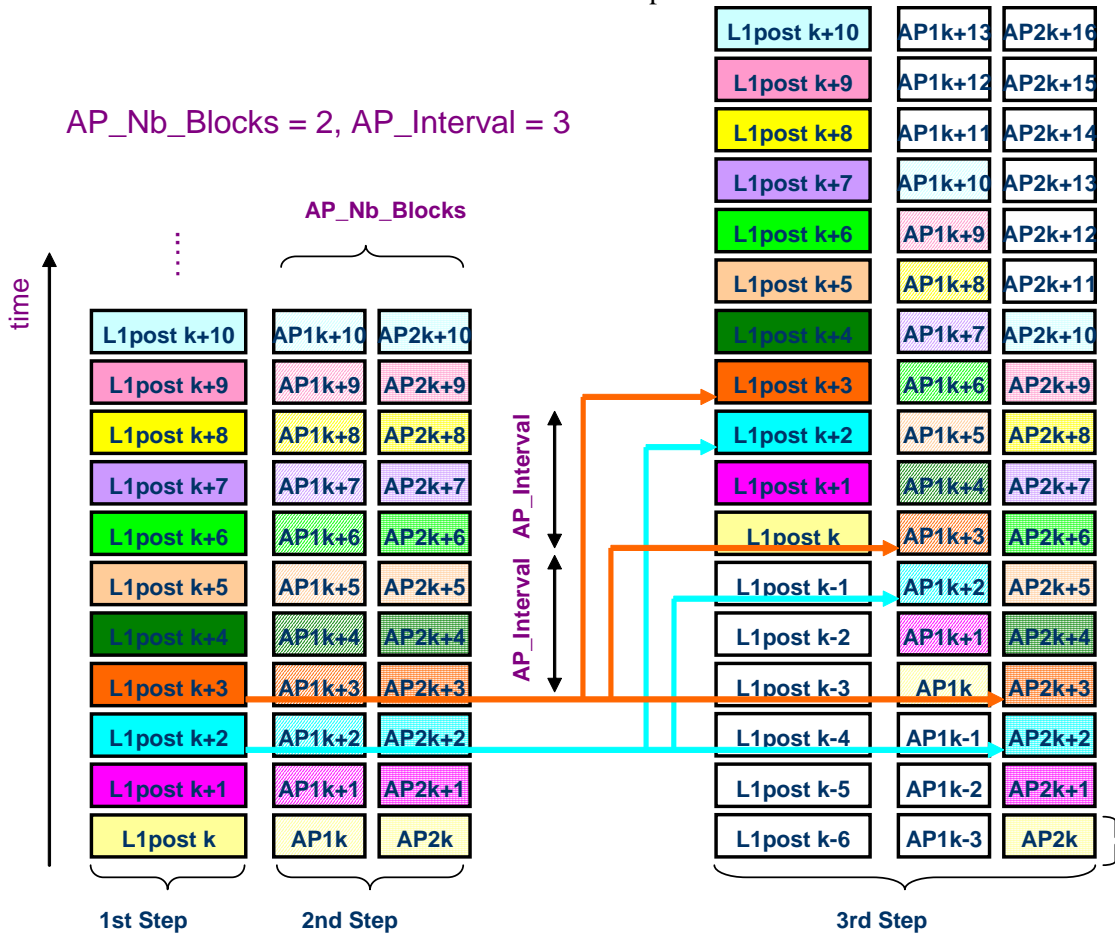


**Figure 34: Total additional parity bits splitting.**

For each frame, additional Parity blocks linked to this frame are mapped in previous frames as the following figure; example is given for additional Number of blocks equals to 2, and additional parity frame interval equals to 3.

Lastly, native L1 post is transmitted synchronously with Additional Parity blocks relative to other frames. Reader shall note Additional Parity blocks corresponding to different frames are transmitted in the same P2 field.

Once bits encoded, they are grouped and mapped into QPSK symbols into the OFDM cells, according to the DVB-T2 specifications. Note that  $L1\text{ pre} + L1\text{ post} + \text{Additional parity cells}$  should be less than  $[CP2] \times [NP2]$  (T2 specification parameters).



- 1st Step : L1 post native encoding is buffered
- 2nd Step : Additional Parity blocks are computed and buffered
- 3rd Step : AP blocks are transmitted in advance, every AP\_interval frames

Figure 35: Example of realization.

## 4.2.3 Simulations results

### 4.2.3.1 Software device

L1 encoding simulations have been carried out using a C-ANSI simulator, compliant with DVB-T2 specifications. According to the previous section, Additional Parity algorithm (encoding and spreading) is implemented.

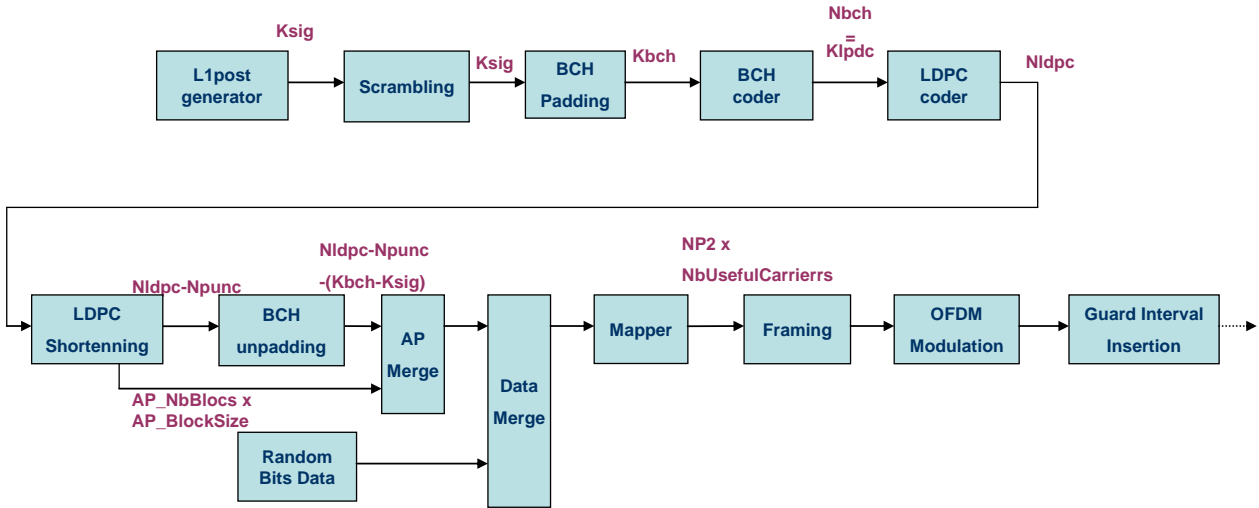


Figure 36: L1 encoding + AP transmitter architecture.

### 4.2.3.2 Validation

Validation of the software was done according to Nokia/Samsung simulations [24] when the LDPC code is very low punctured. Other curves (1 or 5 PLP) are not plotted, but they converge at higher C/N.

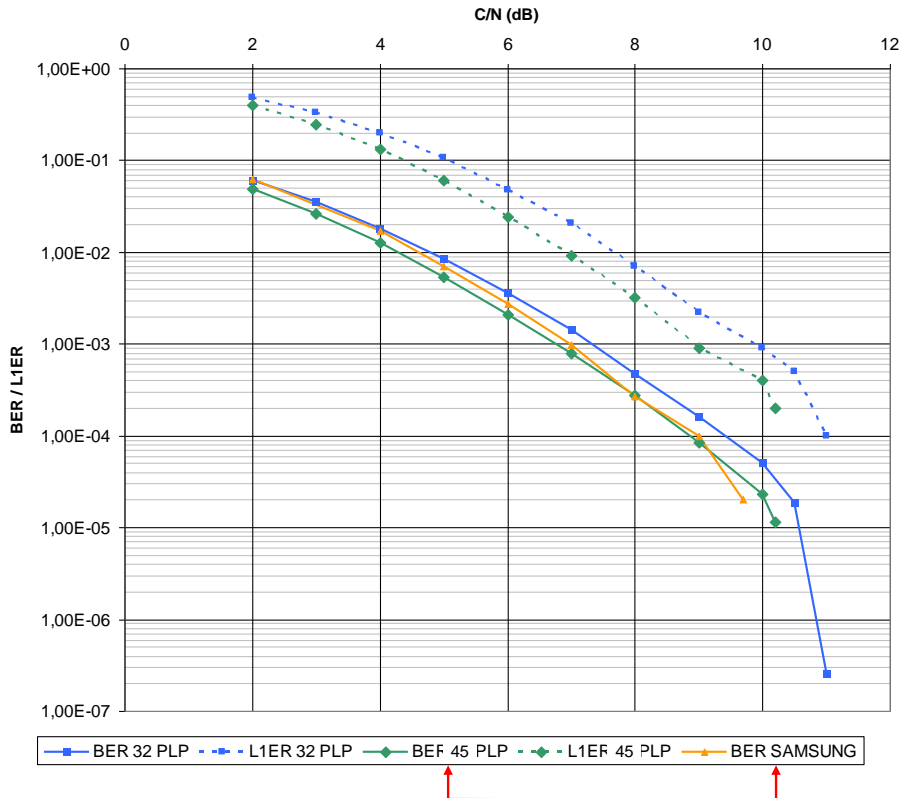


Figure 37: Validation curve of the chain.

Simulations have been run in TU6 channel, with 80 Hz Doppler, on a QPSK  $\frac{1}{2}$  modulation under 8 MHz bandwidth. About OFDM parameters,  $\frac{1}{4}$  guard interval ratio was chosen associated with 8k FFT mode. Frame periodicity was set to 0.25s. Additional parity block was bypassed.

### 4.2.3.3 Simulations Hypothesis

Hypotheses are given hereafter.

Channel	LMS ITS Channel with 40° elevation, 60 Km/h
ModCod	QPSK $\frac{1}{2}$ , LDPC 16K
Bandwidth, OFDM	BW = 5 MHz, FFT 2k, Guard Interval 1/8
NGH Frame period	250 ms
Additional parity	5, 10, 20 Frame interval

About the NGH framing, reader shall note that there is only NGH frame in the stream, because only satellite link is considered in this study.

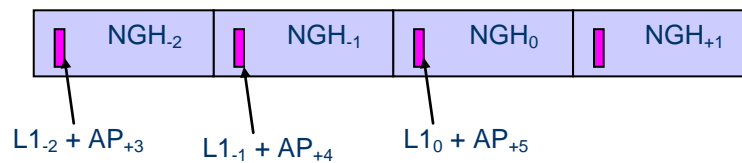


**Figure 38: Framing for the study: only NGH frames.**

On the below table, summary of Additional Parity parameters are given. Note that different parameters on Nb\_AP\_cells\_per\_block and Nb\_blocks, keep the same amount of additional parity, as explained in the previous section.

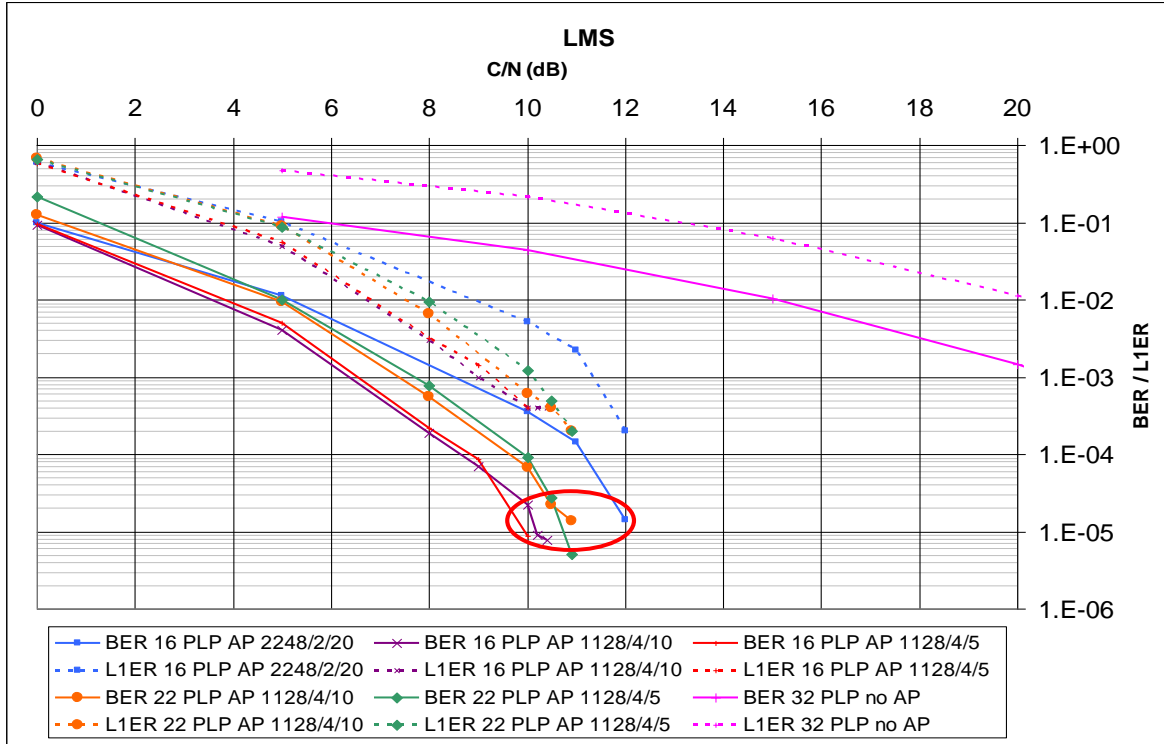
NbPLP	Nb AP cells per block	Nb blocks	Frame Interval	Interleaving length	Overhead on LDPC parity	Effective Coding Rate
16	2248	2	20	10 s	243.29%	0.169
16	1128	4	10	10 s	244.16%	0.169
16	1128	4	5	5 s	244.16%	0.169
22	1128	4	10	10 s	189.26%	0.201
22	1128	4	5	5 s	189.26%	0.201

The choice of these parameters would make it possible to deal with:

- The effect of the parity blocks spreading granularity.
- The interleaving duration.
- The Coding Rate.

Chosen configurations may appear oversized, but the aim of the study was to demonstrate that additional parity with spreading is a robust solution, despite small parameters changes.

#### 4.2.3.4 Results



Legend : number of PLP ; AP\_1block\_cell\_size /AP\_Nb\_Blocks/AP\_interval

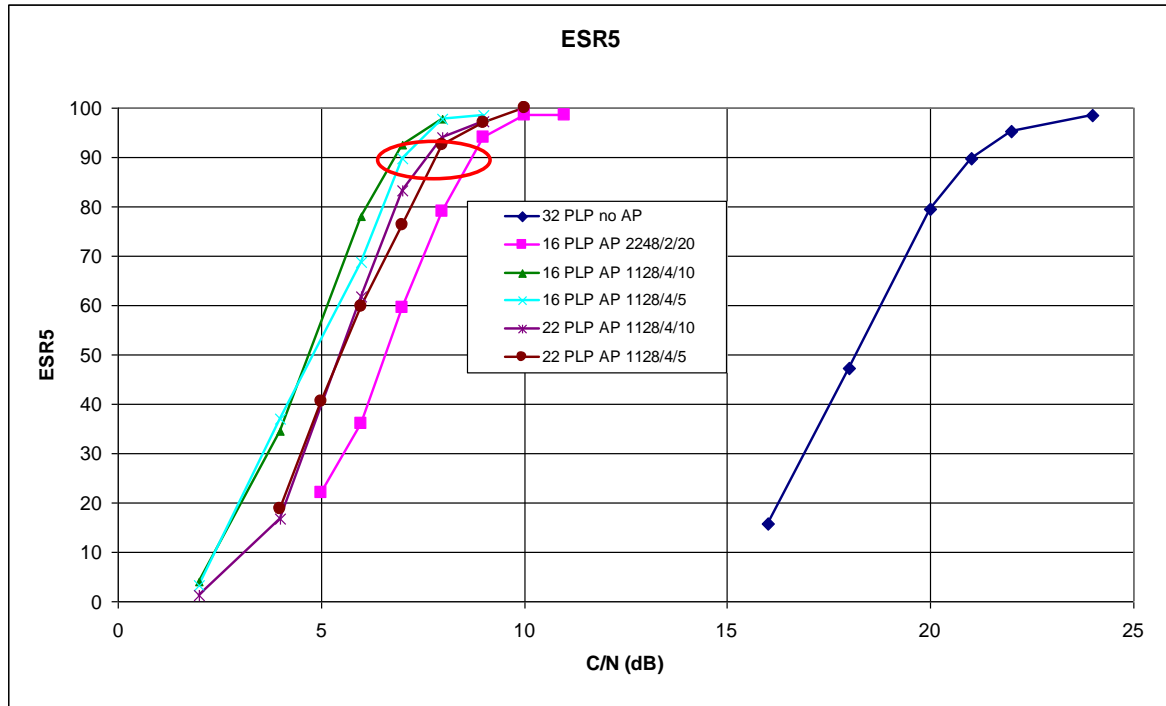
**Figure 39: Additional parity BER/L1ER results.**

Results show that  $BER=10^{-5}$  is reached between 10 and 12 dB of SNR, depending on the configuration. L1 Error Rate  $10^{-4}$  is expected at least around 11 dB of SNR.

Although wide additional parity brings very good results compared to L1 detection Error Rate without additional parity, it can be pointed out that spreading the same additional parity amount over the same interleaving duration is giving better results when 4 AP blocks are used instead of 2.

Besides, given a 60 km/h speed parameter, 5s interleaving seems to be sufficient to counteract channel effects, because results are closed to 10s interleaving. Lastly, it can be seen that applying using Coding rate 0.17 instead of 0.2 brings around 0.7 dB gain.

In a satellite environment, ESR5 criteria may take more sense than usual Modulation Error Ratio (MER). This is why results are also presented with this metric. Results in Figure 39 above show that order between different curves is the same as BER curves. Besides, the C/N area where the criteria is 90% fulfilled (agreed reference point in satellite community and especially in DVB-SH standard) is around 7 to 9 dB.



Legend : number of PLP ; AP\_1block\_cell\_size /AP\_Nb\_Blocks/AP\_interval

Figure 40: Additional parity ESR5 results.

#### 4.2.4 Comparison with NGH adopted solution

In September 2011, Samsung presented simulation results based on the Additional Parity definitive definition (see TR1.1). Main differences between the CNES solution and additional parity are:

- The using of BPSK modulation, instead of the QPSK modulation (3 dB gain on  $E_s/N_0$ ).
- The use of 4K LDPC instead of 16K LDPC.
- The definition of 3 effective coding rates, taking into account the Additional parity:  $\sim 1/3$ ,  $\sim 1/5$ ,  $\sim 1/6$ , instead of constant amount of parity bits.
- Additional parity is put in the previous NGH frame, instead of spread additional parity blocks in several previous frames.

About simulations setting differences, note that:

- Samsung have used a LMS-SU (Sub-Urban) satellite channel, which is a bit more favorable than LMS-ITS (Intermediate Tree Shadowing) channel.
- Terrestrial NGH framing was used (NGH---DVB-T2---NGH) with 600ms gap duration between 2 NGH frames: DVB-T2 frame was 400 ms duration whereas DVB-NGH frame included into Future Extension Frame has only 200ms duration.
- Coding rate was  $\sim 1/6$  (with BPSK).

Compared to CNES simulations (LMS-ITS, QPSK with effective coding rate  $\sim 1/5$ , LDPC 4K), ESR5 criteria reaches 90% fulfillment at 3 or 4 dB, that is showing clearly better results, but not really comparable

(modulation, channel, coding rate, code size). In fact, no matter about this, because Samsung has made the proof that their proposal was enough robust for a suburban reception.

Nevertheless, weakness of the proposal is that there is no possibility (only using Additional parity device) to split additional parity in several previous frames, especially for satellite link with only 250 ms between two NGH frames (compared to 600 ms used in the Samsung simulations).

#### **4.2.5 Conclusion and warnings**

Thanks to Samsung, Additional Parity, powerful mean of robustness for L1 signaling, has been introduced in NGH standardization process. In this study it has been demonstrated that this technology was getting more efficient when associated with spreading. Nevertheless, despite of hard receiving conditions in satellite mobile environment, it has been seen that reduced spreading could be introduced providing more robust modulation (BPSK), very low coding rate ( $\sim 1/6$ ) and reduced size code (LDPC 4K), as it is approved now in the NGH standard.

Adopted decision is well suited for the scenario with a 600ms spreading duration between satellite frames (scenario with satellite frames put in two long DVB-T2 frames and used in SAMSUNG simulations).

Nevertheless, for satellite transmission, only satellite NGH frames are emitted (Stand-alone mode) with 250ms spreading duration that might be a weak point. Fortunately, NGH standard implements another mechanism, Incremental redundancy (not studied here) enabling using another previous frame to carry other bit redundancy.



## 5 SC-OFDM WAVEFORM

### 5.1 Introduction

Satellite systems are due to cope with specific propagation conditions but also stringent technological constraints related to the satellite carrier itself. On top of those lies the power amplifier (PA) that must bring the signal to be transmitted at a level compatible with the receiver sensibility over large areas. In order to guarantee the durability of the satellite, it is critical to keep low the power consumption of the system, and thus to optimize the amplifier power efficiency, i.e. to drive the amplifier close to saturation. Single carrier (SC) modulations also described as time division multiplexing (TDM) modulations have long been the reference scheme for satellite transmissions, e.g. such as in the DVB-S2 system developed in 2003 [5], for their suitability to achieve low power fluctuations compatible with good power efficiency. However, the orthogonal frequency division multiplexing (OFDM) modulation is taking over single carrier schemes thanks to a better flexibility and a comparatively lower complexity when it comes to compensate for high channel degradations. OFDM is now used in many systems such as 3GPP/LTE cellular networks, IEEE 802.11 WiFi solutions, IEEE 802.16 WiMax systems, etc. Dealing with broadcast, the DVB-SH (Satellite to Handhelds) standard developed in 2007 [6] specifies 2 modes of operation, one OFDM mode allowing the deployment of single frequency networks (SFN) on both the terrestrial and satellite links and a second mode with TDM on the satellite link and OFDM on the terrestrial link for multiple frequency networks (MFN).

Despite its obvious advantages, the OFDM modulation is not perfectly well suited for satellite transmissions. Indeed, the more sub-carriers are added together the more the signal behaves like a Gaussian noise with large power fluctuations. The power amplifier shall either be operated in a linear mode far from saturation and thus with a poor power efficiency or in a clipping mode at the cost of significant performance degradations due to saturation. This weakness of OFDM is well known and several means have been studied to reduce its power fluctuations such as the tone reservation (TR) or active constellation extension (ACE) techniques specified in the DVB-T2 standard [10]. However, as it will be shown in the sequel, the gain of these techniques appears to be marginal in the context of satellite transmissions. More recently, the 3GPP selected the single carrier-frequency division multiple access (SC-FDMA) technique for the uplink of LTE networks [12] in the purpose of reducing the power consumption of handled devices. The SC-FDMA scheme is actually a derivation of the orthogonal frequency division multiple access (OFDMA) where each user is allocated with a given sub-set of contiguous OFDM sub-carriers. But unlike in OFDMA, the symbols to be transmitted are precoded in the frequency domain by means of a discrete Fourier transform (DFT) prior OFDM modulation. It is thus possible to benefit from the good PAPR properties of the original symbols to save power in the amplification stage.

It is on the basis of these obvious similarities with the satellite context that the SC-FDMA was proposed as a candidate waveform for the DVB-NGH hybrid profile. A broadcast signal is inherently transmitted towards all receivers. The SC-OFDM terminology was selected to identify the specific case where the whole bandwidth is allocated to all users. As shown in this chapter, the SC-OFDM modulation is clearly suitable for satellite transmissions. It was adopted in the DVB-NGH standard thanks to its ability to preserve a lot of commonalities with pure OFDM while benefiting from the low power fluctuations of single carrier (SC) signals.

The purpose of this chapter is to introduce the principle of the SC-OFDM modulation and to characterize its properties and performance in the particular case of the DVB-NGH hybrid profile. The rest of the chapter is structured as follows. Section 5.2 briefly compares the merits of the different waveforms used for satellite transmissions. Section 5.3 summarizes the specifications of the SC-OFDM modes in the DVB-NGH standard. The last section is dedicated to the analysis of the performances of the SC-OFDM modulation.

## 5.2 Combining the TDM and OFDM strengths

TDM modulations combine low power fluctuations with reasonable receiver complexity using frequency domain equalization (FDE). But SC-FDE schemes do not allow inserting pilot within data in the frequency domain, and present some loss in spectral efficiency due to the roll-off implementation. Moreover, it is generally needed to double the sampling frequency at the receiver for practical implementation of the demodulation. The OFDM can actually be interpreted as a derivation of the SC-FDE approach where it becomes possible to allocate data in both the time and frequency domains and where the roll-off can be set to zero. However, this improved flexibility comes at the expense of a reduced peak to average power ratio (PAPR, see Section 5.4.2). The SC-OFDM modulation actually combines the advantages of the two worlds, the low power fluctuations of the SC modulation and the flexibility and high spectral efficiency of the OFDM waveform. As shown on Figure 41, this is obtained by generating the frequency domain samples of the OFDM modulation by means of a discrete Fourier transform (DFT) applied onto preferably constant amplitude samples. It is thus possible to recover the low PAPR properties of the original symbols in the time domain after OFDM modulation. In the case of the SC-FDE technique, the translation in the frequency domain at the receiver is used to perform the equalization. Similarly for the SC-OFDM, the translation in the frequency domain at the transmitter can be used to perform the sub-carrier mapping of user data and reference pilot just like in the OFDM modulation. Moreover, null sub-carriers can (must) be inserted at the edges of the frequency multiplex in order to perform a zero roll-off oversampling.

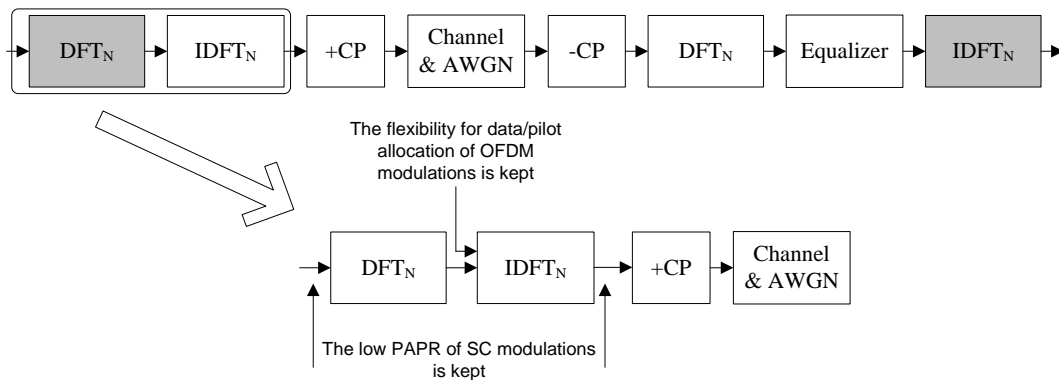


**Figure 41: From OFDM to SC-OFDM.**

Figure 42 illustrates the relationships between the SC-OFDM, OFDM and SC-FDE techniques. As shown on this figure, the first DFT at the transmitter can actually be computed over  $M$  samples where  $M \leq N$ . The result of the  $M$ -point DFT is then mapped in the central part of the OFDM multiplex padding the unallocated sub-carriers with zeros. The resulting signal is simply the zero roll-off oversampled version of the original  $M$ -sample signal, thus leading to the preservation of the original low PAPR. As explained in the introductory

section, the name SC-OFDM was derived from the SC-FDMA terminology used in the 3GPP/LTE system where this technique is used in combination to frequency division multiple access in uplink. In the present case, all users can demodulate the signal that is transmitted over the whole bandwidth. Other approaches are possible: it is possible for instance to alternatively insert  $m-1$  null sub-carrier between each sample obtained at the output of the  $M$ -point DFT. In this case, the resulting signal is periodic as  $m$  replica of the original signal, thus keeping its low PAPR property. Other alternatives have been devised to define multiple access schemes in cellular networks (IFDMA, MC-CDMA, SS-MC-MA, etc). The computation of the first DFT can also be interpreted as a spreading on the symbols to be transmitted. For that reason, SC-OFDM is also known as the DFT-spread OFDM modulation.

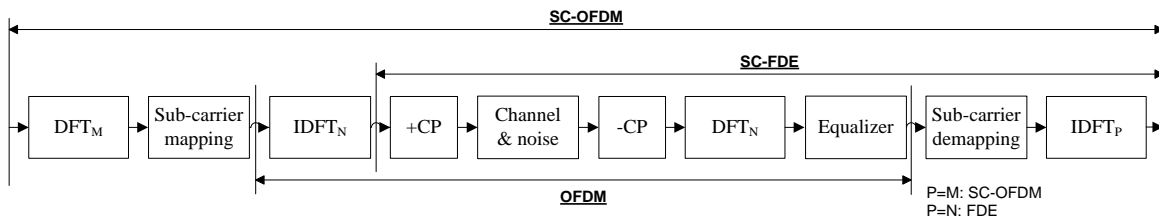


**Figure 42: Relationships between the OFDM, SC-FDE and SC-OFDM modulations.**

The SC-OFDM modulation can be implemented either in the time-domain (IFDMA) or in the frequency-domain (DFT-spread OFDM). The frequency domain implementation is generally preferred, especially at the receiver. The frequency domain implementation of the SC-OFDM transmitter is described in Figure 43. It mainly consists in adding a spreading stage, i.e. a DFT of size  $M$ , to the OFDM transmitter. As already expressed, the SC-OFDM signal can be interpreted as an interpolated version of the signal prior to spreading, the interpolation ratio being equal to  $N/M$ . The interpolation filter being performed by DFT/IDFT is about as sharp as possible. Therefore, the SC-OFDM signal is roughly equivalent to a TDM signal with a zero roll-off.

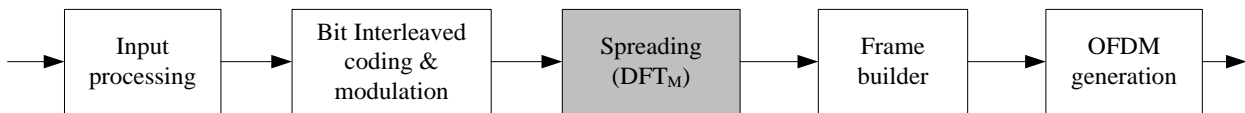


**Figure 43: SC-OFDM transmitter.**

Figure 44 depicts the general architecture of the SC-OFDM receiver in the frequency domain. It clearly appears that the SC-OFDM receiver shows a lot of commonalities with the OFDM receiver. There is only one new function, the de-spreading DFT, and the other modules are only slightly modified with a reasonable increase of complexity. As an illustration, Table 23 compares a possible implementation of the different key functionalities in a multi-carrier receiver for both the OFDM and SC-OFDM modulations. It can be noticed that the functions are very similar except for the occurrence of a summation on the individual OFDM terms when dealing with SC-OFDM. This similarity has actually been one of the rationales for the adoption of the SC-OFDM modulation along with pure OFDM for the satellite segment of the DVB-NGH standard.

**Table 23: Complexity of SC-OFDM versus OFDM.**

	SC-OFDM	OFDM
<b>Demodulation</b>	$r_k'' = DFT\{r_k'\}$	
<b>Equalization (MMSE)</b>	$\hat{s}_k = \frac{H_k^*}{ H_k ^2 + \sigma^2} r_k''$	
<b>De-spreading</b>	$\hat{x}'_n = DFT\{\hat{s}_k\}$	$\hat{x}'_n = \hat{s}_n$
<b>Normalization</b>	$\hat{x}_n = \hat{x}'_n / \tilde{\alpha}, \tilde{\alpha} = \frac{1}{M} \sum_{k=0}^{M-1} \frac{ H_k ^2}{ H_k ^2 + \sigma^2}$	$\hat{x}_n = \hat{x}'_n / \tilde{\alpha}_n, \tilde{\alpha}_n = \frac{ H_n ^2}{ H_n ^2 + \sigma^2}$
<b>LLR weighting</b>	$\Gamma_n^j = \frac{4 \sum_{k=0}^{M-1}  H_k ^2}{\sigma^2} LLR_n^j$	$\Gamma_n^j = \frac{4 H_n ^2}{\sigma^2} LLR_n^j$

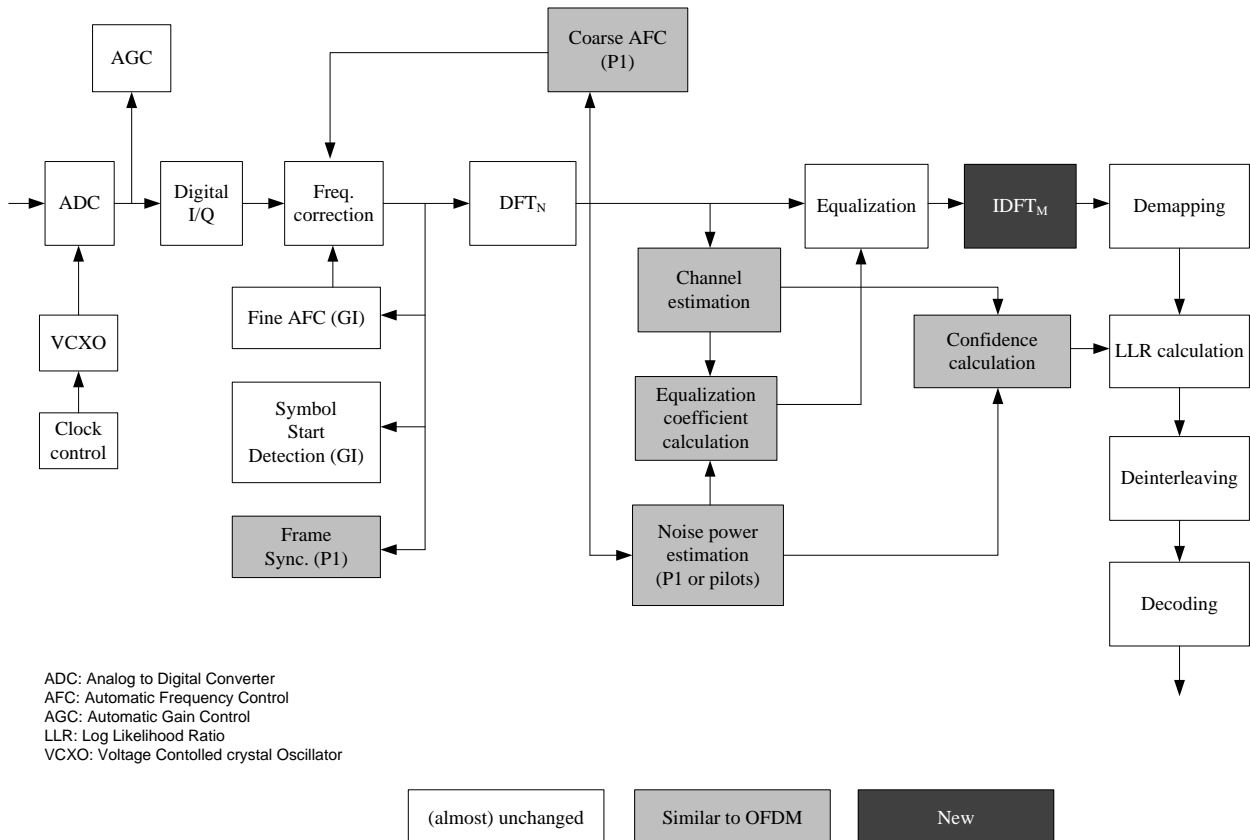


**Figure 44: SC-OFDM receiver.**

## 5.3 SC-OFDM modulation in DVB-NGH

### 5.3.1 System Parameters

The DVB-NGH standard specifies a mandatory sheer terrestrial profile (also called core or base profile) and an optional terrestrial/satellite hybrid profile. The hybrid profile is composed of a main component coming from the terrestrial network and an additional component coming from a satellite. The SC-OFDM modulation has been selected with OFDM as the two reference waveforms for the hybrid profile. Besides defining the transmitted waveforms, the hybrid profile also defines the mechanisms to receive two waveforms simultaneously and combine their outputs into a single stream. The hybrid waveform can be transparent to the receiver, when an identical signal is transmitted by the terrestrial and satellite transmitters (SFN mode), or two different waveforms (MFN mode) can be used. The following hybrid modes are identified:

- **SFN in OFDM:** In this case the OFDM satellite parameter set is applicable to both the terrestrial and satellite components.
- **MFN in OFDM:** In this case the terrestrial component is built according to the Core Profile while the satellite component is set according to the OFDM hybrid profile.
- **SFN in SC-OFDM:** This mode concerns only the case of terrestrial gap fillers that amplify the signal from the satellite (in the same frequency). The SC-OFDM satellite component setting is applicable to both the terrestrial and satellite components.
- **MFN in SC-OFDM on the satellite component and OFDM on the terrestrial component:** The terrestrial component is set according to the core profile while the satellite component is set according to the SC-OFDM mode of the hybrid profile.

The satellite component of the hybrid profile is defined for two bandwidths, 2.5 and 5 MHz for a transmission in the L and S-bands. Table 24 describes the main system parameters defined for the SC-OFDM satellite mode.

**Table 24: Main system parameters for SC-OFDM transmissions in DVB-NGH.**

<b>Bandwidth</b>	2.5 MHz	5 MHz
<b>Sampling Freq.</b>	20/7 MHz	40/7 MHz
<b>FFT Size (<math>N</math>)</b>	512, 1024	512, 1024 and 2048
<b>Guard Interval</b>	1/16 and 1/32 (w.r.t. to $N$ )	
<b>Constellation</b>	QPSK and 16QAM	

### 5.3.2 Pilot Pattern

One strong advantage of OFDM is the possibility to use pilots scattered in the time and frequency domains, a key feature when it comes to estimate the channel at high speeds, i.e. for large Doppler values. As an illustration, Figure 45 depicts the PP1 pilot scheme of the DVB-T2 standard. Note that DVB-T2 specifies 8 different pilot patterns, where PP1 already used in DVB-T offers a good compromise between Doppler and long echoes robustness (see Table 25).

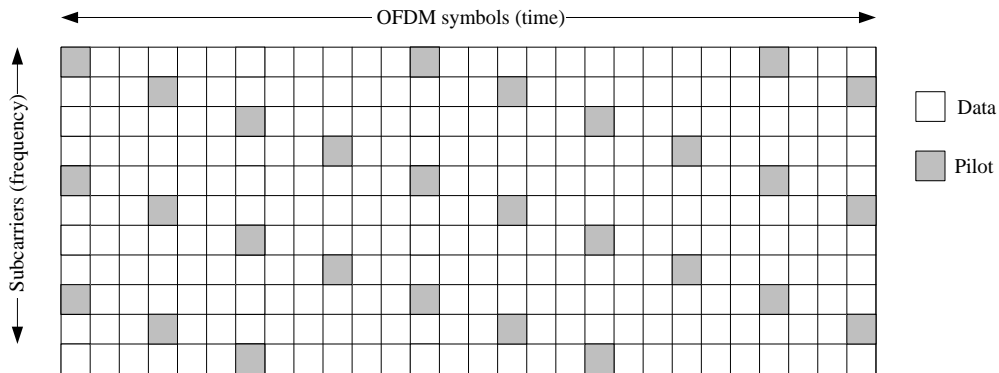


**Figure 45: DVB-T2 PP1 pilot pattern.**

The main issue is that a pilot pattern such as the one on Figure 45 cannot be multiplexed with SC-OFDM data without completely degrading the PAPR structure of the transmitted signal. In such a case, the complementary cumulative distribution function (CCDF) of the transmitted signal amplitude is actually similar to the one of an OFDM signal. To solve this issue, the 3GPP/LTE body selected for the uplink a pilot pattern similar to the one depicted on Figure 46 (see 3GPP/LTE TS 36.211 [12]).

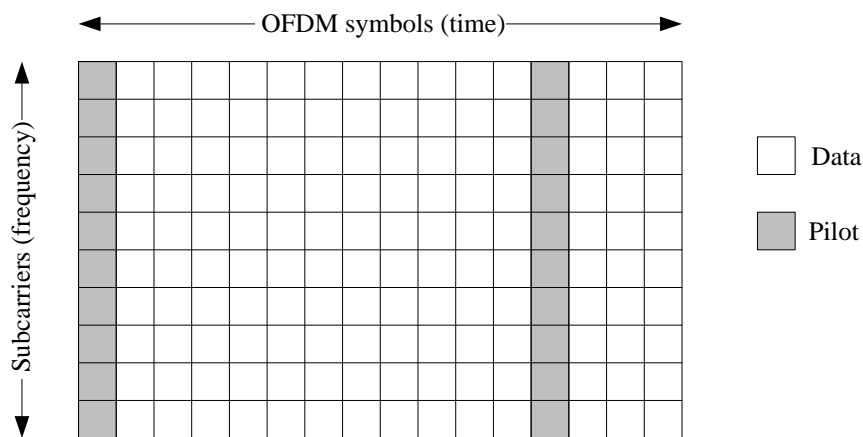


**Figure 46: LTE-like pilot structure for SC-OFDM.**

According to the 3GPP/LTE approach, a complete SC-OFDM symbol (i.e. all the subcarriers), referenced as a pilot symbol, is constituted solely by pilots and is dedicated to channel estimation and synchronization purposes. Such a symbol is regularly inserted in the frame (twice in each 1ms sub-frame made of 14 SC-OFDM symbols). In this case, a classical way of performing channel estimation is represented on Figure 47. The channel is estimated at the pilot positions (cells in the DVB terminology), then the noise level is reduced

by means of a frequency domain smoothing such as a Wiener filter, and finally the channel is estimated at all positions by performing a time interpolation between two pilot symbols. The 3GPP/LTE scheme shows its limits when it comes to implement time interpolation. In order to maximize the user data throughput, one must limit the number of pilot symbols inserted among data cells. For example, in DVB-T2, the pilot insertion rate per sub-carrier depicted in Figure 45 is  $1/12$ . If one wants to keep the same throughput as in the LTE approach, it implies that a full pilot symbol shall be inserted every 12 OFDM symbols. This limits the capability of the system to follow the channel variations of the signal for example due to velocity. According to the Nyquist theorem, if the OFDM rate is  $1/T$ , a bound on the maximum acceptable Doppler frequency is equal to:

$$f_{\max} = \frac{1}{2D_Y T} = \frac{1}{24T} \quad (14)$$

where  $D_Y (= 12)$  is the number of symbols forming one scattered pilot sequence. The bound is actually even lower when considering practical algorithms to perform time interpolation with a reasonable complexity. It must be understood that this bound is due to the pilot structure itself (Figure 46), and not to the related estimation method. With the DVB-T2 scattered pilots showed in Figure 45, the bound falls down to  $(8T)^{-1}$ . The other OFDM pilot patterns specified in the DVB-T2 standard are compared in Table 25.

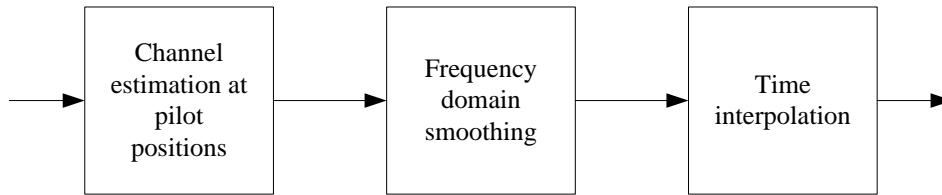


**Figure 47: Typical channel estimation for multi-carrier modulations (OFDM and SC-OFDM).**

The SC-OFDM mode of the NGH hybrid profile specifies a new pilot pattern (defined as PP9) which divides by two the bound of Eq. (14) while preserving the low PAPR structure of SC-OFDM. Typically, Zadoff-Chu (ZC) sequences [13] are used as pilot patterns, due to their low PAPR and their good orthogonality and correlation properties. ZC sequences are constant amplitude zero autocorrelation (CAZAC) sequences, both in the time and frequency domains. Roughly, the generation of the pilot and data structure can be summarized in three steps:

- In the last SC-OFDM symbol of each NGH data section made of 6 symbols (see Figure 49), half of the subcarriers are allocated to DFT-spread data, while the other half of subcarriers convey pilots (see Figure 48). Data and pilots multiplexed in the frequency domain.
- For the pilot subcarriers, a constant amplitude sequence such that its DFT counterpart (in the time domain) has also fixed amplitudes is used. If  $L$  denotes the ZC sequence length ( $L = M/2$ ), then the complex value at each position  $k$  of each  $p$ -root ZC sequence with integer shift  $l$  is (the size  $L$  of the ZC sequence is even here):

$$x_k = e^{-2j\frac{\pi}{L}\left(p\frac{k^2}{2}+lk\right)} \quad (15)$$

As only one sequence is needed for broadcasting, the index  $p$  is set to one ( $p = 1$ ) and the shift  $l$  to zero ( $l = 0$ ).

- This Zadoff-Chu pilot sequence is modified by adding a half period shift:

$$x_k = e^{-2j\frac{\pi}{L}\left(\frac{k^2}{2} + 0.5k\right)} \quad (16)$$

Constant amplitude should be understood as evaluated on a non-oversampled ZC sequence. After oversampling (OFDM modulation and of digital to analog conversion), the ZC sequence is not constant amplitude, but has very low envelope fluctuations, lower than the fluctuations of a typical TDM QPSK sequence.

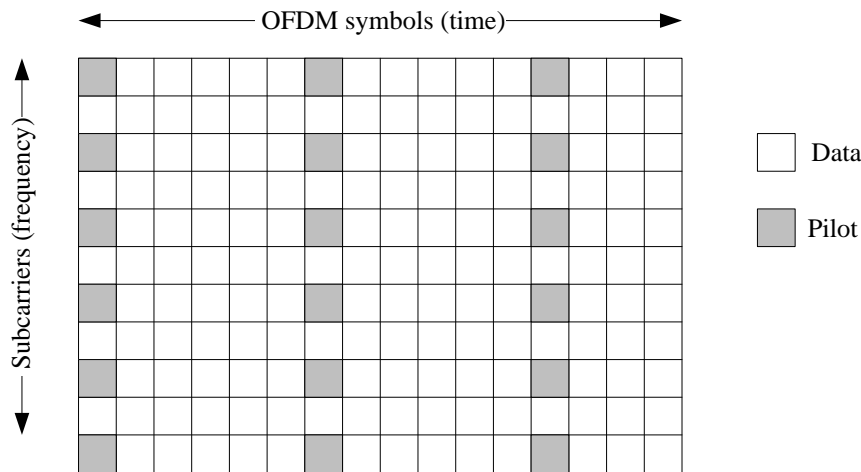


**Figure 48: NGH pilot structure for SC-OFDM.**

The introduction of the fractional time shift is justified as follows: the global signal, in frequency or time dimensions, corresponds to the sum of two signals, data and pilots. As the interpolation is a linear process, the global interpolated signal corresponds also to the sum of two signals: the interpolated data signals and the interpolated pilot signals. For the data in the time domain, if no interpolation is performed and if a x-PSK constellation is used, a constant amplitude is obtained every sample period, and the maximum peaks after interpolation are placed just in-between these time instants. The same phenomenon occurs with the classical Zadoff-Chu sequence. Therefore, in this case, we add two signals, the peaks of which are placed at the same positions. By time shifting the Zadoff-Chu sequence of half a sampling period, the peaks of each signal are now interleaved. This implies that the peaks of the global signal, sum of both, are reduced.

If a non constant constellation is used, e.g. 16QAM, the amplitude is no longer constant every sample period. However, the peaks will still be placed at the same positions, i.e. just in-between these time instants, and the peaks of the global signal will still be reduced by modifying the original ZC pilot sequence.

Table 25 lists the different pilot patterns: PP1 to PP7 for OFDM waveform, PP9 for the SC-OFDM waveform. When comparing the SC-OFDM pattern PP9 to the terrestrial one, It can be noticed that large  $D_y$  values decrease the Doppler performance. However, it can be noted that:

- The lower  $D_x$  values improve the smoothing filter performance and then decreases the noise on the channel estimates.
- The DFT size is generally lower for the satellite component, which will improve Doppler performance.



- As the satellite channel is single path, the use of an Automatic Frequency Control (AFC) improves Doppler performance.

**Table 25: Parameters defining the scattered pilot patterns.**

Pilot pattern	Separation of pilot bearing carriers ( $D_x$ )	Number of symbols forming one scattered pilot sequence ( $D_y$ )
PP1	3	4
PP2	6	2
PP3	6	4
PP4	12	2
PP5	12	4
PP6	24	2
PP7	24	4
PP9	2	6

In accordance with this new pilot scheme, the DVB-NGH specifies a specific frame structure for the hybrid profile (see Figure 49). At the top level, the frame structure is made of super-frames, which are divided into NGH-frames that contain data sections made of 6 consecutive SC-OFDM symbols. As shown on Figure 49, the last symbol of each data section is a PP9 pilot pattern as described above. Note that this structure is typical of the SC-OFDM satellite link. The frame structure for the core profile remains similar to the DVB-T2 structure.

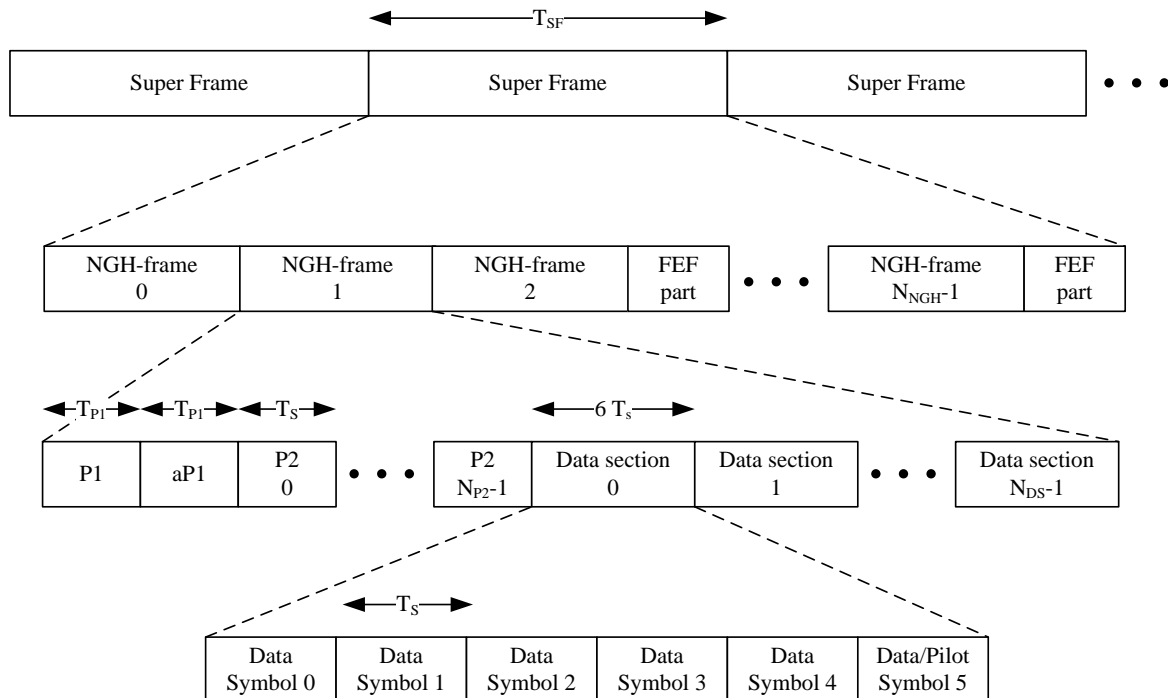


**Figure 49: The DVB-NGH frame structure of the hybrid terrestrial-satellite profile.**

### 5.3.3 MIMO

With an increasing pressure on both the frequencies (analog switch off and digital dividend/digital switch over) and the bandwidth requirements, it is critical to take the most of the available spectrum. Just like most of the recent wireless systems, the DVB-NGH system relies on multi-antenna schemes to either improve the robustness (spatial diversity) or to increase the capacity (spatial multiplexing) of the broadcasting transmissions. The DVB-NGH standard specifies two spatial diversity schemes, a modified Alamouti code and an enhanced SFN solution (the so-called called rate 1 schemes). These two schemes are actually part of the core profile along with SISO for sheer terrestrial transmissions. Spatial multiplexing schemes called rate 2 schemes in DVB-NGH are specified in an optional MIMO profile dedicated to the core profile. In addition, the DVB-NGH specifies a 2x2 enhanced spatial multiplexing (eSM) precoding with an optional phase hopping (PH). In parallel of these schemes dedicated to sheer terrestrial transmissions, the DVB-NGH standard also includes the so-called hybrid MIMO profile that has been devised specifically to facilitate the use of MIMO on the terrestrial and/or satellite elements within a hybrid transmission scenario. This profile encompasses two branches described hereunder.

#### 5.3.3.1 Hybrid MIMO MFN

The hybrid MIMO MFN scenario describes the case where the satellite and terrestrial parts of the transmission are on different carrier frequencies and do not necessarily share any common frame or symbol timing at the physical layer. At least one of the transmission elements (i.e. terrestrial or satellite) must be made using multiple antennas; otherwise the use case lies within the hybrid profile, not the hybrid MIMO profile. Dealing with the single MFN mode implying SC-OFDM (terrestrial component set according to the core profile and a satellite component in SC-OFDM mode), three MIMO configurations can be considered:

- The terrestrial component operates in MIMO according to any scheme from the MIMO profile while the SC-OFDM transmission occurs in SISO.
- The terrestrial component operates in SISO according to the base profile while the SC-OFDM transmission occurs in MIMO using a basic Spatial Multiplexing (SM) scheme neither precoding nor phase hopping).
- Both links operate in MIMO, where the terrestrial component operates in MIMO according to any scheme from the MIMO profile while the satellite link operates in SM mode.

The MIMO SM of the hybrid MIMO profile processing consists in transmitting cell pairs  $(f_{2i}, f_{2i+1})$  on the same SC-OFDM symbol and carrier from Tx-1 and Tx-2 respectively:

$$\begin{pmatrix} g_{2i} \\ g_{2i+1} \end{pmatrix} = \begin{pmatrix} f_{2i} \\ f_{2i+1} \end{pmatrix}, \quad i = 0, 1, \dots, N_{cells} / 2 - 1, \quad (17)$$

where  $i$  is the index of the cell pair within the FEC block and  $N_{cells}$  is the number of cells per FEC block. The insertion of pilots is modified in order to allow for the channel estimation on each transmitter-receiver path. The frequency domain implementation of SC-OFDM makes the SM decoding very simple.

#### 5.3.3.2 Hybrid MIMO SFN

The hybrid MIMO SFN describes the case where the satellite and terrestrial parts of the transmission use the same carrier frequency and radiate synchronized signals intended to create an effective SFN. SC-OFDM is

not an option for the hybrid MIMO SFN profile where a synchronized effective SFN transmission can only exist in OFDM mode (terrestrial emitters other than gap fillers only implement OFDM).

## 5.4 Performance evaluation

The knowledge gathered so far on the SC-OFDM technique has been obtained in the context of broadband cellular networks (SC-FDMA for LTE/UL). It was thus required to check the suitability of the SC-OFDM modulation for satellite broadcasting. In that purpose, the performances of the SC-OFDM modulation have been thoroughly evaluated by means of computer simulations. This section provides key performance related to the use of SC-OFDM in a satellite transmission context.

### 5.4.1 Power amplifier characterization

As previously mentioned, the SC-OFDM was designed to benefit from reduced power fluctuations in comparison to OFDM while keeping the same flexibility. Variation in the amplitude is actually an issue when dealing with power amplification (PA). Basically, a PA amplifies the amplitude of the incoming signal so as to bring its power level to a value compatible with the transmission requirements (coverage, receiver sensibility). A perfect PA provides a linear gain whatever the level of the incoming signal. Practically, a PA can only amplify signal up to a maximum value called the saturation amplitude  $v_{\text{IN(OUT),Sat}}$ . A still ideal but more realistic model is the ideal clipper: all peaks above a certain saturation level are clipped, and all the others remain unchanged (Figure 50, black solid line curve). It is common to characterize the PA by its AM/AM characteristic, giving the output amplitude  $|v_{\text{OUT}}|$  as a function of the input amplitude  $|v_{\text{IN}}|$ . In the case of the ideal clipper, the AM/AM response is defined as:

$$\frac{v_{\text{OUT}}}{v_{\text{OUT,Sat}}} = \begin{cases} \frac{v_{\text{IN}}}{v_{\text{IN,Sat}}}, & |v_{\text{IN}}| \leq v_{\text{IN,Sat}} \\ 1, & \text{otherwise} \end{cases} \quad (18)$$

And the gain of the PA in the linear region is given by  $G_1 = v_{\text{OUT,Sat}} / v_{\text{IN,Sat}}$ . In practice, PA are not perfectly linear but show a power response like the ones depicted on Figure 50 obtained with the well know Rapp model [16]. The impact of the fluctuations in the signal amplitude appears clearly on Figure 50. If the amplitude of the incoming signal falls in the saturation region, then the output signal will be clipped leading to degradations both in-band with the introduction of noise but also out-of-band with unwanted emissions immediately outside the assigned channel bandwidth (shoulders).

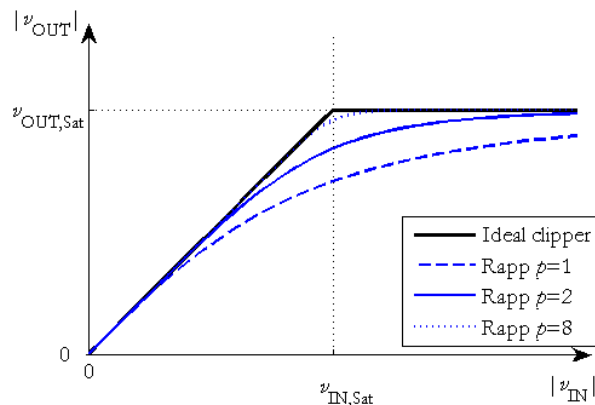


Figure 50: Typical AM/AM PA characteristics.

In order to avoid any degradation on the transmitted signal, it is required to operate the PA solely in its linear region. Typically, the RMS level of the incoming signal is set well below the saturation value so as to leave enough room for higher amplitudes to be amplified without being saturated. The signal is said backed-off from the saturation point. It is common to define the input back-off (IBO) and output back-off (OBO) with respect to the saturation values as respectively:

$$\text{IBO}|_{dB} = -10 \log_{10} \frac{P_{\text{IN,Avg}}}{P_{\text{IN,Sat}}}, \quad (19)$$

$$\text{OBO}|_{dB} = -10 \log_{10} \frac{P_{\text{OUT,Avg}}}{P_{\text{OUT,Sat}}}, \quad (20)$$

where  $P_{\text{IN(OUT),Sat}} = |v_{\text{IN(OUT),Sat}}|^2$  represents the input (output) saturation power and:

$$P_{\text{IN(OUT),Avg}} = \lim_{T \rightarrow \infty} \frac{1}{T} \int_0^T |v_{\text{IN(OUT)}}(t)|^2 dt, \quad (21)$$

is the mean power of a signal  $v(t)$  at the PA's input (output).

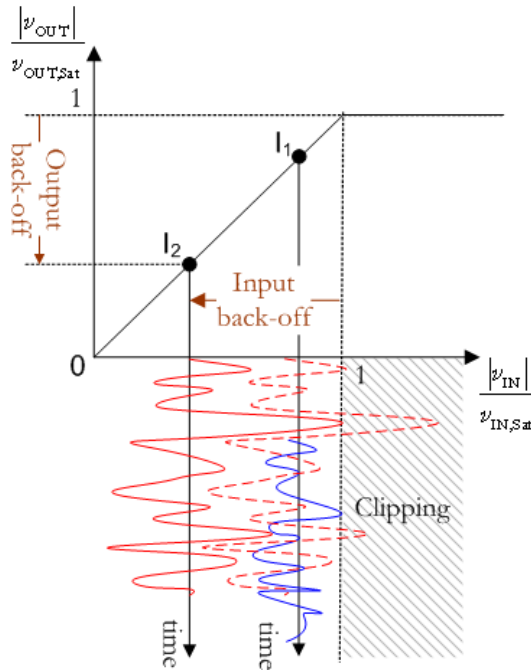


**Figure 51: Backing-off signals with different dynamic ranges.**

As shown on Figure 51 (red curves), depending on the operating point ( $I_1$  or  $I_2$ ), the same signal may suffer or not from clipping effects. In order to avoid significant degradations, an OFDM signal requires an IBO of 10-15 dBs while a SC signal can afford an IBO of a few dBs. Using signal with large power fluctuations has two main impacts: it requires high-end PAs with a large linear region and leads to a poor power efficiency. The power efficiency of a PA is measured as the ratio of the radiated output power with respect to the power consumed to operate the PA.

The power efficiency can be defined as follows:

$$\xi = \frac{P_{OUT,Avg}}{P_{OUT,Avg} + P_{DC}} \quad (22)$$

where  $P_{DC}$  is the power consumed by the PA on top of the radiated power (e.g. polarization current). It is clear from this definition, that the efficiency of the PA is higher when the average output power is close to the saturation point. For a given transmission, reducing the IBO without saturation enables increasing the power efficiency (blue curve) or relying on a PA with reduced constraints in terms of linearity. This is the kind of advantage that led to the selection of the SC-OFDM modulation for the uplink transmission in the 3GPP/LTE cellular system. Several techniques have been devised to reduce the PAPR of the OFDM modulation. One of them, namely the Tone-Reservation (TR) approach [14] was selected in the DVB-T2 standard [10]. For consistency, the performance of SC-OFDM has been measured against both pure OFDM and OFDM-TR for a number of relevant parameters.

### 5.4.2 Peak to average power ratio (PAPR)

Classically, the power fluctuations are measured using the complementary cumulative distribution function (CCDF) of the PAPR, defined as [15]:

$$\text{CCDF}(\text{PAPR}) = \Pr\{\text{PAPR} > \gamma^2\}. \quad (23)$$

The parameter  $\gamma^2$  is a threshold, expressed in dB, and the CCDF value indicates the probability that the PAPR surpasses this threshold. Should we consider a signal (normalized to unitary mean power, for simplicity) passing through an ideal clipper PA,  $\gamma^2$  has a direct physical interpretation: it can be assimilated to the input back-off. Indeed, for a signal working at  $\gamma^2$  dB of IBO to go into saturation and suffer clipping, it would be necessary that its PAPR be higher than  $\gamma^2$ . The probability in (23) is also called clipping probability. Figure 52 displays the result of the evaluation of the CCDF of the PAPR with the following parameters: QPSK,  $M=512$  (modulation),  $N=420$  (spreading), oversampling factor equal to 4.

Figure 52 clearly shows the advantage of the SC-OFDM modulation over the OFDM with a gain of 2.8 dB in terms of admissible IBO for a clipping probability of  $10^{-3}$ . It can also be noticed that the tone reservation technique is not really well suited for satellite networks where the link budget and the transmitter power amplifier efficiency issues lead to very small back-offs. For the same clipping probability, the advantage of the SC-OFDM still holds against the OFDM with tone reservation but with a lower gain of 1.2 dB.

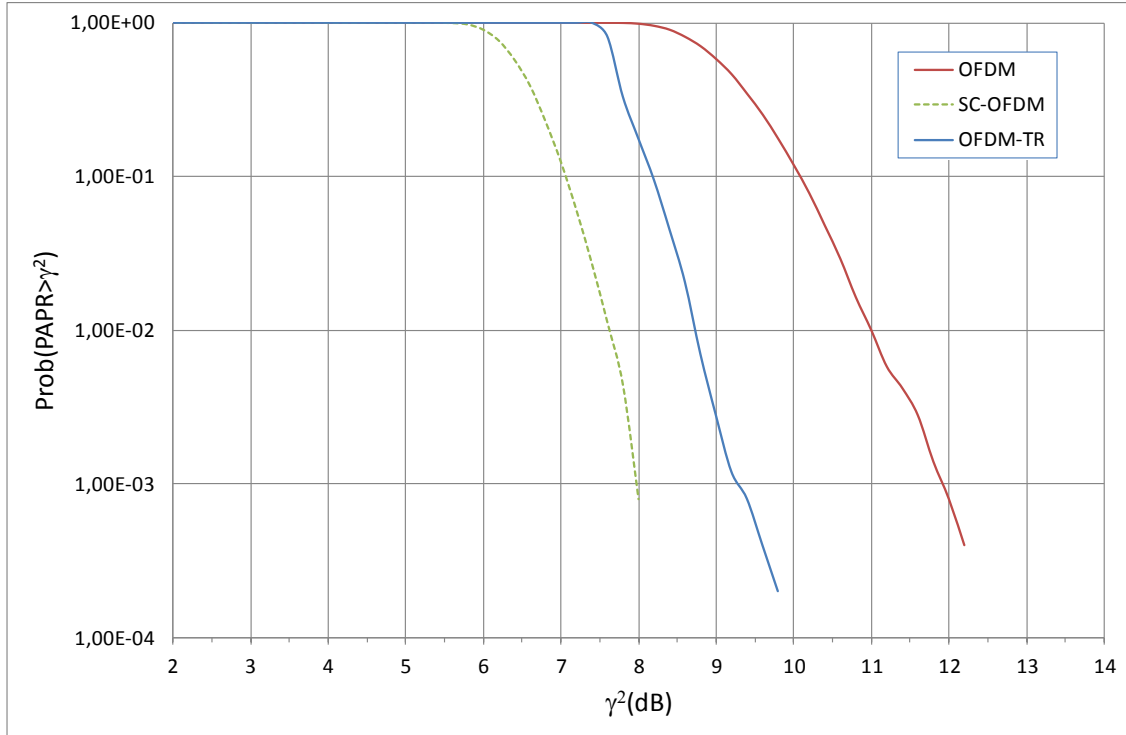


Figure 52: CCDF of PAPR for SC-OFDM, OFDM and OFDM-TR.

### 5.4.3 Instantaneous normalized power (INP)

While the CCDF of PAPR is a very popular notion, it has one important drawback. A certain clipping probability ensures that at least one peak per block has an important amplitude and is susceptible to suffer clipping or severe distortion, but gives no information on how many samples in that block are distorted [15]. Yet, in practical scenarios it is of great interest to know how many samples have a certain level and are thus susceptible to be distorted, as all of these samples cause degradation [17]. Indeed, severely clipping one single peak in a large block has a negligible effect on the MER or spectrum shape, while distortion (even mild) of a large number of samples might have unacceptable consequences. From this point of view, it is important to consider a more refined analysis taking into account all the signal samples. This can be done by means of considering the distribution of the instantaneous normalized power (INP) [15]:

$$\text{CCDF}(\text{INP}) = \Pr \left\{ \frac{\overbrace{|v[n]|^2}^{\text{INP}(v)}}{\frac{1}{N_s} \sum_{k=0}^{N_s-1} |v[k]|^2} > \gamma^2 \right\}, \quad (24)$$

where  $N_s$  is the number of samples considered to evaluate the INP. Note that the INP is defined in the discrete time domain. One must pay attention that the behavior of a signal in the continuous and discrete time domains may not be the same. Continuous and discrete performances will be equivalent only when oversampling the discrete signal at a sufficient level. The CCDF of INP indicates the probability that the INP at a sample level exceeds a certain threshold  $\gamma^2$ . If we look at the range of important values of  $\gamma^2$  for the CCDF of PAPR, the probability that one sample in a block exceeds such a level is very weak, and should a

sample exceed this level it is highly likely to be the only one in that block: The CCDF of INP and the CCDF of PAPR tend asymptotically to the same value. But in the range of lower values of  $\gamma^2$ , the CCDF of INP has a better resolution and shows effects that CCDF of PAPR tends to mask.

Figure 53 displays the result of the evaluation of the CCDF of the INP with the same parameters as in the previous section for the OFDM and SC-OFDM modulations. The figure also gives the CCDF of the INP for the TDM waveform with different roll-offs and the PAPR reduction technique for OFDM specified in DVB-T2, the so-called tone reservation algorithm (TR). These curves confirm the good PAPR properties of the SC-OFDM that outperforms both the OFDM and OFDM-TR modulation even at low IBOs. TDM waveforms exhibit better performance than SC-OFDM but only for roll-offs above 0%, i.e. not for the same spectral occupancy. It occurs that the (SC-)OFDM modulation with rectangular window is spectrally equivalent to TDM with a roll-off of 0%. An evolution of the SC-OFDM (Extended and Weighted SC-OFDM) modulation was devised to allow for controlling the frequency bandwidth with a roll-off factor just like for TDM. Without going into details on its actual principle, Figure 53 shows that the extended SC-OFDM behaves like TDM for the same value of roll-off except for very large power values. But, if the application of zero roll-off is readily achieved for SC-OFDM, it implies severe filtering issues for TDM waveforms. With an increasing pressure on the spectrum, it was decided to keep the SC-OFDM in its original form, i.e. with a roll-off of 0% (smallest bandwidth). *The main result of this study is that the SC-OFDM modulation is strictly similar to TDM modulations in terms of PAPR for the same spectral occupancy.*

The Tone Reservation algorithm brings an improvement to OFDM for INP probability less than  $4 \cdot 10^{-3}$ , corresponding to a signal power greater than 7 dB. For a terrestrial system and linear amplifiers, this brings an improvement if large input back-offs are considered, i.e. very low out-of-band emission. If operating a PA with large IBO is not a big issue for terrestrial transmission, it is not at all the case for satellite transmissions where limiting the power consumption is critical. Satellite PAs are often driven with IBOs of a few dBs thus leading to a high saturation of the signal. This is compensated by the use of robust modulation and coding schemes. From Figure 53, it is clear that for a satellite system and a foreseen IBO of about 1 dB, TR does not bring any advantage.

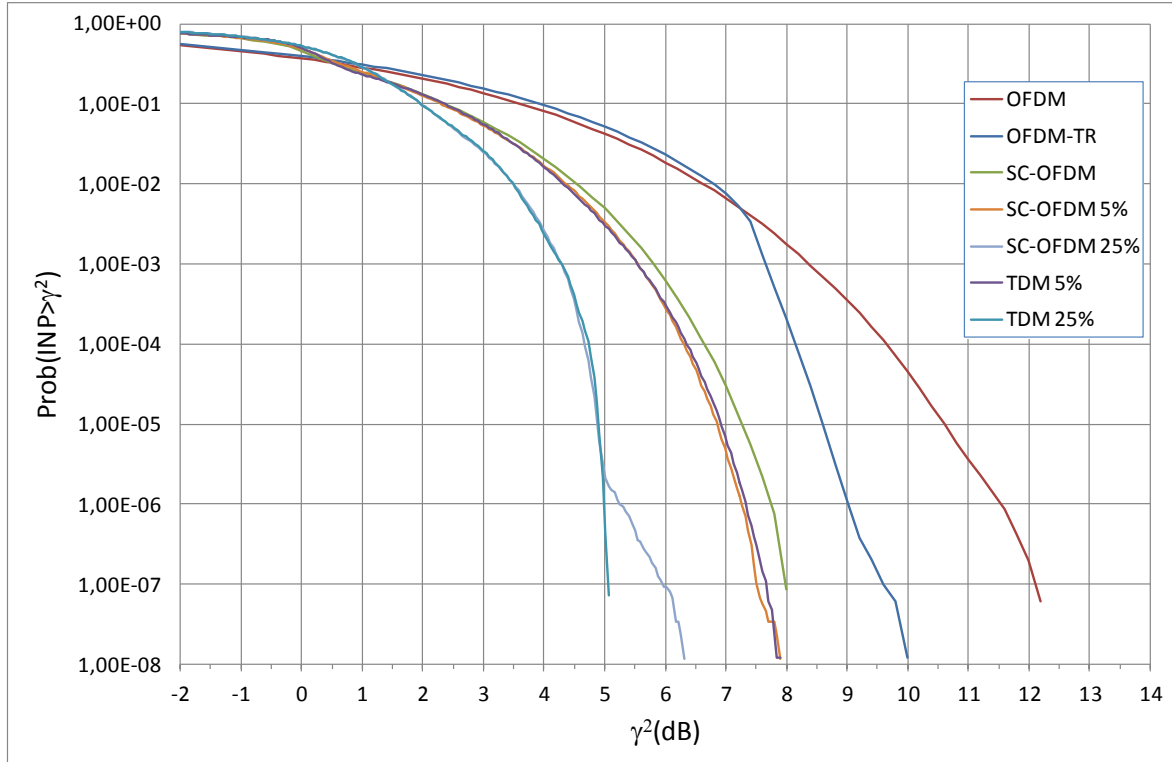


Figure 53: CCDF of INP for SC-OFDM, OFDM and OFDM-TR.

#### 5.4.4 Satellite Pilot Pattern (PP9)

As explained in Section 5.3.3, the DVB-NGH standard specifies a pilot pattern specifically dedicated to the SC-OFDM transmission mode. Figure 54 plots the CCDF of INP of the hybrid data and pilot SC-OFDM symbols. Simulation parameters considered a FFT size of 0.5k ( $N = 512$ ,  $M = 432$ ) and QPSK signal mapping. An oversampling factor of 4 was considered. Results in Figure 54 confirm the overall low envelope fluctuations of the hybrid data and SC-OFDM pilot symbol. At a clipping probability per sample of  $2 \cdot 10^{-2}$  SC-OFDM outperforms OFDM by 2 dB and the hybrid symbol has close performance to SC-OFDM, with a slight degradation of 0.4 dB. Since the hybrid symbol appears in a frame once every 6 SC-OFDM symbols, this slight degradation has overall no impact on the performance. At higher clipping probabilities the performance difference between SC-OFDM and OFDM is even higher, and the hybrid symbol has lower envelope variations than the SC-OFDM data symbol. To illustrate the performance of the PP9 pilot scheme, Figure 55 compares the performance of SC-OFDM in an AWGN channel with perfect and real channel estimation. Real channel estimation is carried out according to the scheme introduced in Figure 47 with Wiener filtering. The real channel estimation introduces a loss of 1.2dB, i.e. typical of what is measured in the case of pure OFDM.



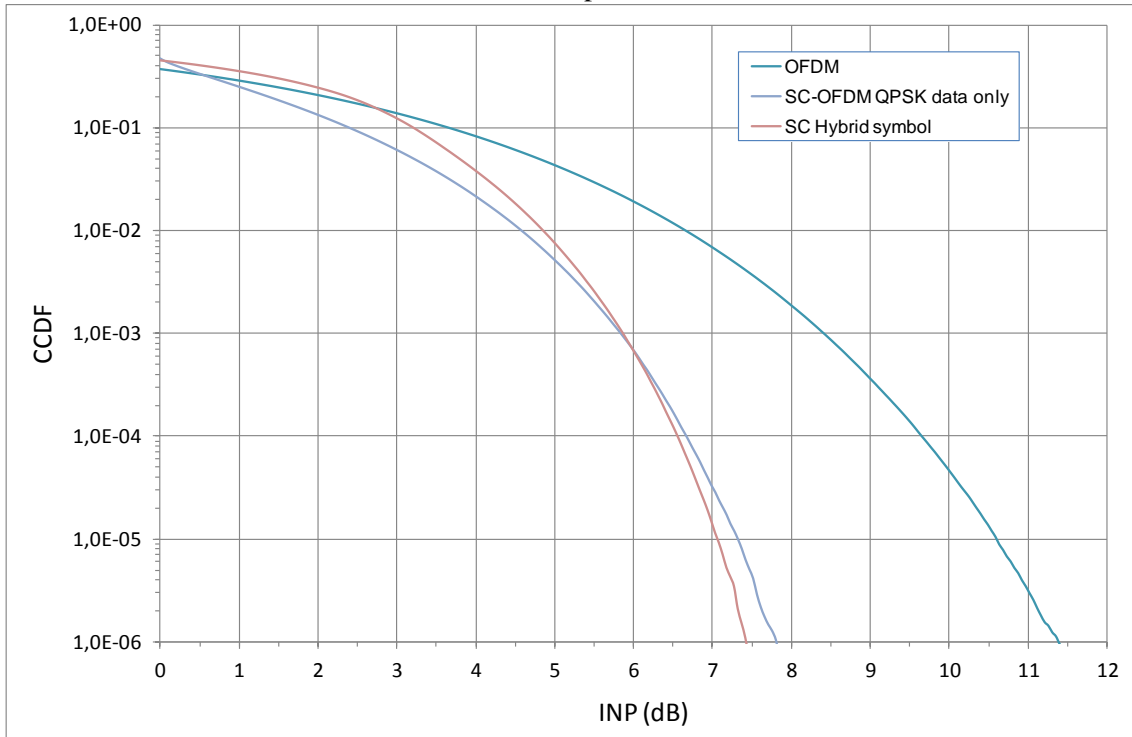


Figure 54: CCDF of INP of OFDM, SC-OFDM and SC-OFDM hybrid pilot.

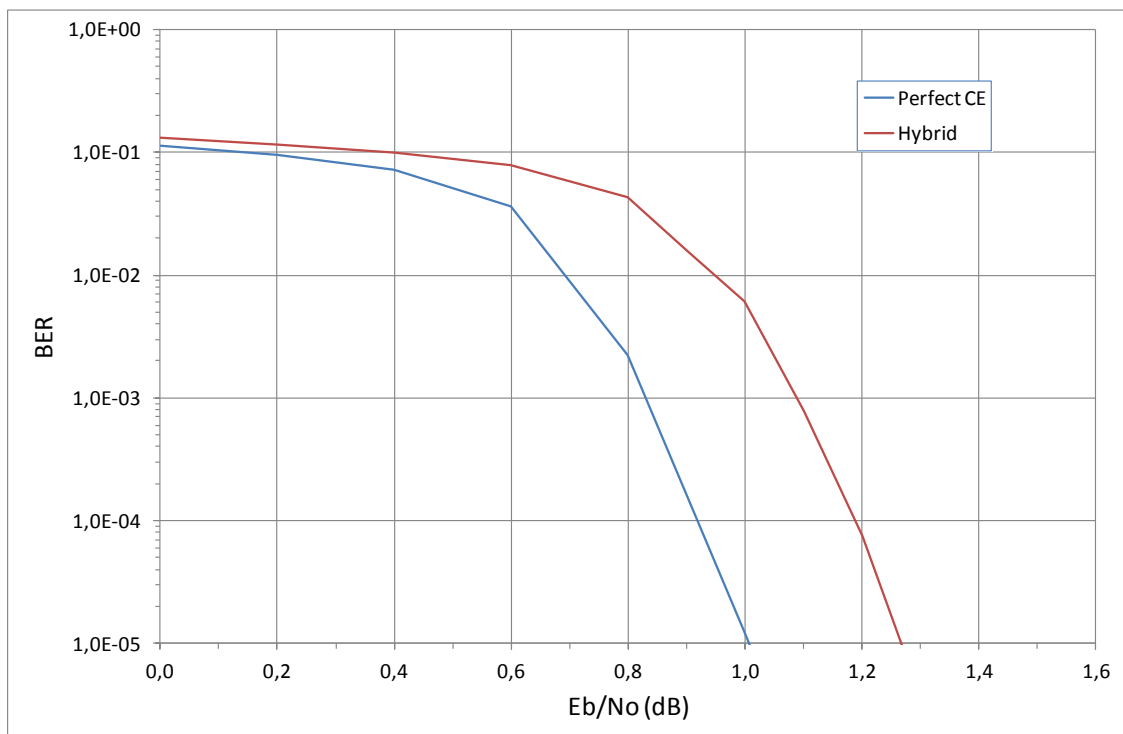


Figure 55: Performance of the PP9 pilot scheme with real channel estimation (CE). QPSK 4/9, LDPC 16k, N = 512, GI = 1/32, AWGN.

### 5.4.5 Modulation error ratio (MER)

The CCDF of the PAPR and INP provides a direct insight on the power fluctuations of the signal. As mentioned above, satellites often operate with very low IBOs. The PAPR reduction brought by the SC-OFDM modulation with respect to OFDM is thus not sufficient to transmit without saturation. It is thus of great interest to quantify and compare the impact of the saturation on those modulations. The saturation of the incoming signal by the PA introduces within the signal bandwidth interference that can be assimilated to an additional noise. The impact of the PA non-linearity on the modulation itself (independently from channel coding) is commonly evaluated using the modulation error ratio (MER). The MER basically measures the level of noise introduced by the degradation onto the demodulated constellation samples. The MER is defined in dBs as follows:

$$MER = 10 \log_{10} \frac{P_{signal}}{P_{error}}, \quad (25)$$

where  $P_{error}$  is the RMS power of the error vector, and  $P_{signal}$  is the RMS power of ideal transmitted signal. Note that the MER is closely related to the error vector magnitude (EVM) [18]. The MER was measured for two power amplifiers, an ideal clipper and the linearized TWTA amplifier as used in DVB-S2 [5]. Figure 56 and Figure 57 display the result of the evaluation of the MER respectively for the ideal clipping and linearized TWTA PAs with the following parameters: QPSK,  $M=512$  (modulation),  $N=420$  (spreading), oversampling factor equal to 4.

The MER evaluation confirms that the SC-OFDM is significantly more robust than the OFDM to saturation with a gain of ~3 dBs. The MER evaluation also shows that the TR method does not bring a significant improvement in a satellite environment, i.e. with a linearized amplifier not so linear, whatever the IBO. Even with an ideal amplifier and for small IBO (less than 5 dB), TR does not bring any improvement over OFDM and remains less robust than SC-OFDM.

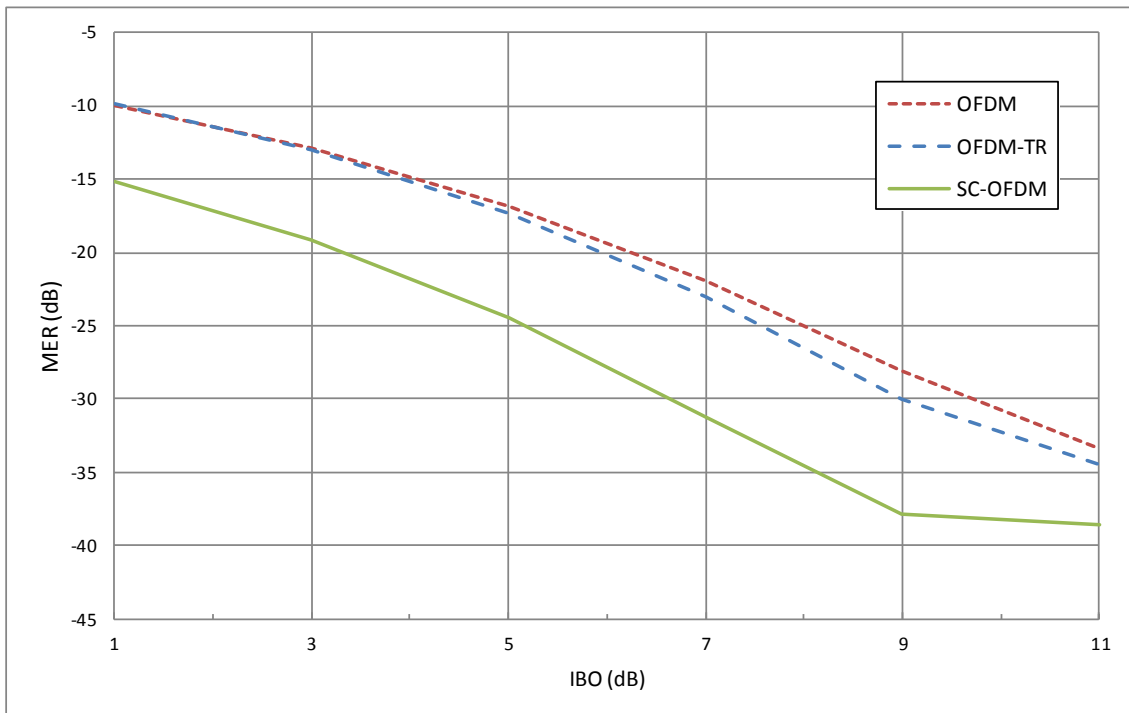


Figure 56: MER for SC-OFDM, OFDM and OFDM-TR – linearized TWTA PA.

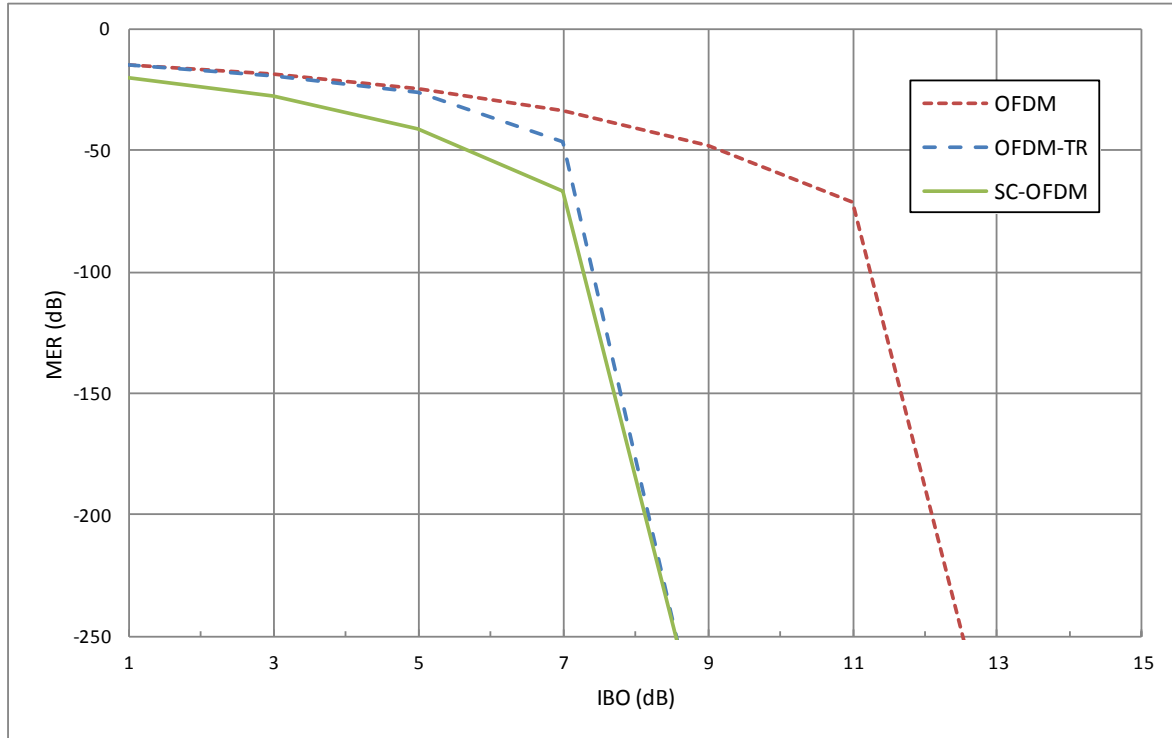


Figure 57: MER for SC-OFDM, OFDM and OFDM-TR – Ideal clipping PA.

#### 5.4.6 Bit error rate (BER) and total degradation (TD)

When dealing with coded modulations, it is common to evaluate performance in terms of bit error rate (BER) with respect to the signal-to-noise ratio (SNR). In the present case, the objective is to evaluate the losses due to the PA non-linear effects in comparison with the ideal case (linear PA without saturation). As previously explained, a PA should ideally be operated close to its saturation point. Assuming a perfect amplifier, the application of an IBO means that the SNR shall be IBO dBs larger to reach the reference level of performance. In practice, it is obviously not possible to increase the SNR - the application of a given IBO actually results in a reduction of the transmitted power and thus of the coverage. Moreover, the AM/AM response of real power amplifiers is not perfectly linear especially close to the saturation region and the actual loss in SNR is given by the OBO associated to the IBO. The OBO thus represents the first cause of in-band degradations when dealing with non-linear PAs. The second cause of degradation is the in-band noise introduced by the saturation applied onto the incoming signal. It is common to evaluate this degradation as the loss in SNR for a given reference value of target BER between the non-linear amplifier and an ideal linear amplifier for a given output back-off OBO [15]:

$$TD = OBO + [SNR_{PA} - SNR_{linear}]_{BER_{ref}} = OBO + \Delta SNR. \quad (26)$$

When the back-off is high, there is virtually no in-band distortion and thus no distortion-related BER loss ( $\Delta SNR \ll OBO$ ). When working at low OBO, in-band distortions increase,  $\Delta SNR$  loss is important and becomes the predominant term in the total degradation. There is an optimal working point  $I_{opt}$ , which ensures a compromise between OBO and  $\Delta SNR$  and yields a minimum total degradation.

Figure 58 and Figure 59 respectively depicts the BER performance of the OFDM and SC-OFDM modulations assuming an AWGN channel and the linearized TWTA amplifier model. The simulation parameters are given in Table 26 below.

Modulation	OFDM	SC-OFDM
Constellation	QPSK	QPSK
Channel coding	LDPC 16k, 4/9	LDPC 16k, 4/9
FFT size	2048	512
Guard Interval	1/32	1/32

**Table 26: Parameters for BER and TD simulations**

The BER is given for a set of IBOs as a function of a reference  $E_b/N_0$  i.e. the one that will be measured with a linear PA with the same gain operated at the saturation point of the actual PA or equivalently with no amplifier considering that the PA model is normalized in power with a unitary gain for IBO=0. This representation enables to directly measure the combined effect of the OBO and interference noise. The total degradation is simply given by the shift between the ideal reference curve and the measured curve. The Total Degradation for a BER value of  $10^{-5}$  has been extracted from those evaluations as shown on Figure 60. In order to distinguish the impact of the OBO against the one of the saturation noise, Figure 60 also depicts the OBO as a function of the IBO.

It appears from these curves that the optimum IBO for the OFDM is 2 dB leading to a TD of 2.95 dB while the optimum IBO for the SC-OFDM is 1 dB leading to a TD of 1.35 dB. This shows that the SC-OFDM enables operating closer to the saturation point than the OFDM, thus improving the power efficiency of the amplifier for a reduced consumption or an increased coverage. In addition, this comes with a TD smaller of 1.6 dB in favor of SC-OFDM, which means the ability to increase the coverage for a given level of performance.

The results have been given so far under the assumption of a QPSK modulation alphabet. Figure 61 compares the total degradation measured in the case of the QPSK and 16QAM. Due to its higher PAPR, 16QAM requires an IBO greater than 1 dB with a TD of 2.1 dB, logically but not significantly greater than what can be obtained in QPSK.

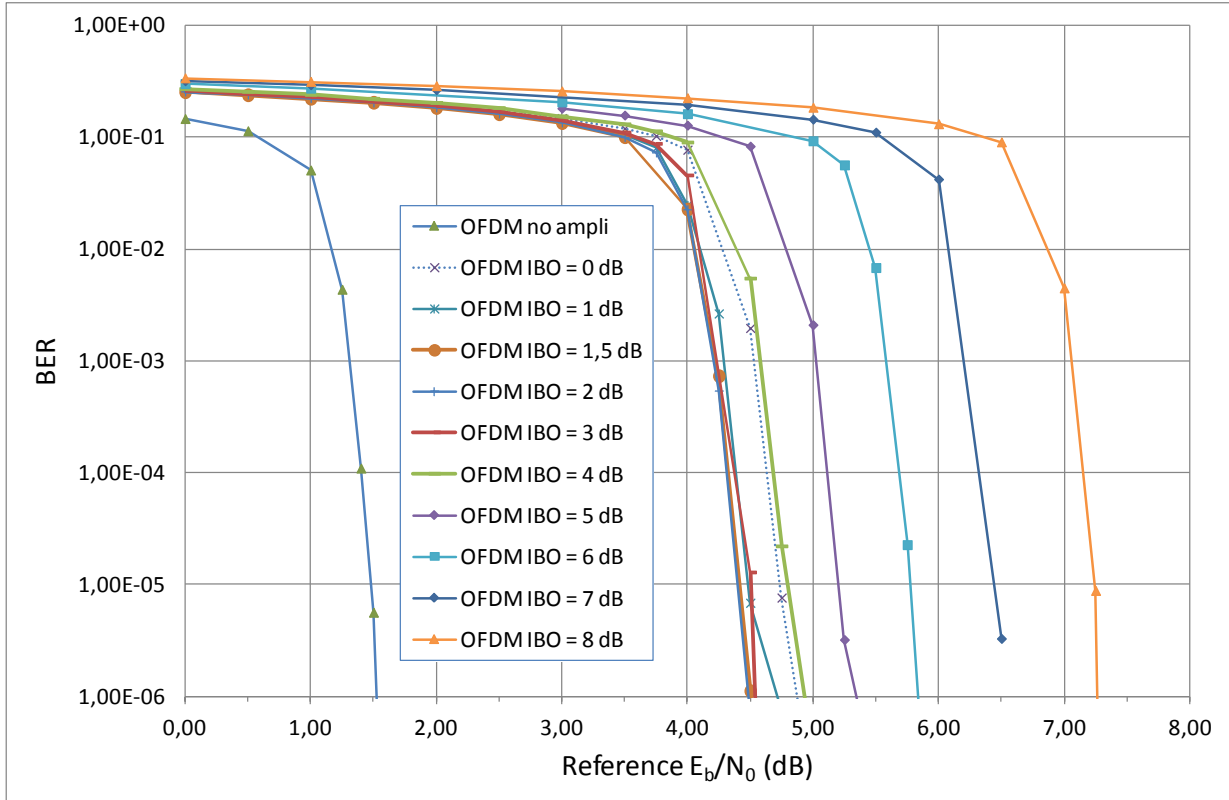


Figure 58: BER performance – OFDM.

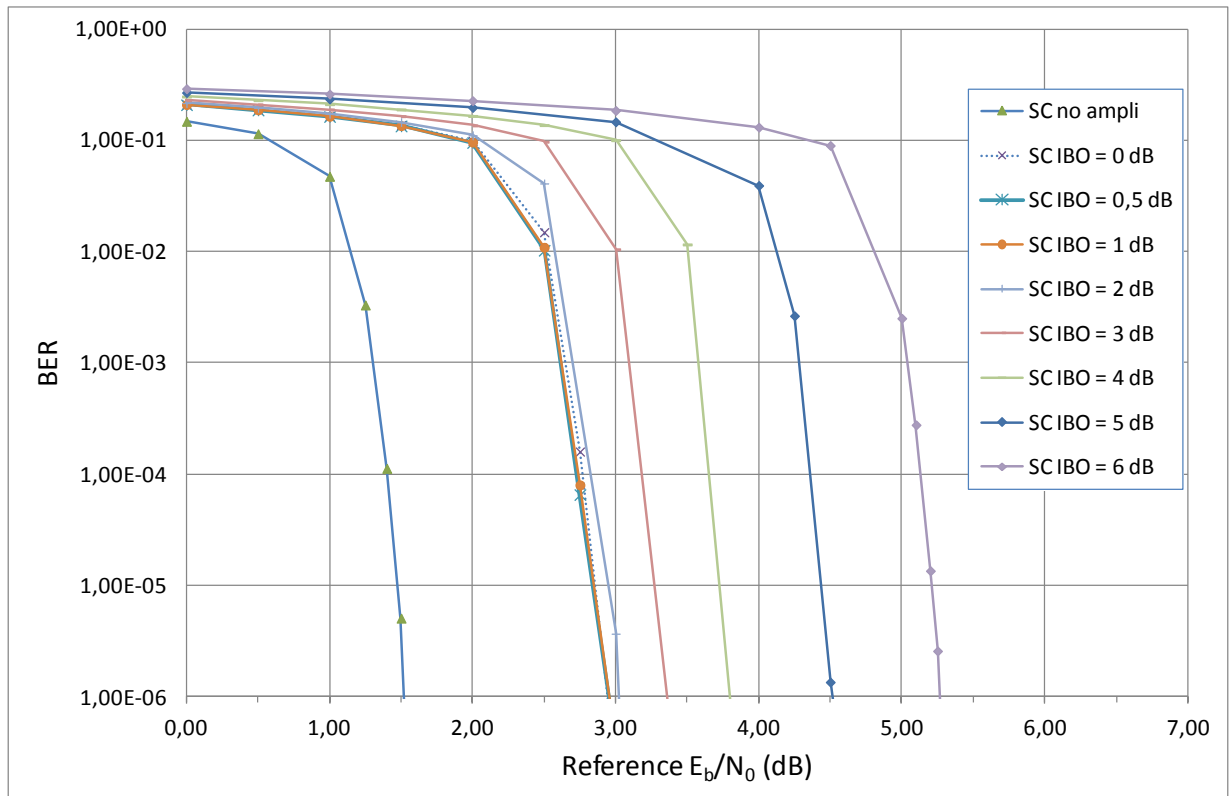


Figure 59: BER performance – SC-OFDM.

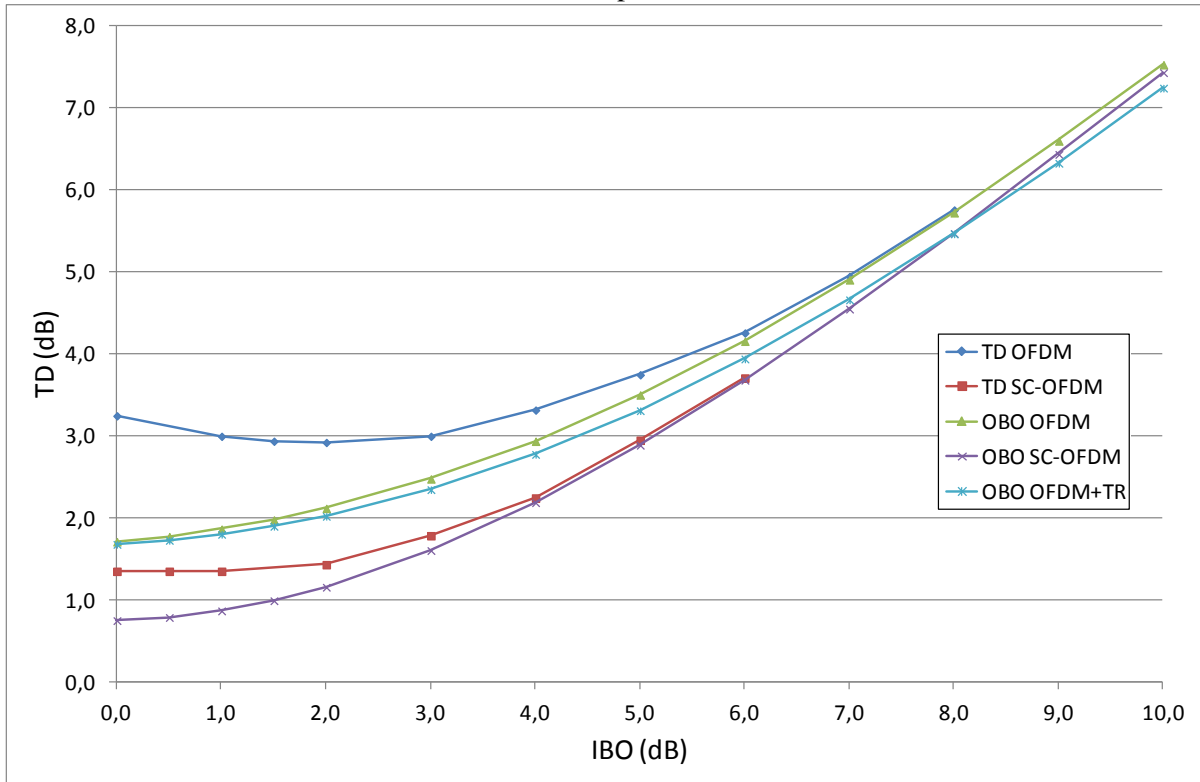


Figure 60: Total degradation and OBO performance.

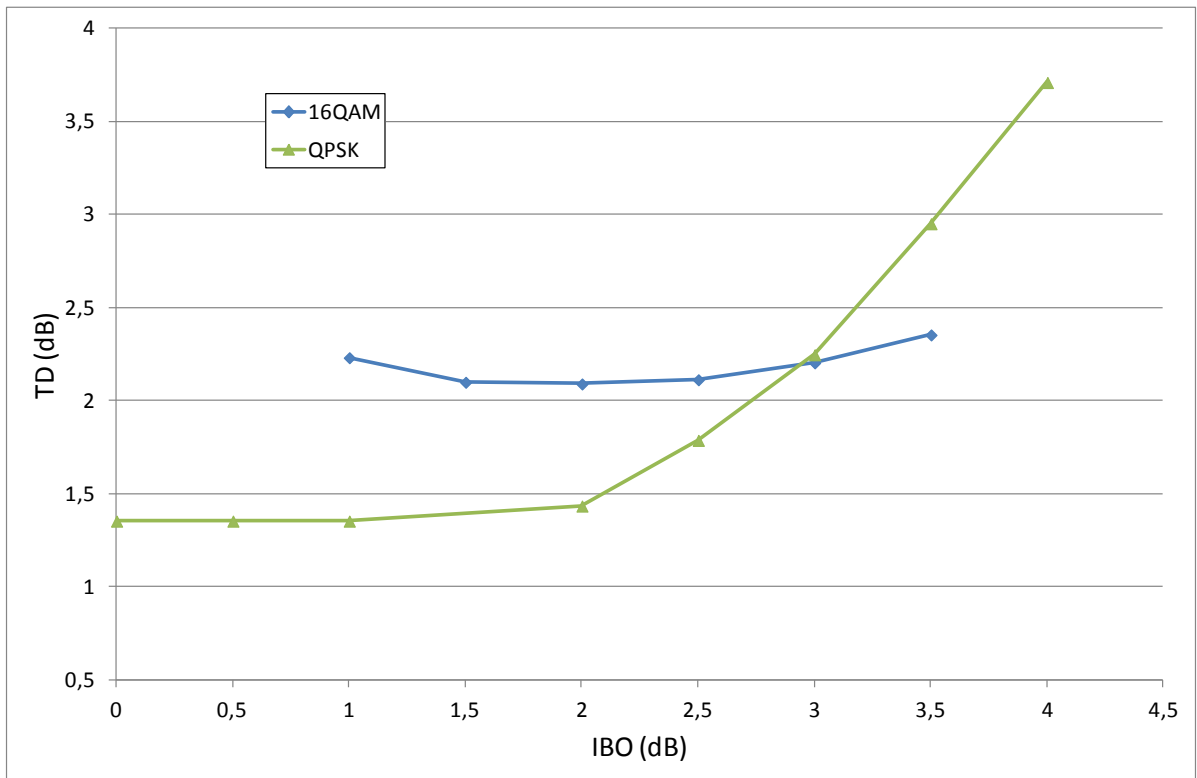


Figure 61: Total degradation and OBO performance - Linearized TWTA PA, AWGN channel – 4/9, LDPC 16k, NFFT = 512, M = 432, GI = 1/32.

### 5.4.7 Doppler performances

As mentioned in the DVB commercial requirements, DVB-NGH networks are expected to support moving terminals for speeds up to 350 km/h. The requirement applies to the satellite segment and thus to the SC-OFDM modulation. The SC-OFDM has been evaluated by simulation using the Land Mobile Satellite (LMS) model from CNES as described in [19] for an elevation angle of  $40^\circ$  (Rice fading with  $K=5$ ). The simulation parameters are given in Table 27.

The pilot pattern inserted for channel estimation is the PP9 scheme, the only one supported for SC-OFDM satellite transmissions. Figure 62 depicts the result of the BER evaluation for 3 different speeds: 100, 500 and 1000 km/h. Figure 62 confirms the robustness of the SC-OFDM modulation to Doppler degradations with a degradation of  $\sim 2$  dB for a speed of 100 km/h and 3.5 dB for 1000 km/h. Those results are provided without taking into account the gain of 30% typically obtained when considering an elevation angle of  $40^\circ$  for the satellite. SC-OFDM actually behaves closely to OFDM with respect to Doppler in the satellite channel that does not show a lot of frequency selectivity. The support of high speeds here is due to use of a 512 sub-carriers multiplex and the occurrence of the specular component that enables to perform an efficient AFC.

**Table 27: Parameters for Doppler simulations.**

Parameter	Value
Carrier Frequency	2.2 GHz
Bandwidth	5 MHz
FFT size	512
Guard Interval	1/32
Constellation	QPSK
Channel coding	LDPC R = 4/9
Time interleaving	100 ms

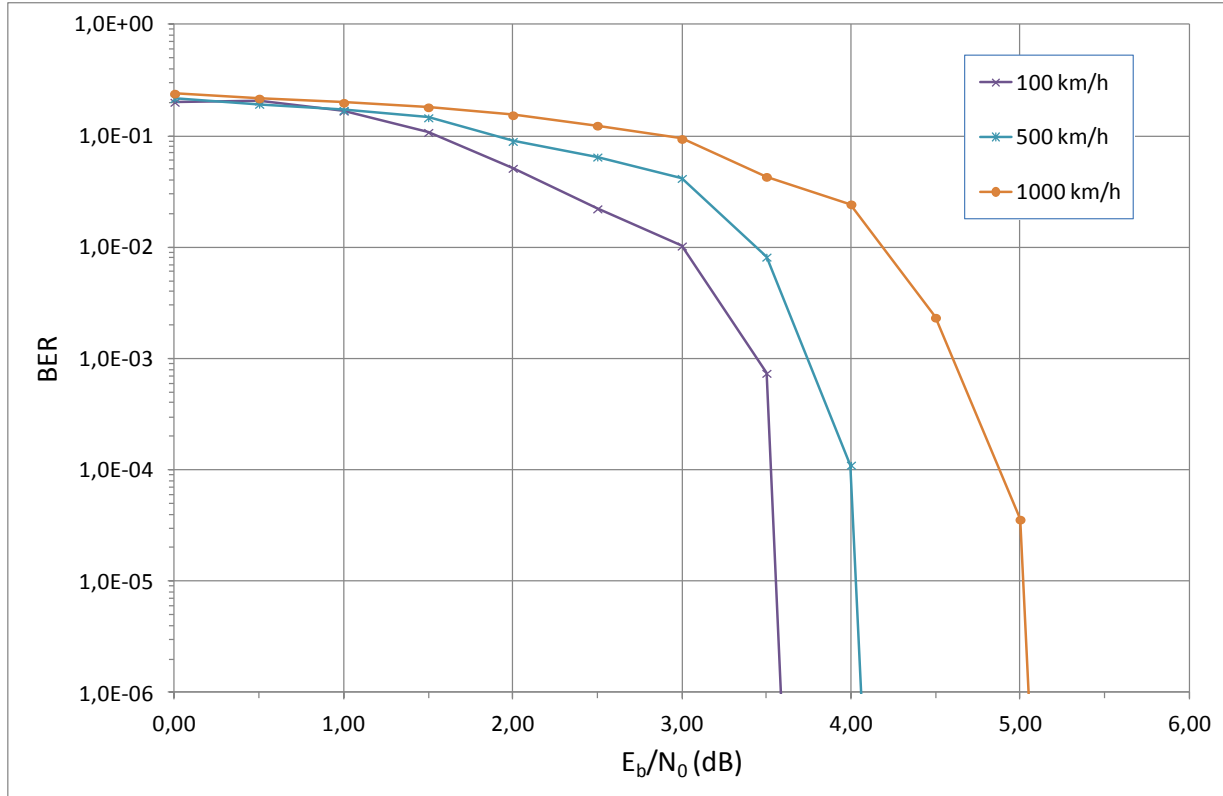


**Figure 62: Doppler performance of the SC-OFDM modulation.**

### 5.4.8 MIMO performances

As mentioned in Section 5.3.3, a  $2 \times 2$  spatial multiplexing scheme can be used to perform a MIMO SC-OFDM transmission from the satellite in the hybrid MFN context. The common assumption for Rate 2 MIMO in DVB-NGH is the enhanced SM (eSM) scheme where a rotation precoding matrix is applied onto the reference SDM scheme. This scheme was not selected for SC-OFDM transmissions as it breaks the PAPR properties of the modulation. This is shown on Figure 63 that depicts the MER of the transmitted SC-OFDM signal after passing through the linearized TWTA PA model. The simulations have been performed for a 5 MHz bandwidth, a FFT size of 512 points, in QPSK and two angles for the eSM scheme,  $22^\circ$  and  $45^\circ$ . The MER curves show that for the IBO of interest (1 dB), an eSM with an angle of  $22^\circ$  (resp.  $45^\circ$ ) brings a MER degradation of about 1.1 dB (resp. 1.6 dB).



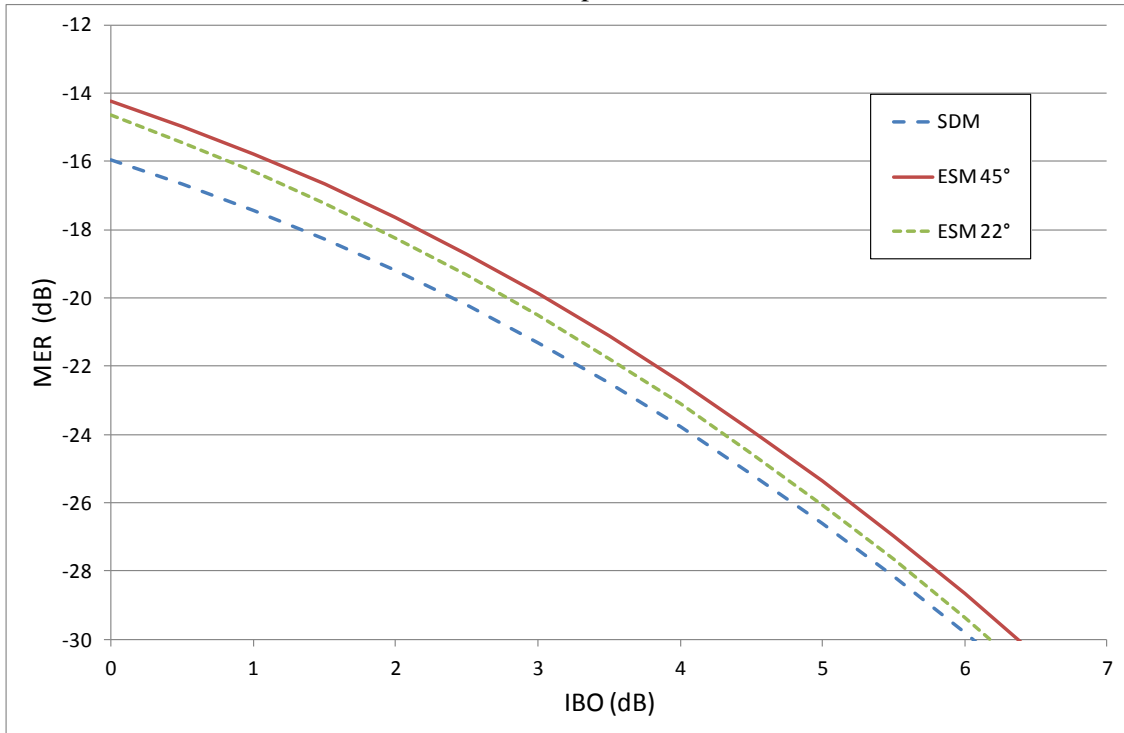


**Figure 63: MER for eSM and SDM schemes.**

The actual performance of the SM scheme on the SC-OFDM has been evaluated by simulation with a modified version of the BBC channel model [20]. The BBC model is a simple hybrid 4×2 SFN model. It has been modified to obtain a 2×2 sheer satellite model with the following parameters:

- Counter-rotating circular polarization.
- Single-tap Ricean variable  $K = 5$ .
- Satellite cross-polar discrimination:  $\alpha = 2$ .

Figure 64 depicts the BER performance assuming a speed of 60 km/h, perfect channel estimation and a simple MMSE MIMO decoding. The SM scheme brings a degradation of only ~0.5 dB with respect to the ideal two SISO parallel transmissions. In comparison to a 16QAM SIMO transmission, the SM scheme provides about 1.9 dB of improvement for the same spectral efficiency. Those results are actually close to the ones obtained in OFDM, when no power amplifier is used.

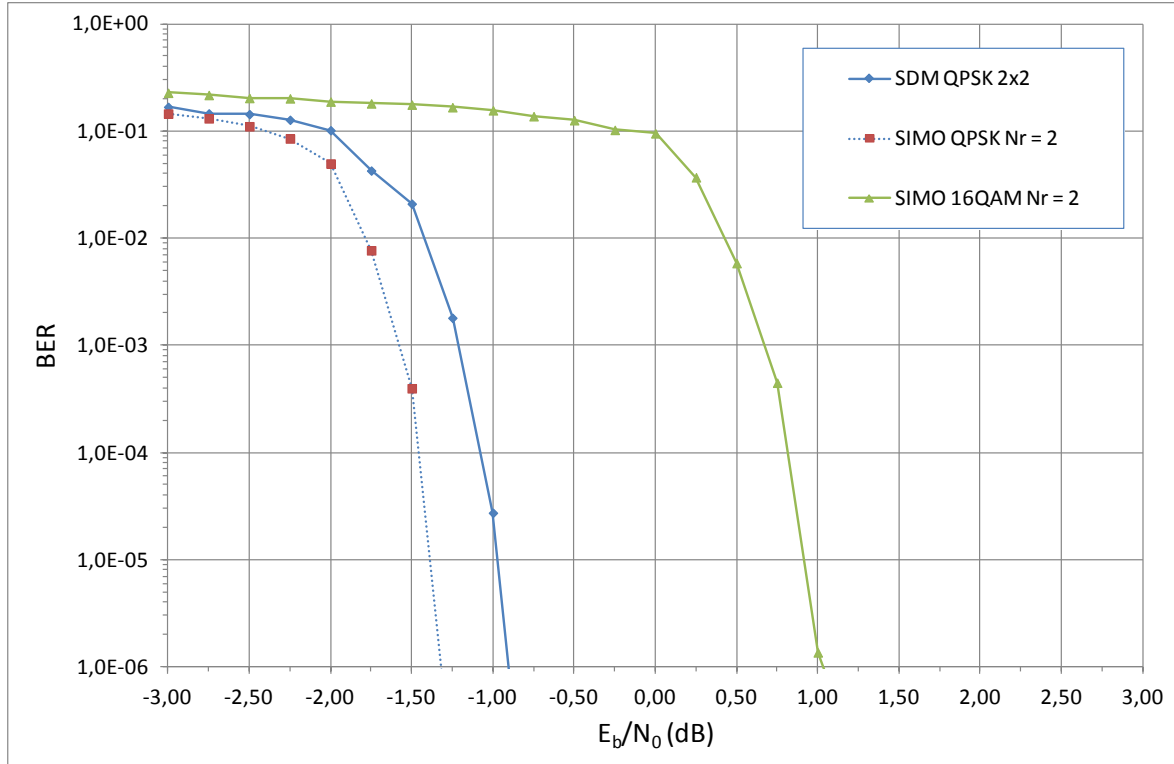


Figure 64: BER performance for the SM scheme in SC-OFDM.

Table 28: Parameters for MIMO SM simulations.

Parameter	Value
Carrier Frequency	2.2 GHz
Bandwidth	5 MHz
FFT size	512
Guard Interval	1/32
Constellation	QPSK
Channel coding	LDPC R = 4/9
Time interleaving	1 s

## 5.5 Conclusion

This chapter was dedicated to the new waveform selected to implement the transmissions on the satellite link of the DVB-NGH standard, namely the single carrier-orthogonal frequency division multiplexing (SC-OFDM) modulation. This introduction to the SC-OFDM waveform was conducted according to three perspectives. The SC-OFDM is first compared to the two other modulations commonly used for satellite transmissions, the TDM and OFDM waveforms. It is shown that the SC-OFDM modulation enables keeping the low power fluctuations of TDM signals while benefiting from the flexibility and high spectral efficiency of the OFDM modulation. The chapter then focuses on the intrinsic robustness of the SC-OFDM modulation



## Technical Report TR4.2

to the Power Amplifier non-linear degradations with the ability to operate with a reduced OBO in comparison to OFDM and a total degradation improved by 1.5 dB. It is thus possible to improve the power efficiency of the PA while improving the coverage. It must be pointed out that this result still holds when considering the PAPR reduction solutions such as the Tone Reservation approach used in DVB-T2. This kind of solution actually performs well for large IBOs but not for the small IBOs (a few dBs) commonly used in satellite transmissions. In a third wing, the chapter shows that the SC-OFDM behaves similarly to OFDM when it comes to compensate for the degradation due to the channel and mobility, either in SISO or MIMO. These results clearly demonstrate the interest of the SC-OFDM modulation in the context of satellite transmissions.

## 6 SYNCHRONIZATION IN THE SATELLITE CONTEXT – APPLICATION TO THE SC-OFDM WAVEFORM

This chapter deals with synchronization in the satellite context with application to the SC-OFDM waveform adopted along with pure OFDM for the satellite link of the NGH Hybrid Profile. Just like in DVB-T2, data is transmitted as frames starting with the so-called P1 symbol [10], [11]. This symbol is meant to serve for the synchronization of the receiver. After a short remainder about the SC-OFDM modulation already described in Section 5, this section briefly introduces the most common synchronization algorithms as described in the literature. A comprehensive set of new algorithms is then described in details with their respective performances. The impact of these algorithms on SC-OFDM transmissions is finally evaluated in terms of bit error rate (BER) for different propagation channels.

### 6.1 SC-OFDM waveform

The waveform considered in this section is the SC-OFDM modulation retained as a solution along with pure OFDM for the satellite link in MFN configurations. The NGH standard specifies a set of system parameters covering the different needs for SAT transmission. We focus here on a specific configuration:

- Carrier frequency = 2.2 GHz
- Bandwidth = 5 MHz
- FFT size = 512 sub-carriers
- Modulation = QPSK
- LDPC/BCH code rate of 1/3 or 1/2
- Pilot pattern = PP9 (See Figure 65)

According to the specification for the size of the de-interleaving buffer, the time interleaving can vary between 0.2 second up to several seconds.

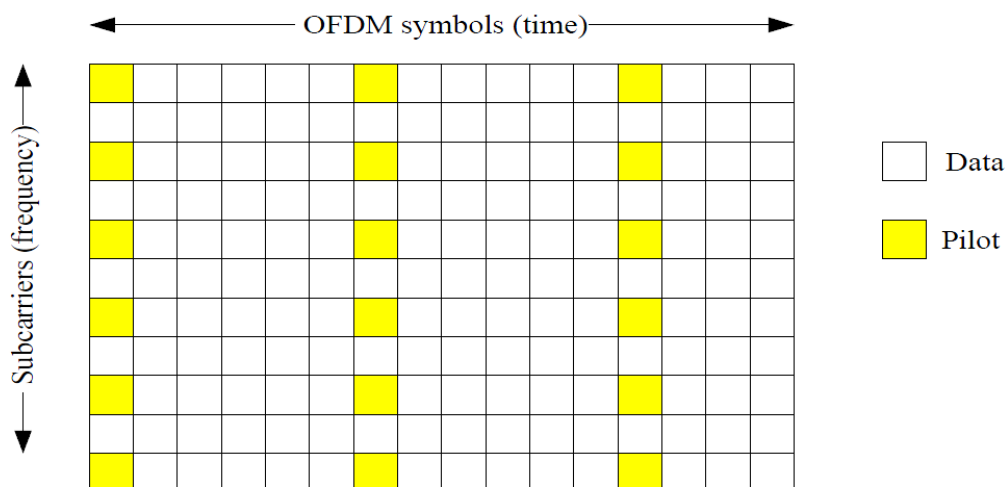


Figure 65: PP9 pilot pattern for SC-OFDM transmission.

Transmission occurs according to the frame format for SC-OFDM as described in the NGH standard. It is supposed here that the frame is made of one P1 symbol, one P2 symbol (where L1 signaling is carried within a PP9 hybrid symbol) and 61 blocks of six SC-OFDM symbols terminated by a PP9 reference symbol (thus leading to a total of 367 SC-OFDM symbols).

## 6.2 State of the art

DVB-T2 introduced a special frame structure for synchronization and signal acquisition. The P1 symbol is located before each data frame and its first purpose is to allow for the fast recognition of the T2 signals (or signal present in the FEFs). The P1 contains signaling data providing the transmission type and basic transmission parameters needed by the receiver to be able to process the remaining part of the data frame. The P1 symbol is also meant to allow for the robust acquisition of the time and frequency synchronizations. The remaining part of the present section focuses on the mechanisms used for P1 detection and time/frequency synchronization. A number of algorithms are presented along with performance simulation results for various propagation channels.

### 6.2.1 P1 symbol

The P1 symbol is a 1K OFDM symbol with two guard intervals (C and B) that are frequency shifted in order to enable the receiver to distinguish this preamble from conventional multi-carrier symbols with a standard cyclic prefix [10], [11]. The general structure of the P1 symbol is depicted on Figure 66 and Figure 67.

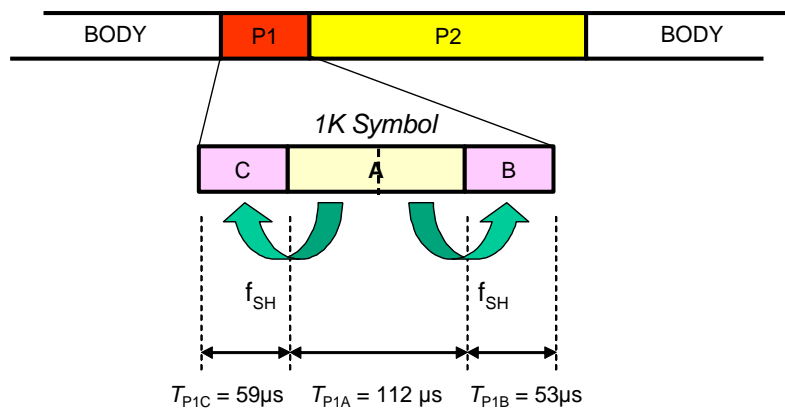


**Figure 66: P1 symbol structure in the time domain.**

All the useful carriers of the 1K symbol are not used. About a half of them are set to zero in order to facilitate the detection of the P1 symbol even with a large frequency offset (up to 500 kHz). The 384 active carriers are used to code 7 bits of information leading to 128 different P1 symbols.

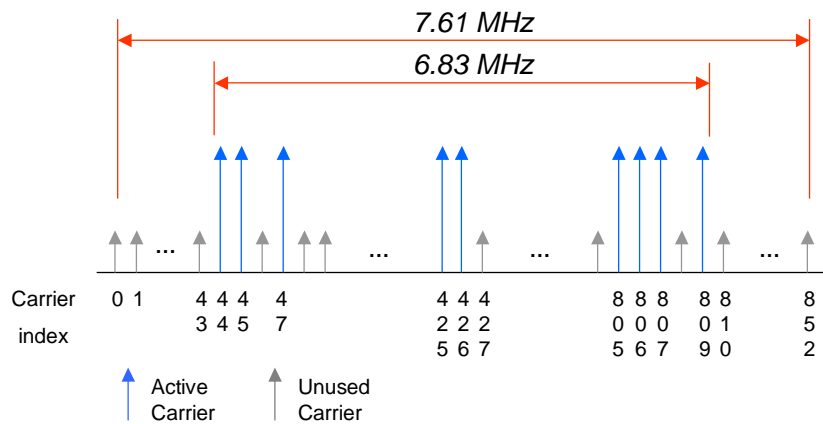


**Figure 67: P1 symbol structure in the frequency domain (only the A part).**

The DVB-T2 implementation guidelines [11] suggest a technique for time and frequency synchronization, exploiting the correlation among the main part of the received P1 symbol and the two guard intervals. This approach allows for a robust acquisition of the time and frequency synchronization. For better performance, a refined synchronization may be needed. Figure 68 below presents an example of simple synchronization mechanism only based on the correlation of P1 symbol.

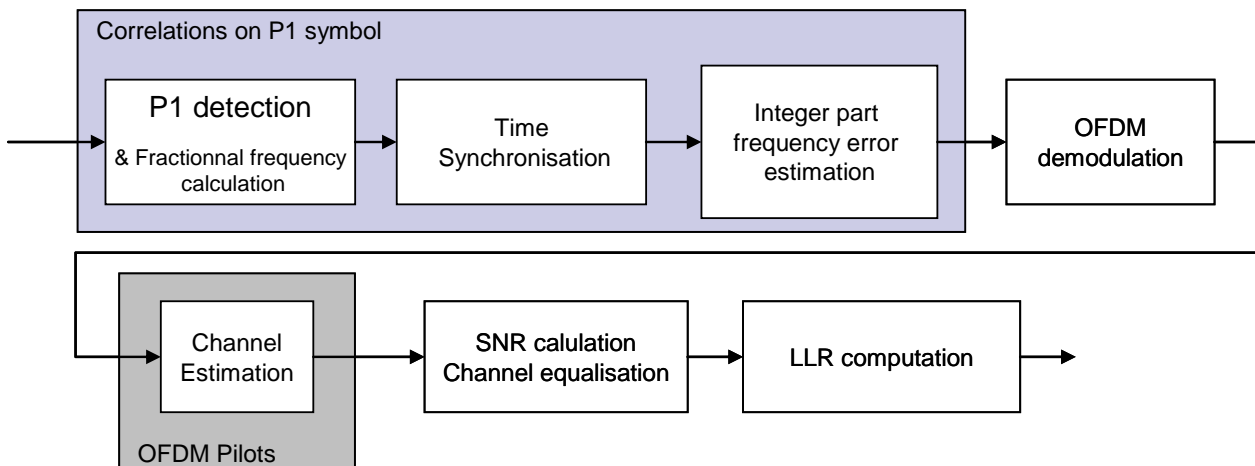


**Figure 68: Typical architecture of a DVB-T2/NGH receiver.**

The receiver starts by performing the detection of the P1 symbol. The detection algorithm provides an estimation of the fractional part of the frequency error and a coarse estimation of the start of the P1 symbol (plus or minus a few samples at high SNR and plus or minus hundreds of samples at very low SNR). It is then possible to evaluate the integer part of the frequency error using the knowledge by the receiver of the specific positions of the modulated and null subcarriers in the P1 symbol. Following the frequency synchronization, the time synchronization is performed and aims at finding the exact position of the first sample in the received P1 symbol (it is performed by correlation). After completion of these algorithms, the signal is synchronized in time but a residual frequency error may still be present and degrade the channel estimation mechanism. Indeed in order to have good channel estimation, an average in time is performed and the residual frequency error may cause the phase of the signal to vary too much during the time averaging.

In order to guaranty a reasonable low residual frequency error, an additional algorithm is used to obtain a fine frequency synchronization using the pilot of the hybrid symbols. This algorithm requires that the initial frequency error does not make the phase rotate more than  $2\pi$  between two hybrid symbols. In order to enhance the performance on propagation channel of type LMS ITS, it is possible to add an estimation of the frequency error after the time synchronization and before the fine frequency synchronization.

### 6.2.2 P1 detection

As described in DVB-T2 guidelines, the detection of P1 can be performed using the algorithm described on Figure 69 by calculating the correlation over the central symbol A with its 2 guard intervals B and C.

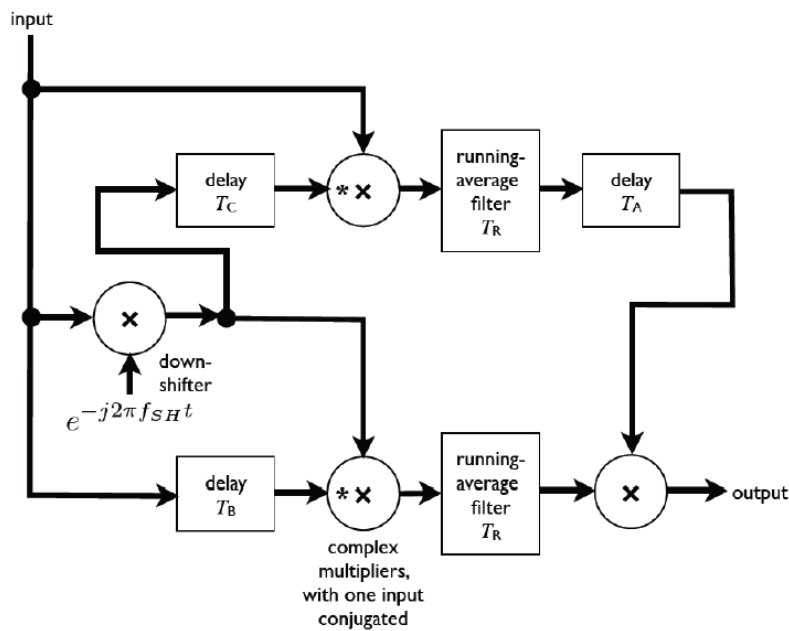


Figure 69: Block diagram of a P1 detection algorithm.

As shown on Figure 70, the correlation between A and B gives a complex pulse whose magnitude is a trapezoid of base  $(T_A+T_B)$  and top  $(T_A-T_B)$ .

The correlation between A and C gives also a trapezoid of base  $(T_A+T_C)$  and top  $(T_A-T_C)$ .

The two trapezoids are then multiplied together and a coarse estimation of the P1 symbol position is given by the center of the resulting trapezoid while the fractional part of the frequency offset is given by its argument.

The detection of a valid detection trapezoid can be obtained by defining an adequate threshold.

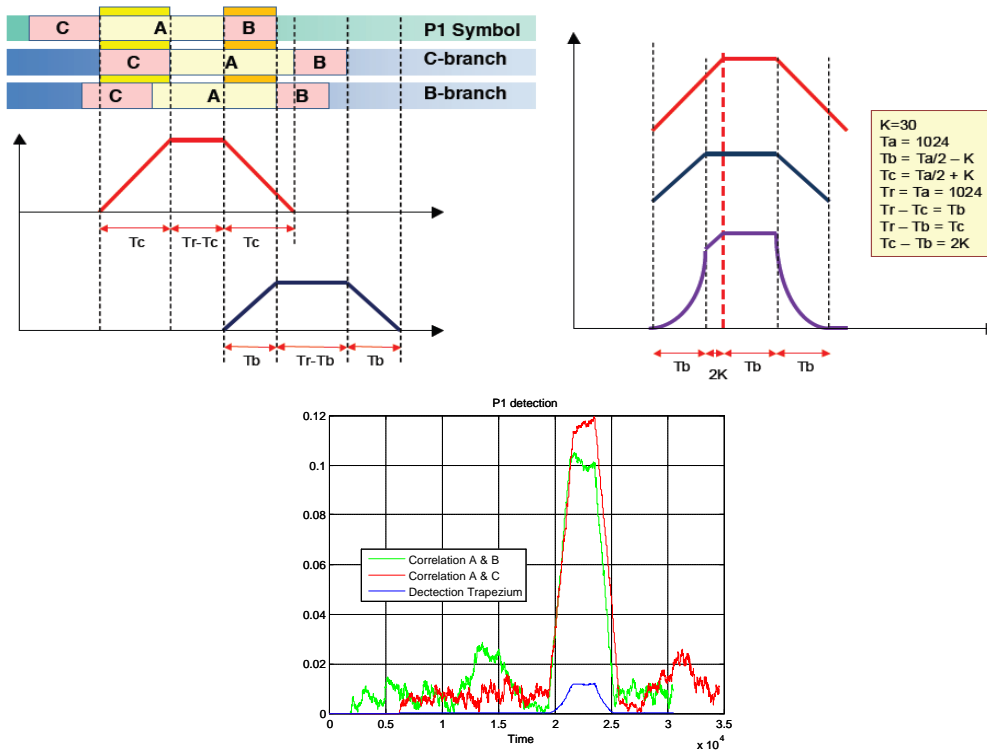


Figure 70: Principle of the correlation algorithm for P1 detection.

### 6.2.3 Fine time synchronization

At the output of the correlation, a coarse estimation of the start of P1 is obtained. The fine synchronization consists in estimating the sample corresponding to the start of the P1 symbol.

It is assumed that the receiver stores in memory the “X128” symbol corresponding to the “average” of the 128 possible P1 configurations.

Considering an oversampling factor (OVF) of 4, the X128 symbol is composed of 8192 samples. The fine synchronization is performed by correlating the input stream with the X128 symbol. The P1 symbol being composed of 8192 samples, the correlation for one position is rather time/resource consuming but also robust towards noise.

Unfortunately, any frequency error decreases the strength of the correlation peak that can vanish if the frequency error is greater or equal to the subcarriers interval. Alternatives to be more robust to frequency errors are:

- Perform the correlation with the module of X128 and the received signal. This solution is insensitive to frequency error but less robust to noise.
- Perform the frequency synchronization prior to the time synchronization.



## 6.2.4 Estimation of the integer part of the frequency error

The correlation performed during P1 detection provides an estimate of the fractional frequency error. The integer part is then to be determined. The P1 symbol that is composed of 384 active sub-carriers over 1024 is aimed at enabling this synchronization. The integer part is obtained by performing the correlation between:

- The FFT of P1 symbol without the guard intervals (that is to say the “A” part of P1 that is a 4096 points FFT considering an oversampling factor of 4).
- A reference vector of 1024 “zeros” except at the position of the active sub-carriers.

Just like for time synchronization:

- If a complex correlation is performed (that is to say the active subcarriers of the reference vector have the value +1 or -1), good time synchronization is needed to obtain a clear correlation peak.
- If the correlation is made using the modules (that is to say the active subcarriers of the reference vector have the value +1), the correlation is robust towards time synchronization errors but more sensitive to noise.

## 6.2.5 First estimation of the residual frequency error

The fractional frequency error is first estimated during P1 detection. In certain cases, this estimation is not precise enough to estimate the residual frequency error between the hybrid symbols because of a low SNR.

If the SNR increases over a NGH frame, e.g. in the case of the LMS ITS channel, the LLR provided by the decoder may be high (because the SNR is high) but with an erroneous sign (because of the residual frequency error that has not been corrected). This could lead to errors in reception despite the fact that the average SNR on the transmission is high enough to be error free.

In order to solve this issue, an additional fine frequency estimator can be implemented after the time synchronization stage and before the frequency error estimation on the pilot symbols. This estimator needs to know which P1 symbol among the 128 possible values has been received. The 8192 sample of the received P1 are correlated with the P1 symbol stored in memory of the receiver. The P1 samples without noise can be written as:

$$P1 = [|P1_1| e^{j(Arg(P1_1)+2\pi df 1+\phi_0)} \quad \dots \quad |P1_{8192}| e^{j(Arg(P1_{8192})+2\pi df 8192+\phi_0)}]. \quad (27)$$

After multiplying by its conjugate defined as:

$$P1^* = [|P1_1| e^{-j(Arg(P1_1))} \quad \dots \quad |P1_{8192}| e^{-j(Arg(P1_{8192}))}], \quad (28)$$

we obtain:

$$|P1|^2 = [|P1_1|^2 e^{j(2\pi df 1+\phi_0)} \quad \dots \quad |P1_{8192}|^2 e^{j(2\pi df 8192+\phi_0)}]. \quad (29)$$

The first 4096 correlation products are then correlated with the last 4096 correlation products, and a 4096 sample vector is obtained:

$$[|P1_1|^2 |P1_{4097}|^2 e^{-j(2\pi df 4096)} \quad \dots \quad |P1_{4096}|^2 |P1_{8192}|^2 e^{-j(2\pi df 4096)}], \quad (30)$$

The frequency error  $df$  is obtained as the argument of the sum of this 4096 correlation product.

## 6.2.6 Estimate of the residual frequency error

After the P1 synchronization, time and frequency synchronization is obtained, however a residual frequency error remains. After synchronization, the channel estimation is performed using the PP9 pilot symbols as follows:

- The channel is evaluated for each pilot,
- The channel is filtered and an interpolation is performed to obtain an estimate of the hybrid symbols over all the subcarriers,
- For each subcarrier, the channel is averaged in time over  $N$  hybrid symbols,
- For each subcarrier, a linear interpolation is made of the channel between two hybrid symbols.

In complex notation, the frequency is equivalent to the rotation velocity of the phase. If the frequency error is greater than  $1/2N$ , the phase turns more than  $\pi$  radians over  $N$  hybrid symbols, and consequently the channel estimation is biased at step 3 when the channel estimate is averaged over  $N$  hybrid symbols. It is needed to add an estimator capable of reducing the residual frequency error.

Recall that the PP9 pilot symbols are spread every  $K=6$  SC-OFDM symbols. The residual frequency error is less than the inverse of the period of the hybrids symbols. It is assumed that between two hybrid symbols the phase of the signal does not rotate more than  $\pi/2$  (See Figure 65). The difference of the signal is equivalent to the rotation velocity of the phase. The frequency  $\delta k$  is then estimated by differentiating the phase divided by the time between the pilots  $P$  of two consecutive hybrid symbols:

$$\delta k \approx \frac{1}{2\pi} \frac{1}{KN_{FFT} \left(1 + \frac{1}{GI}\right)} \text{Arg} \left( E \left\{ P_k^* P_{k+1} \right\} \right), \quad (31)$$

where  $E \left\{ P_k^* P_{k+1} \right\}$  is the correlation between  $N_p$  pilots of the hybrid symbols  $k$  and  $k+1$ :

$$E \left\{ P_k^* P_{k+1} \right\} = \frac{1}{N_p} \sum_{i=1}^{N_p} P_{k,i}^* P_{k+1,i}, \quad (32)$$

In order to have an accurate estimation, it is needed that between 2 hybrid symbols, the signal phase rotation is lower than  $\pi/2$ , i.e.:

$$\left| df - \hat{df} \right| < \frac{1}{2 T_{symp} K \left(1 + \frac{1}{GI}\right)}, \quad (33)$$

with  $T_{symp}$  SC-OFDM symbol time in the guard interval.

## 6.3 Improvement of the P1 detection

This section describes algorithms that aim at improving the performance of SC-OFDM synchronization.

### 6.3.1 Filtering prior to P1 detection

In the case of a dynamic Rice channel, the SNR can drop dramatically and reach values below -10dB. In order to increase the chance of a correct P1 detection in this case, the samples are filtered prior to the correlation. The filter is used for data demodulation; it only aims at removing the noise out of the useful band. Considering that the 384 active subcarriers of P1 start at index 44 and end at index 809, the bandwidth of the filter is, assuming an oversampling factor of 4 by symbol:

$$B = \frac{809 - 44}{1024 * 4} \approx 0,187, \quad (34)$$

Thus leading to a gain of  $10 \times \log_{10} 0.187^{-1} \approx 7dB$  on P1 detection.

### 6.3.2 Detection threshold computation

This section describes a possible threshold calculation for the P1 detection algorithm described in Section 6.2.2. The proposed solution is based on the following algorithm.

Considering that:

$X_1$  and  $X_2$  are two independent Gaussian variables, with null mean and standard deviation  $\sigma_X$  and variance  $\sigma_X^2$ , the following rules apply:

1. The product  $X_1 X_2$  follows a "normal product law" with standard deviation  $\sigma_X^2$
2. The sum of  $N$  variables  $Y_1 + Y_2 \dots + Y_N$ , having an arbitrary distribution, but centered and independent with standard deviation  $\sigma_X$  is a normal law of standard deviation  $\sqrt{N}\sigma_X$ , and variance  $N\sigma_X^2$
3. The Euclidian norm  $\frac{\sqrt{X_1^2 + X_2^2}}{\sigma_X}$  is a Chi distribution with two degree of freedom
4. If there is a value  $K$  and a probability  $p$  so that:

$$\Pr \left\{ \frac{\sqrt{X_1^2 + X_2^2}}{\sigma_X} > K \right\} = p, \quad (35)$$

Then:

$$\Pr \left\{ \sqrt{X_1^2 + X_2^2} > K\sigma_X \right\} = p. \quad (36)$$

The general architecture of the P1 detection algorithm is recalled on Figure 71. Let's assume that P1 is not present and the input signal  $X$  is only a white noise with zero mean and variance of  $\sigma_X^2$ .

On Figure 71,  $U$  and  $V$  are both the result of the product of two independent variables normally distributed with zero mean. They consequently have a normal product distribution of zero mean and variance  $\sigma_X^4$ .

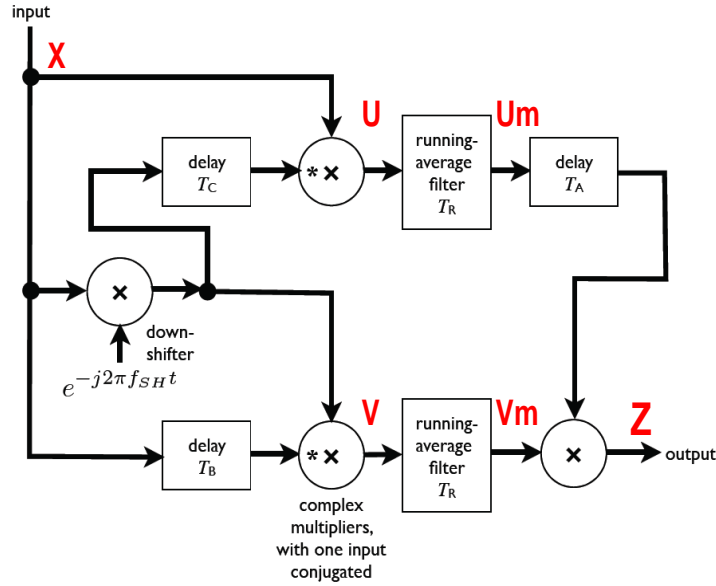


**Figure 71: Block diagram of a P1 detection algorithm.**

$U_m = \frac{1}{T_R} \sum_{i=1}^{T_R} U_i$  and  $V_m = \frac{1}{T_R} \sum_{i=1}^{T_R} V_i$  are the sum of  $T_R$  independent variables  $U_i$  divided by  $T_R$ . According to the axiom 2 in the above theorem,  $U_m$  and  $V_m$  can be modeled as centered Gaussian variables of standard deviation  $\sigma_{U_m} = \frac{1}{T_R} \sqrt{T_R} \sigma_U$ , and variance  $\sigma_{U_m}^2 = \frac{1}{T_R} \sigma^2_U = \frac{\sigma_X^4}{T_R}$ .

If the input signal  $X$  is noise of variance  $\sigma^2$ , correlated with a period  $t$ :

$$\begin{aligned}
 E\{X_i X_{i-j}^*\} &= 0 \text{ if } j \geq t \\
 E\{X_i X_{i-j}^*\} &\neq 0 \text{ if } j < t
 \end{aligned}$$

$U$  and  $V$  are the result of the product of two independent variables  $X_1$  and  $X_2$ , that have the same distribution, and each auto-correlated with the same period  $t$ , so  $U$  and  $V$  are also auto-correlated with a period  $t$ :

$$E\{U_i U_{i-j}^*\} = E\{X_1(i) X_2(i) X_1^*(i-j) X_2^*(i-j)\} = E\{X_1(i) X_1^*(i-j)\} \times E\{X_2(i) X_2^*(i-j)\}, \quad (37)$$

So  $E\{U_i U_{i-j}^*\} = 0$  if  $E\{X_i X_{i-j}^*\} = 0$ , which is equivalent to  $j \geq t$ .

$U_m$  is the result of the sum of  $T_R$  variables, that can be divided in  $T_R/t$  sub-groups of independent variables:

$$U_m = \frac{1}{T_R} \sum_{i=1}^{T_R} U_i = \frac{1}{T_R} \sum_{i=1}^{T_R/t} \left( \sum_{j=1}^t U_{i^*t+j} \right). \quad (38)$$

The sum of  $t$  correlated variables is modeled as  $\sum_{j=1}^t U_{i^*t+j}$  by the sum of the same variable:

$$\sum_{j=1}^t U_{i^*t+j} = tU_{i^*t+1}. \quad (39)$$

The standard deviation of this sum is  $t\sigma_U$ .

Considering the axiom 2,  $U_m$  has a normal distribution of standard deviation:

$$\sigma_{U_m} = \frac{1}{T_R} \sqrt{\frac{T_R}{t}} t\sigma_U = \sqrt{\frac{t}{T_R}} \sigma_U \text{ and of variance } \sigma_{U_m}^2 = \frac{t}{T_R} \sigma_U^2 = \frac{t\sigma_X^4}{T_R}.$$

The conclusion is:

$$\text{If } X \text{ is a white noise, then } \sigma_{U_m}^2 = \frac{\sigma_X^4}{T_R}.$$

$$\text{If } X \text{ is a noise filtered by a filter of bandwidth } B = 1/t, \text{ or a signal of band } = 1/t \text{ then } \sigma_{U_m}^2 = \frac{t\sigma_X^4}{T_R} = \frac{\sigma_X^4}{BT_R}.$$

If  $X$  is the simulated DVB-NGH signal, then the band  $B$  is equal to the useful band of the signal divided by the observation band, that is to say:

$$B = \frac{N_u}{OVS \times N_{FFT}} = \frac{426}{4 \times 512}. \quad (40)$$

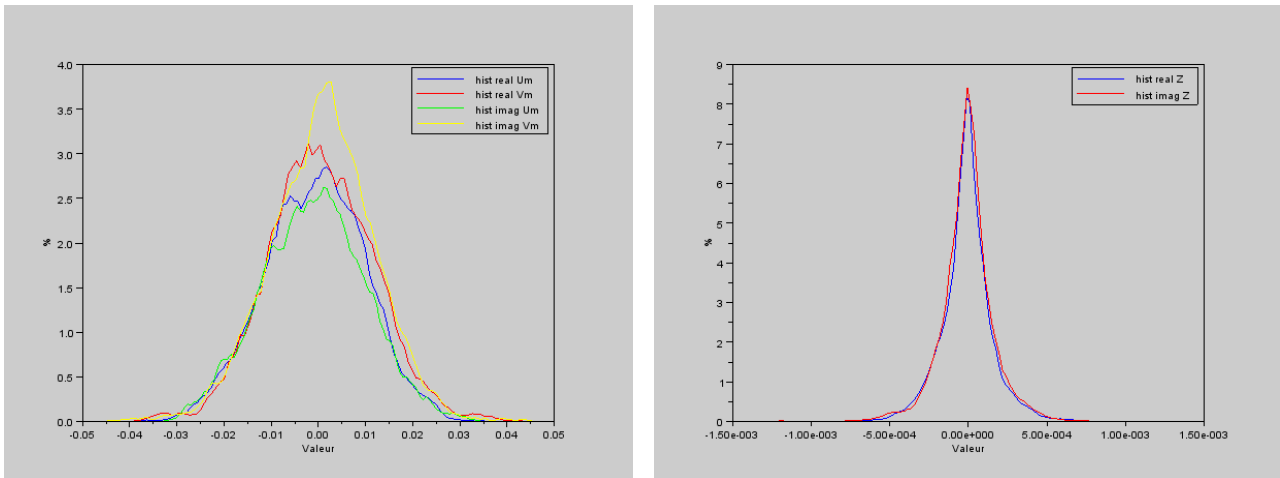


**Figure 72: For white noise in input, distribution of the output of the average filters (left) and distribution of the output of the detection algorithm.**

### 6.3.2.1 Variable threshold depending of SNR

$U_m$  and  $V_m$  are two variables with a Gaussian distribution. The variance of  $U_m$  and  $V_m$  is dependant of the power and the band of the input signal; it can easily be computed. Considering the axioms (3) and (4), it is possible to compute the threshold using  $\|U_m\|^2$  and  $\|V_m\|^2$ .

There is a probability  $p$  that  $\|U_m\|^2 > K(p)\sigma_{\text{Re}\{U_m\}}^2$  where:

1.  $K(p)$  the inverse chi-square function calculated with the probability  $p$ .
2. The variance of the real or imaginary part of  $U_m$  :  $\sigma_{\text{Re}\{U_m\}}^2 = \sigma_{\text{Im}\{U_m\}}^2 = \frac{\sigma_{U_m}^2}{2}$

The output  $Z$  of the detection algorithm is the product of two normally distributed variables  $V_m$  and  $U_m$  with zero mean and finite variance. Considering the axiom (1), the variable  $Z$  is a distribution of normal product law. In order to compute a threshold based on  $\|Z\|^2$  it is needed to know:

- The variance of  $\|Z\|^2$
- The inverse function of the cumulated distribution

As  $\|Z\|^2 = \|U_m\|^2 \|V_m\|^2$ , the threshold on  $\|Z\|^2$  is approximated like the product of the threshold on  $\|U_m\|^2$  and  $\|V_m\|^2$ .

It is assumed that  $X$ , the input signal of the P1 detection algorithm, is composed of a white noise with power  $P_n$  and a useful signal with power  $P_s$  and bandwidth  $B_s$ .

If the SNR is high, this threshold shall be high to avoid false alarm and to obtain a precise estimate of the fractional frequency error.

If the SNR is low, the threshold shall be chosen in order to maximize the chance of detecting P1.

In order to find a good compromise between the two recommendations, the proposed threshold is a combination of two values:

$$S_Z = S_Z^{\text{noise}} + S_Z^{\text{signal}} = K_n^2 \left( \frac{P_n^2}{T_R} \right) + K_s^2 \left( \frac{P_s^2}{T_R B_s} \right)^2, \quad (41)$$

with  $K_n = 5$  and  $K_s = 55$  for example.

If a filter of bandwidth  $B_F \leq B_s$  is added before the P1 detection, then the noise is not white anymore and the threshold becomes:

$$S_Z = S_Z^{\text{noise}} + S_Z^{\text{signal}} = K_n^2 \left( \frac{P_n^2}{T_R B_F} \right)^2 + K_s^2 \left( \frac{P_s^2}{T_R B_F} \right)^2, \quad (42)$$

where  $P_n$  and  $P_s$  are respectively the power of noise and signal after filtering.

Then, it is obtained that:

- At low SNR, a threshold with a value corresponding to the Khi-2 inverse value equals to about  $K_n$
- At high SNR a threshold with a value corresponding to the Khi-2 inverse value equals to about  $K_s$

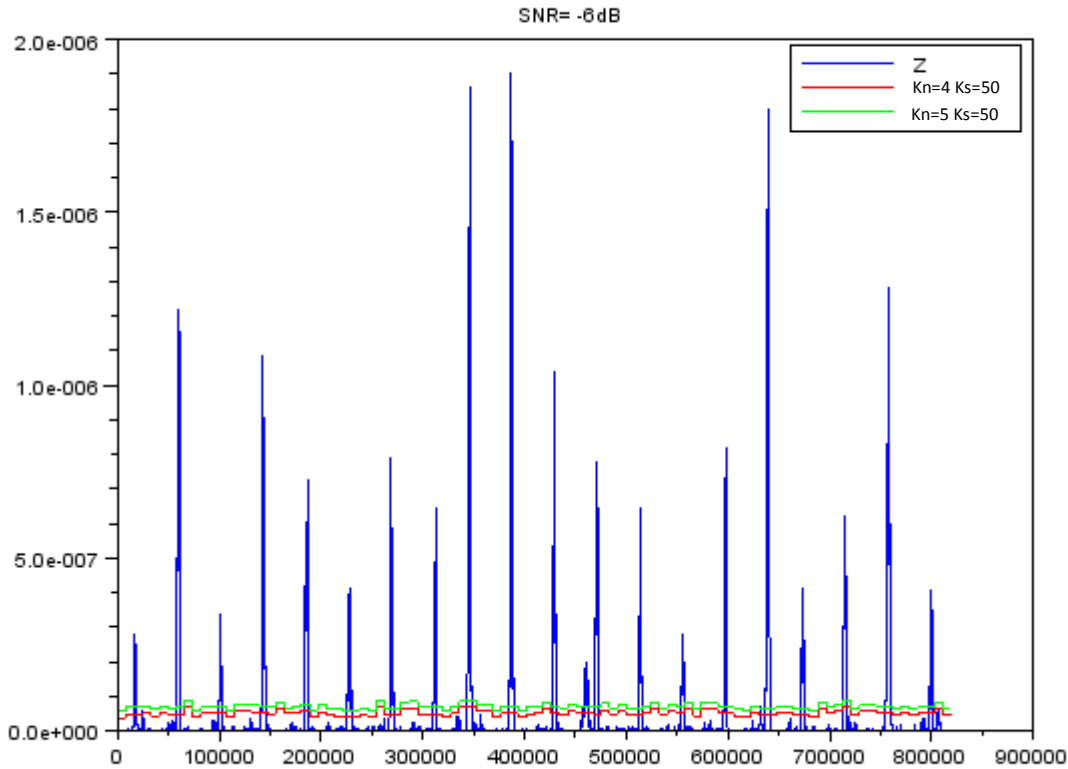


Figure 73: Output of the P1 detection ( $Z$  in blue), and two values of threshold.

### 6.3.2.2 Fixed threshold

If the signal is filtered before the P1 detection with mean power  $P$ , then the variance of  $U_m$  and  $V_m$  is given by:

$$\sigma_{U_m}^2 = \frac{P^2}{B_F T_R}, \quad (43)$$

The output  $Z$  of the detection algorithm is the product of  $U_m$  and  $V_m$  and consequently has a normal product distribution with zero mean and variance  $\sigma_{U_m}^4$ .

The distribution of  $\|Z\|^2$  is unknown but it can be approximated by running simulations.

It can be noticed that if  $U_m$  and  $V_m$  have a unitary variance and that there is a probability  $p$  so that  $\|Z\|^2$  is greater than  $K$ .

Consequently, if  $U_m$  and  $V_m$  have a variance  $\sigma_{U_m}^2$ ,  $\|Z\|^2$  has a probability  $p$  to be greater than  $K\sigma_{U_m}^4$ .

It is then possible to define a threshold in function of  $\sigma_{U_m}^2$ , that is to say in function of the mean power of the input signal, by choosing an appropriate value for  $K$ . The following table gives the probabilities to be greater than the measured threshold  $K\sigma_{U_m}^4$ .

**Table 29: Probabilities of exceeding the threshold.**

K	$\Pr( Z ^2 > K\sigma_{U_m}^2)$
5	0.0326786
10	0.0059646
15	0.0015966
20	0.0005128
25	0.0001874
30	0.0000754
35	0.0000316
40	0.0000129
45	0.0000064
50	0.0000028
55	0.0000011

It is then possible to simply determine the threshold by measuring the power  $P$  of the signal at the input of the P1 detection algorithm:

$$S_z = K \left( \frac{P^2}{B_F T_R} \right)^2. \quad (44)$$

### 6.3.3 Performances

The performance of the algorithm described in the previous section has been evaluated under the following assumptions:

- 512 subcarriers with 426 modulated subcarriers
- Gaussian noise with SNR computed for an OFDM signal
- Oversampling factor of 4

The input signal is filtered prior to P1 detection. The threshold is computed with a perfect knowledge of the SNR and  $K_n = 5$  and  $K_s = 50$ . A P1 is declared as detected when at least 420 consecutive points of  $\|Z\|^2$  are above the threshold.

#### 6.3.3.1 Detection performance

The performance of the P1 detection algorithm has been evaluated over 2000 P1 symbols for each SNR. Results are given in Table 30.

Conclusion:

- At SNR = -8dB the non detection rate is 30%
- The false alarm probability is about 1/1000



**Table 30: P1 detection performance.**

SNR	Detection error ratio	Number of false alarms
-8	0,2955	26
-5	0,003	6
-2	0	0
1	0	1
4	0	0
7	0	1
10	0	0
13	0	0
16	0	2

### 6.3.3.2 Coarse time synchronization precision

For each detected P1, the error in coarse time estimation is computed. A large error can be considered as a false alarm, in particular if the error is greater than the search window of the following time/frequency synchronization algorithms. Table 31 below gives for various SNR, the ratio of P1 that have not been detected and the percentage of coarse estimation that are greater than 100, 1000, 1200 or 2000 samples.

**Table 31: Coarse time synchronization performance.**

SNR	% ND	% > 100	% > 1000	% > 1200	% > 2000
-8	20%	70%	13%	6%	4%
-6.5	0%	85%	9%	5%	3%
-5	0%	67%	2%	1%	1%
-3	0%	46%	0%	0%	0%

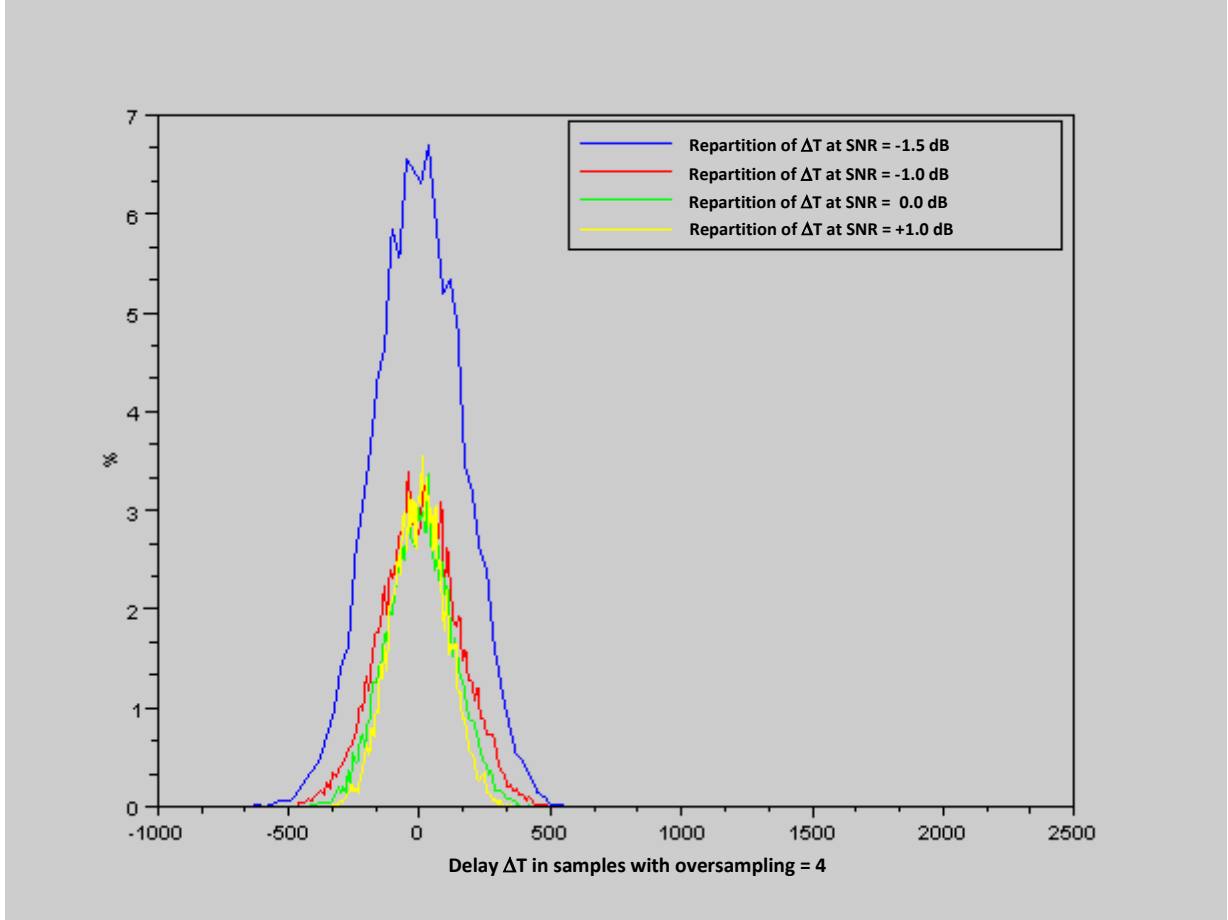


**Figure 74: Error distribution of the coarse time estimation of the start of P1 (without filtering).**

### 6.3.3.3 Frequency fractional error estimation precision

In parallel to the coarse time estimation, the receiver also performs the detection of the fractional part of the frequency offset. After the integer part is computed, the residual frequency error can easily be estimated using the SC-OFDM hybrid symbols if the phase between two hybrid symbols rotates less than  $\pi$  radians. The maximal error of the P1 detection algorithm shall not be greater than half of the inverse of time between two hybrid symbols:

$$df_{\max} = \frac{SC - OFDM_{\text{carrierspacing}}}{2T_{\text{Hybrid}} \left(1 + \frac{1}{GI}\right)}, \quad (45)$$

where:

- $SC - OFDM_{\text{carrierspacing}}$  is the spacing between the subcarriers of the SC-OFDM symbols,
- $T_{\text{Hybrid}}$  is the period of the hybrid symbols, expressed in number of SC-OFDM symbols,
- $GI^{-1}$  is the fraction of SC-OFDM symbol copied as guard interval ( $GI=4, 8, 16$  or  $32$ ).

Table 32 below gives the percentage of the estimated fractional frequency error greater than  $df_{\max}$  with:

- SC\_OFDM symbols with  $N_{\text{FFT}} = 512$ ,  $GI=8$

- $T_{Hybrid}=6$ .

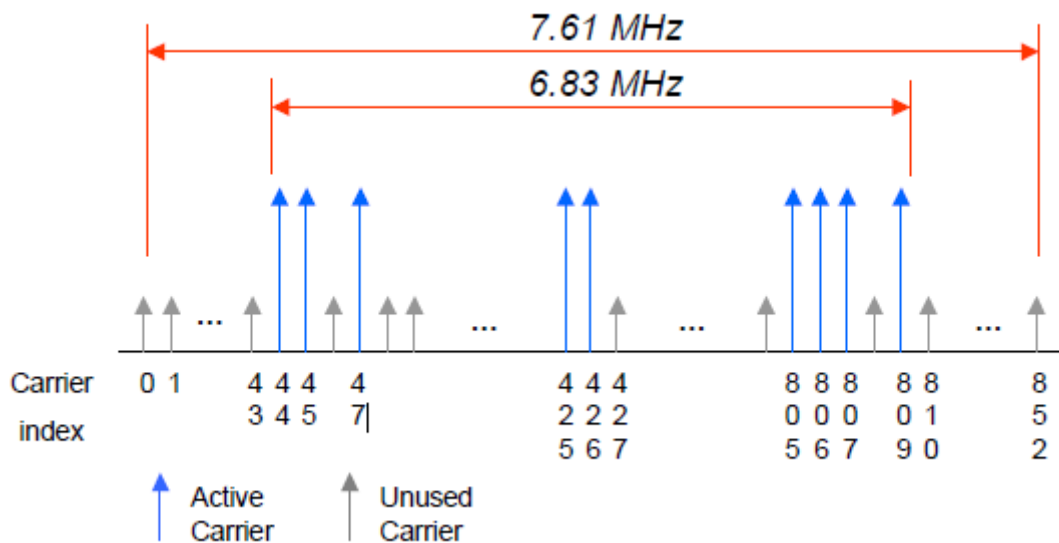
**Table 32: Error rate of the fractional frequency error estimate.**

GI	SNR = -8dB	SNR = -6.5dB	SNR = -5dB	SNR = -2dB
1/4	7,0%	4,55%	0,3%	0,0%
1/8	4,0%	1,84%	0,2%	0,0%
1/16	3,3%	1,26%	0,2%	0,0%
1/32	3,0%	0,87%	0,2%	0,0%

## 6.4 Estimation of the integer part of the frequency offset

### 6.4.1 Description of the algorithms

This section presents two methods for estimating the integer part of the frequency offset. After P1 detection, only a coarse estimation of the timing offset  $\tau_0$  of the start of P1 symbol is known and the maximum tolerable error on  $\tau_0$  is the fine synchronization search space. The non regular spreading of the active carriers of P1 symbol is used to estimate the integer part of the frequency (See Figure 75).

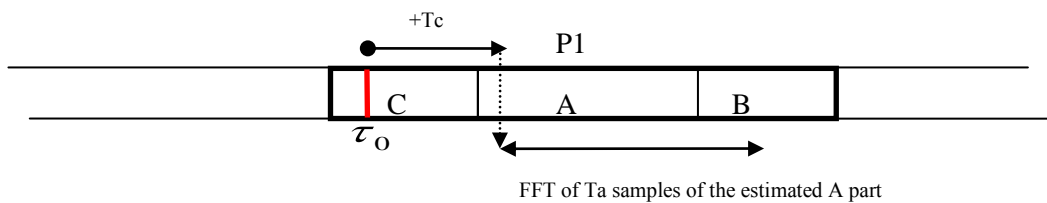

**Figure 75: Spectrum mask of the P1 symbol.**

The two proposed methods are:

- Method 1 : module correction
  - The FFT is performed on the A part of the P1 symbol which is coarsely synchronized:  $1024 \times \text{oversampling factor (OVF)}$  samples over the time interval:  $\tau_0 + T_C$  to  $\tau_0 + T_C + T_A - 1$
  - A correlation is performed between this FFT and a reference vector with zeros except where active carriers are present where the is a 1

- The frequency error is obtained by the index of the correlation peak.
- Method 2 : complex correlation
  - The first sample is taken at  $\tau_0 - \text{FINE\_SYNCHRO\_SEARCH\_SPACE} + T_C$ , the FFT is performed on  $1024 \times \text{OVF}$  samples from the start.
  - The correlation is performed between this FFT and a reference vector composed of zeros except where the X128 symbol has non zero values that are +1 or -1 (carriers are BPSK modulated).
  - It is needed to be synchronized in time with less that  $\text{OVF}$  samples of error in order to have a correlation peak. So the computation is performed by shifting from 1 to  $\text{OVF}$  samples in the data flow and doing several FFT and correlations.
  - It stops at sample  $\tau_0 + \text{FINE\_SYNCHRO\_SEARCH\_SPACE} + T_C$ .
  - The frequency error is given by the index of the maximum of the correlation peak.
  - If a maximum is found, then the start of P1 symbol is known with a precision of  $\pm \text{OVF}/2$ .

Method 1 :



Method 2 :

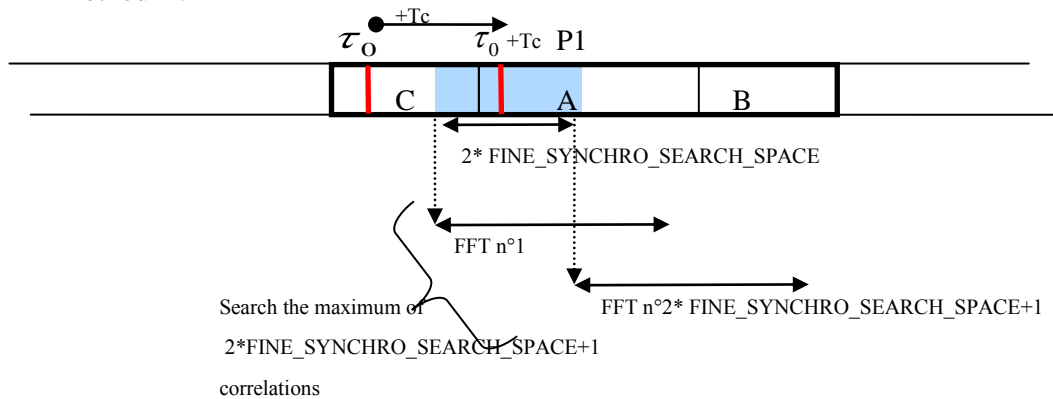


**Figure 76 : Illustration of the 2 methods for the integer frequency offset estimation (IFS).**

Method 2 is more robust to noise, but is also more complex. However, the total complexity IFS + FTS of the 2 methods is equivalent, because with Method 2 the precision of time synchronization after FTS reduces the number of correlation to perform for the FTS.

Table 33 presents the complexity ratio between the two methods:

- "search step" is the number of samples of the shift to perform FFT+correlation if method 2 is used.
- FFT size can be reduced to 2048 instead of  $4 \times 1024 = 4096$  (if one sample over 2 is used).
- The number of FFT with method 2 is calculated with  $\text{Erreur\_max\_CTS} = 1200$  samples.

- "NB corr X128" is the number of correlation with the symbol X128 necessary to perform the fine time synchronization.
- "Nop M1" is the number of operation of method 1 + the fine frequency synchronization performed with  $2 \times \text{Error\_max\_CTS}$  correlations with the X128 symbol.
- It can be noticed that the complexity are of the same order with the two methods.

**Table 33: Comparison of complexity between Method 1 and Method 2.**

Search step	size FFT	Number of FFT	NB Corr X128	Nop M1	Nop M2	Ratio Nop M2/M1
1	2048	2400	0	19660800	37524527,2	1,9
2	2048	1200	3	19660800	18786839,6	1,0
3	2048	800	4	19660800	12540943,7	0,6
4	2048	600	5	19660800	9422091,81	0,5
1	4096	2400	0	19660800	81814968,5	4,2
2	4096	1200	3	19660800	40932060,3	2,1
3	4096	800	4	19660800	27304424,2	1,4
4	4096	600	5	19660800	20494702,1	1,0

## 6.4.2 Performance evaluation

This section illustrates the performance of the 2 aforementioned methods for estimating the integer part of the carrier frequency offset. Figure 77 gives the percentage of success of the integer frequency error estimation for Method 1 with respect to the precision of the initial coarse time synchronization for various SNR. Figure 78 gives the same kind of result for Method 2.

It appears from those results that Method 2 is more robust to noise. However considering the SNR used for the systems simulations (around 0 dB) Method 1 will also provide good results.

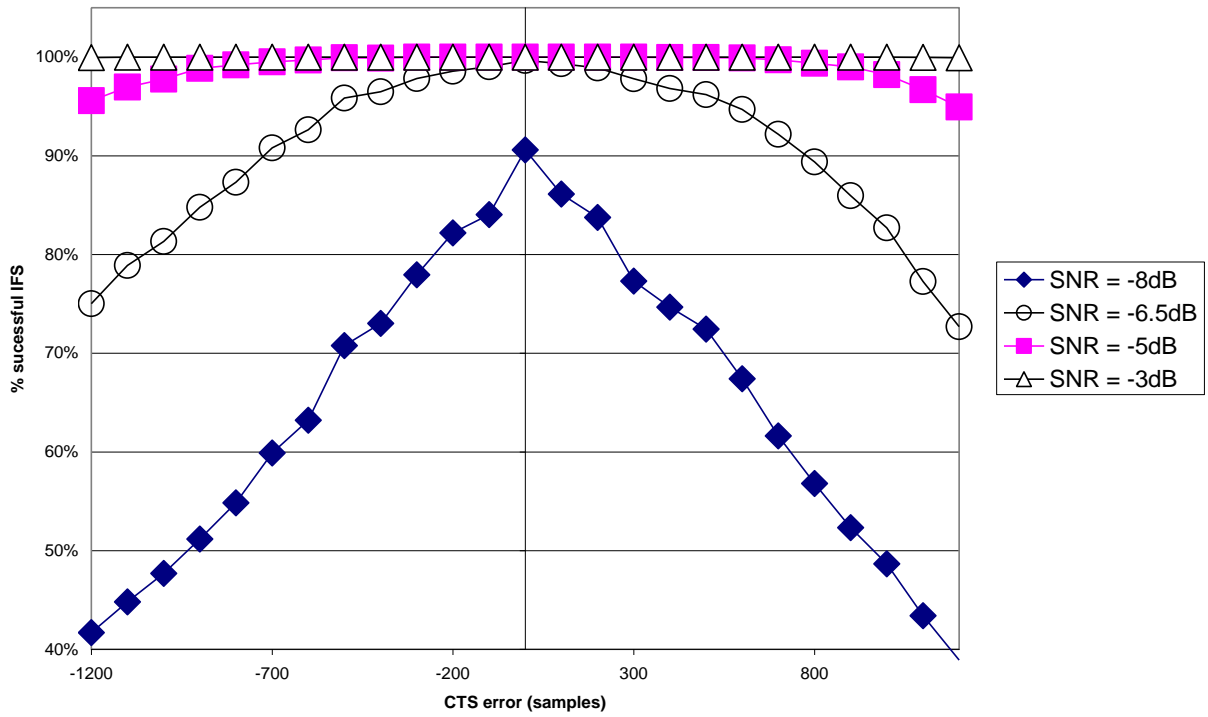


Figure 77: IFS detection performance - Method 1.

IFS performances with complex correlation

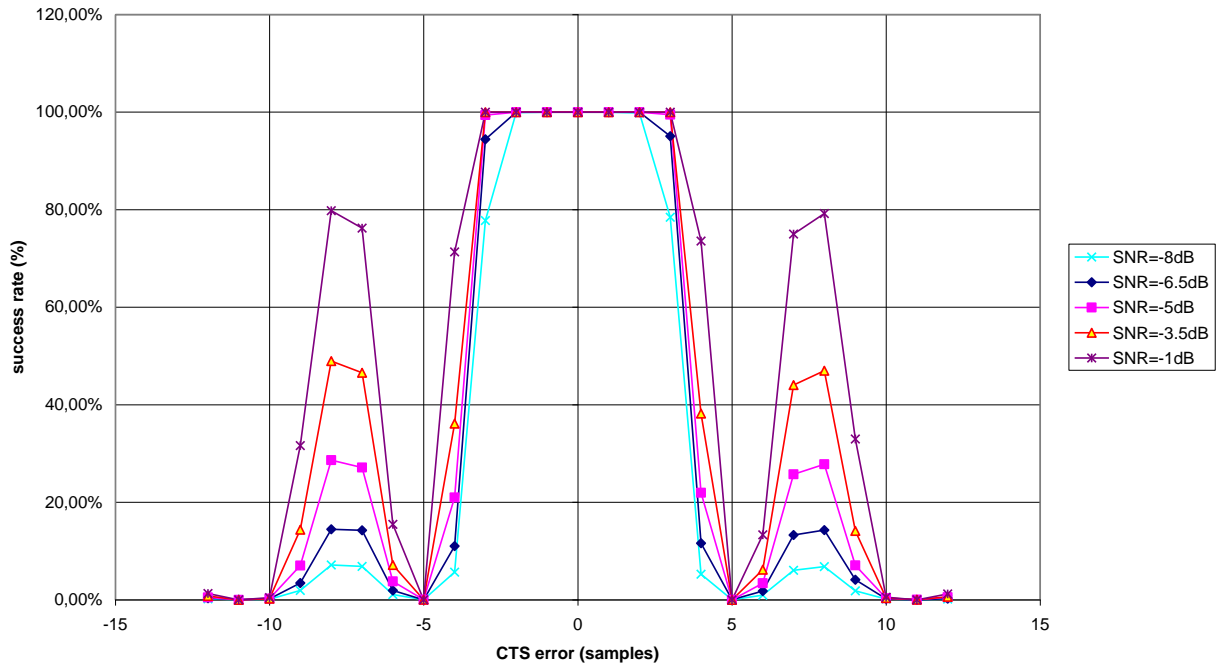


Figure 78: IFS detection performance - Method 2.

## 6.5 Time synchronization

### 6.5.1 Algorithm description

The time synchronization is performed after the integer frequency error estimation. The inputs are:

- A coarse estimation  $\tau_0$  of the start of the P1 symbol obtained after P1 detection,
- The estimate of the frequency error.

The observed SNR being as low as -8dB (minimal SNR for detection) the correlation  $\gamma$  with the X128 symbol shall be performed in complex in order to be robust to noise in AWGN channel:

- The signal is corrected with the estimated frequency.
- The maximum is searched of the complex correlation products  $\|\gamma_N\|^2$  between the samples  $x_k$  of the X128 and the samples  $y_{k-N}$  of the input signal:

$$\|\gamma_N\|^2 = \left\| \sum_{k=1}^M x_k y_{k-N}^* \right\|^2. \quad (46)$$

Note that  $\|\gamma_N\|^2$  is a complex correlation and not a module correlation ( $\gamma_N = \sum_{k=1}^M \|x_k\|^2 \|y_{k-N}\|^2$ ).

- In order to compute the correlation product  $\|\gamma_N\|^2$  with the X128 symbol, 8192 complex products are needed, X128 being composed of 8192 samples: this operation is computationally consuming.
- The parameter FINE\_SYNCHRO\_SEARCH\_SPACE corresponds to the worst time error on  $\tau_0$ , the calculation of  $\|\gamma_N\|^2$  is made for  $N$  going from  $\tau_0 - \text{FINE\_SYNCHRO\_SEARCH\_SPACE}$  to  $\tau_0 + \text{FINE\_SYNCHRO\_SEARCH\_SPACE}$ , that is  $2 \times \text{FINE\_SYNCHRO\_SEARCH\_SPACE} + 1$  correlations  $\|\gamma_N\|^2$ .
- Each correlation product  $\|\gamma_N\|^2$  is calculated over 8192 points, the needed memory is:
 
$$2 \times \text{FINE\_SYNCHRO\_SEARCH\_SPACE} + 1 + 8192.$$
- FINE\_SYNCHRO\_SEARCH\_SPACE is set to 1200 samples if the integer part of the frequency error was estimated using Method 1 and 3 samples if the integer part of the frequency error was estimated with Method 2.

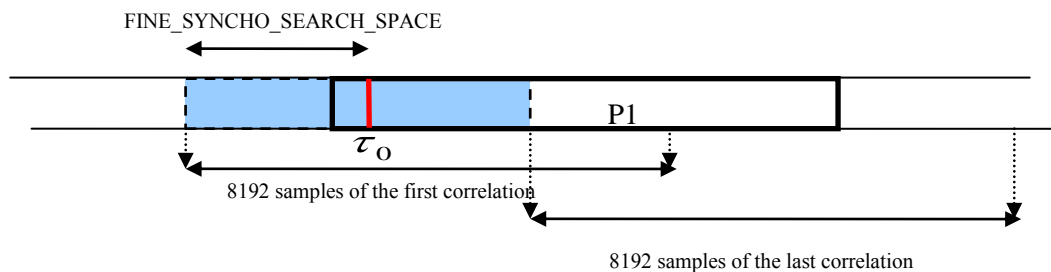


**Figure 79: Illustration of the fine time synchronization implementation (FTS).**

## 6.5.2 Performances evaluation

Without any frequency error, the correlation between the P1 symbol with unitary power and the X128 is defined as:

$$\gamma = \frac{1}{8192} \sum_{k=1}^{8192} x_k X128_{k-N}^* , \quad (47)$$

where:

- $x_k$  is a complex white Gaussian noise  $n = n_I + jn_Q$  with variance  $\sigma_n^2 = \sigma_{\text{Re}(n)}^2 + \sigma_{\text{Im}(n)}^2 = 2\sigma_{\text{Re}(n)}^2$ ,
- The determinist X128 symbol is assumed with power 1.

Eq. (47) is the result of the sum of 8192 independent variables  $x_k X128_{k-N}^*$  of variance  $\sigma_n^2$ . As a consequence,  $\gamma$  is a random complex variable with a variance given by:

$$\sigma_\gamma^2 = \left( \frac{1}{8192} \right)^2 8192 \sigma_n^2 = \frac{\sigma_n^2}{8192} , \quad (48)$$

As the sum of two zero-mean squared independent Gaussian variables  $\gamma_I$  and  $\gamma_Q$ ,  $\|\gamma\|^2 = \gamma_I^2 + \gamma_Q^2$  follows a Khi square law with two degrees of freedom.  $\gamma_I$  and  $\gamma_Q$  have variance equal to:

$$\sigma_{\text{Re}\{\gamma\}}^2 = \sigma_{\text{Im}\{\gamma\}}^2 = \frac{\sigma_n^2}{2} \frac{1}{8192} . \quad (49)$$

Consequently, it is possible to compute the value of  $\sigma_n^2$  in order to have  $\|\gamma\|^2 = 0.33$  with probability  $p$ :

$$\sigma_n^2 = \frac{0.33 \times 8192 \times 2}{\text{Khideuxinverse}(p)} , \quad (50)$$

under the assumption of a SC-OFDM transmission data with  $N_{\text{FFT}} = 512$  and  $N_u = 426$ , a unitary mean power (because 0.33 is the value if the power of P1 is 1), and an oversampling factor of 4. It is finally possible to derive the SNR from the noise power as:

$$\text{SNR} = 10 \log_{10} \left( \frac{4 \times \frac{512}{426}}{P_{\text{noise}}} \right) , \quad (51)$$

Table 34 provides the SNR value required to obtain different target probabilities.

**Table 34: Probability of bad fine time synchronization vs. SNR and intermediate metrics.**

Pr(Corr>0,33)	KHI2INV(p)	Pnoise	SNR
1,E-01	4,61	1 174,05	-24
1,E-02	9,21	587,03	-21
1,E-03	13,82	391,35	-19
1,E-04	18,42	293,51	-18
1,E-05	23,03	234,81	-17
1,E-06	27,63	195,68	-16



From Table 34, it can be noticed that the fine time synchronization is very robust, mainly due to the high number (8192) of mean computations performed to obtain a correlation product.

In conclusion, the fine time synchronization can only fail if:

- The coarse time estimation  $\tau_0$  computed during P1 detection is greater than FINE\_SYNCHRO\_SEARCH\_SPACE
- The frequency error estimation is in the order of magnitude of 50% of a subcarrier.

Figure 80 below shows the values of  $\|\gamma\|^2$  obtained for various P1, various random chooses, and various frequency errors (estimated in % of a SC-OFDM subcarrier with N\_FFT = 512, that is half of the error in % of a P1 subcarrier) and SNR = 0dB.

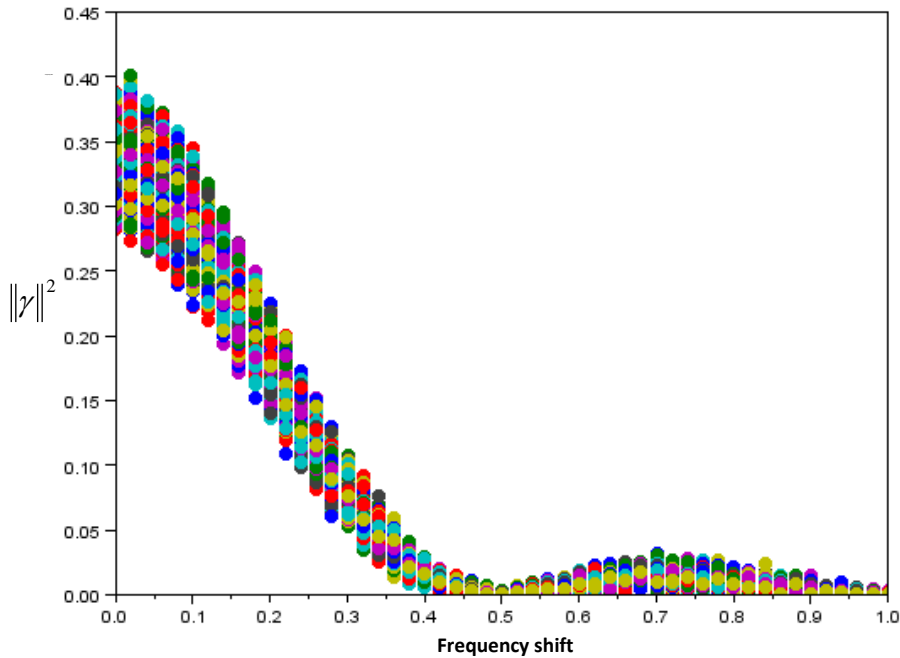


Figure 80: Values of various correlations between P1 and X128 symbol.

### 6.5.3 False alarm computation

Let's consider the following correlation:

$$\gamma = \frac{1}{8192} \sum_{k=1}^{8192} x_k X128_{k-N}^* \quad (52)$$

with:

- $x_k = s_k + n_k$
- $s_k$ , an SC-OFDM signal with a power  $\sigma_s^2$  and a bandwidth  $b = \frac{426}{4 \times 512}$  (426 useful carriers over 512, observed with 4 samples by symbol)

- $n_k$  white Gaussian complex noise with variance  $\sigma_n^2$

It can be shown that the variance of the correlation  $\gamma$  is given by:

$$\sigma_\gamma^2 = \frac{1}{8192} \frac{\sigma_n^2}{2} + \frac{1}{8192} \frac{\sigma_s^2}{2b}. \quad (53)$$

The squared module  $\|\gamma\|^2$  follows a Khi square law with two degrees of freedom. The false alarm threshold with a probability  $p$  is obtained as:

$$Threshold = \sigma_\gamma^2 \text{Khi}2^{-1}(p), \quad (54)$$

If after fine time synchronization, the maximum of  $\|\gamma\|^2$  is below the threshold, it is assumed that the correlation was not performed on a P1 symbol and consequently the frame is not validated.

It is also possible to compute a threshold based on the correlation value between a P1 of power  $\sigma_s^2$  shifted in frequency and the X128 symbol:

- If  $df=0$  then  $\|\gamma\|^2 = 0.33\sigma_s^2$
- If  $df > 0.3\%$  of a SC-OFDM subcarrier then  $\|\gamma\|^2 < 0.1\sigma_s^2$
- It is needed to have  $df < \frac{1}{2} \frac{1}{T_{Hybrid} \left(1 + \frac{1}{GI}\right)} = 0.074$  if  $T_{Hybrid} = 6$  and  $GI = 8$  so it is possible to use a threshold of  $0.1 \times \sigma_s^2$  in order to validate a P1 frame.

The power values  $\sigma_n^2$  and  $\sigma_s^2$  are estimated using:

- The estimated SNR given by the P1 detection block
- The total power at the input of the algorithm  $\sigma_n^2 + \sigma_s^2$
- The formula  $SNR = 10 \log_{10} \left( \frac{1}{b} \frac{\sigma_s^2}{\sigma_n^2} \right)$  with  $b$  the useful band of the signal  $s$ .

## 6.6 Fine frequency synchronization over pilot symbols

### 6.6.1 Description of the algorithm

The residual frequency error  $df$  is estimated as follows:

$$\widehat{df}_k = \frac{1}{T_{Hybrid}} \text{Arg} \left\{ E \left\{ P_k^* P_{k+1} \right\} \right\} = \frac{1}{T_{Hybrid}} \text{Arg} \left\{ \frac{1}{N_p} \sum_{i=1}^{N_p} P_{k,i}^* P_{k+1,i} \right\}, \quad (55)$$

where:

- $i$  is the index of the subcarrier and  $k$  the index of the hybrid symbol,
- $T_{Hybrid}$  is the time between two hybrid symbols (expressed in seconds in order to have  $\widehat{df}$  in Hz, or expressed in number of symbols if  $\widehat{df}$  is to be expressed relatively to the subcarrier space),

- $Arg\{Z\} = \tan^{-1}\{\text{Im}\{Z\} / \text{Re}\{Z\}\}$ .

Considering that the SNR varies during the frame and that it is not possible to determine if an estimate of  $\widehat{df}_k$  is correct,  $\widehat{df}_k$  is estimated for each pair of hybrid symbols and  $\widehat{df}_k$  is used to correct data symbols between symbols  $k$  and  $k+1$ . It is possible to accumulate the correlation products between the pilot subcarriers over more than 2 hybrid symbols:

$$\widehat{df}_a = \frac{1}{T_{Hybrid}} Arg\left\{E\left\{P_k^* P_{k+1}\right\}\right\} = \frac{1}{T_{Hybrid}} Arg\left\{\frac{1}{K} \frac{1}{N_p} \sum_{k=a}^{K+a-1} \sum_{i=1}^{N_p} P_{k,i}^* P_{k+1,i}\right\}, \quad (56)$$

with  $K$  lying between 1 and the total number of possible sums, that is to say the total number of hybrid symbols in the frame minus 1.

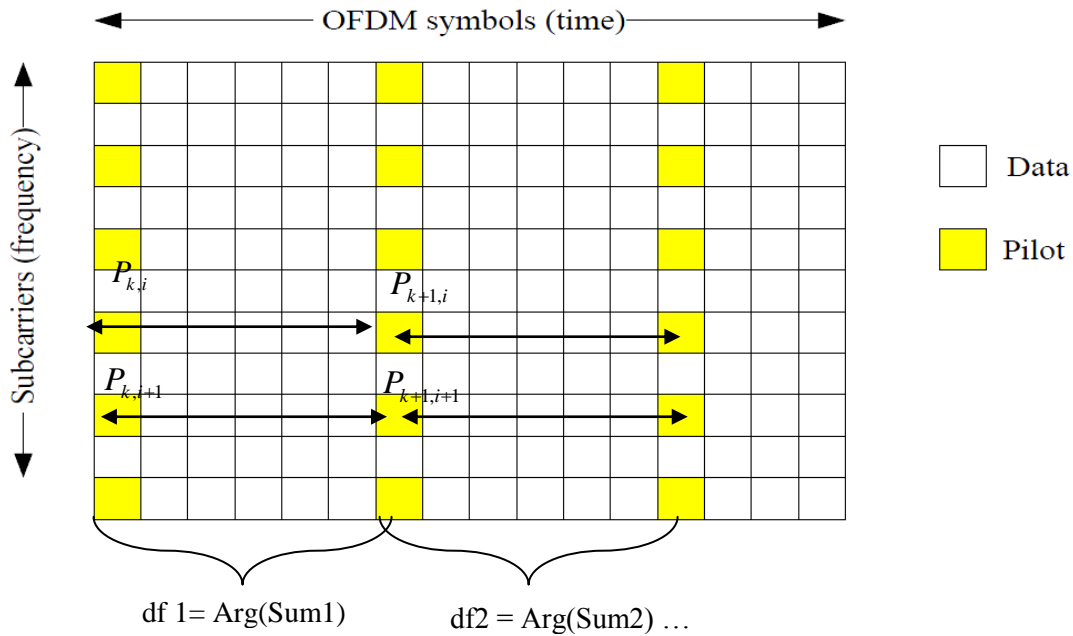


**Figure 81: Illustration of fine frequency estimation.**

## 6.6.2 Performances evaluation

Let's consider the fine time estimate defined as:

$$\widehat{df}_k = \frac{1}{2\pi T_{Hybrid}} Arg\left\{\frac{1}{N_p} \sum_{i=1}^{N_p} P_{k,i}^* P_{k+1,i}\right\}. \quad (57)$$

The received signal  $P_{k,i}$  is given by:

$$P_{k,i} = H_{k,i} X_{k,i} + N_{k,i}, \quad (58)$$

where  $X_{k,i}$  is the pilot,  $H_{k,i}$  the channel coefficient and  $N_{k,i}$  the noise with power  $\sigma_n^2$ .

In (57), the sum  $\sum_{i=1}^{N_p} P_{k,i}^* P_{k+1,i}$  follows a normal law with variance  $N_p (\sigma_n^4 + 2\sigma_n^2)$ . Thus we have:

$$\begin{aligned}
 E\left\{(H_{k,i}X_{k,i} + N_{k,i})(H_{k+1,i}X_{k+1,i} + N_{k+1,i})^*\right\} &= E\left\{(HX + N_{k,i})(HX + N_{k+1,i})^*\right\} \\
 &= \|HX\|^2 + E\{N_{k,i}N_{k+1,i}^*\} + 2E\{HXN\} \\
 &= \|HX\|^2,
 \end{aligned} \tag{59}$$

and:

$$\begin{aligned}
 E\left\{\left\|(H_{k,i}X_{k,i} + N_{k,i})(H_{k+1,i}X_{k+1,i} + N_{k+1,i})^*\right\|^2\right\} &= E\left\{\left\|(HX + N_{k,i})(HX + N_{k+1,i})^*\right\|^2\right\} \\
 &= E\left\{\|HX\|^2 + N_{k,i}N_{k+1,i}^* + 2HXN\right\} \\
 &= \|HX\|^4 + E\left\{\|N_{k,i}N_{k+1,i}^*\|^2\right\} + 4E\left\{\|HXN\|^2\right\} \\
 &= \|HX\|^4 + \sigma_n^4 + 4\frac{\sigma_n^2}{2}.
 \end{aligned} \tag{60}$$

Finally, we have:

$$\text{Var}\left\{\frac{1}{N_p} \sum_{i=1}^{N_p} P_{k,i}^* P_{k+1,i}\right\} = \frac{1}{N_p} (\sigma_n^4 + 2\sigma_n^2). \tag{61}$$

By writing  $C = (I + jQ) + (n_I + jn_Q)$  with  $(I + jQ)$  a determinist constant complex number of power 1 and  $n_I + jn_Q$  a complex white noise of variance  $\sigma_n^2$  and assuming  $Q \ll I$  (that is  $Q/I$  close to zero and  $I$  close to 1) and  $E\{n_I^2\} \ll 1$ , then:

$$\text{Var}\{\text{Arg}\{C\}\} = \frac{\sigma_n^2}{2}. \tag{62}$$

This can be demonstrated as follows:

$$\begin{aligned}
 \text{Var}\left\{\tan^{-1}\left(\frac{\text{Im}\{C\}}{\text{Re}\{C\}}\right)\right\} &\approx \text{Var}\left\{\frac{\text{Im}\{C\}}{\text{Re}\{C\}}\right\} = E\left\{\frac{\left(\text{Im}\{C\} - E\{\text{Im}\{C\}\}\right)^2}{\left(\text{Re}\{C\} - E\{\text{Re}\{C\}\}\right)^2}\right\} \\
 &= E\left\{\frac{(Q + n_Q)^2}{(I + n_I)^2}\right\} - E\left\{\frac{Q + n_Q}{I + n_I}\right\}^2 \\
 &= \frac{E\{Q^2\} + E\{n_Q^2\}}{E\{I^2\} + E\{n_I^2\}} - E\left(\frac{Q}{I}\right)^2 \\
 \text{Var}\left\{\tan^{-1}\left(\frac{\text{Im}\{C\}}{\text{Re}\{C\}}\right)\right\} &\approx \text{Var}\left\{\frac{\text{Im}\{C\}}{\text{Re}\{C\}}\right\} = \frac{E\{n_Q^2\}}{1 + E\{n_I^2\}} \approx E\{n_Q^2\} \\
 &\approx \frac{\sigma_n^2}{2}
 \end{aligned} \tag{63}$$

Using this approximation, the standard deviation of the residual frequency error is given by:

$$\sigma_{df} = \frac{1}{2\pi T_{Hybrid}} \sqrt{\frac{\sigma_n^4 + 2\sigma_n^2}{2N_p}}. \quad (64)$$

Figure 82 and Figure 83 compares the simulated and theoretical values of the standard deviation of the sum of the correlations of the pilot symbols and the standard deviation of the residual frequency error that has been estimated. Those figures clearly validate the approximation obtained above.

It is possible to compute the probability  $p$  to have an estimated error greater than the expected precision, knowing the SNR so the value of  $\sigma_n^2$ :

$$\Pr \left\{ \left| df - \hat{df} \right| > f \right\} = \text{erfc} \left\{ \frac{f}{\sqrt{2\sigma_{df}^2}} \right\}. \quad (65)$$

If the channel estimator performs a temporal mean over 5 hybrid symbols, we obtain:

$$f_{\max} = \frac{1}{2 \times 5 \times T_{hybrid}}. \quad (66)$$

Table 35 gives the probability of the fine time error exceeding different thresholds for a set of SNR. Similarly, Figure 84 gives the error rate of the algorithm FFS for various SNR. It appears that the frequency estimation works correctly around the SNR at which the decoder is able to correct most of the errors (that is to say starting from SNR= -1dB for the modulation QPSK 1/2).

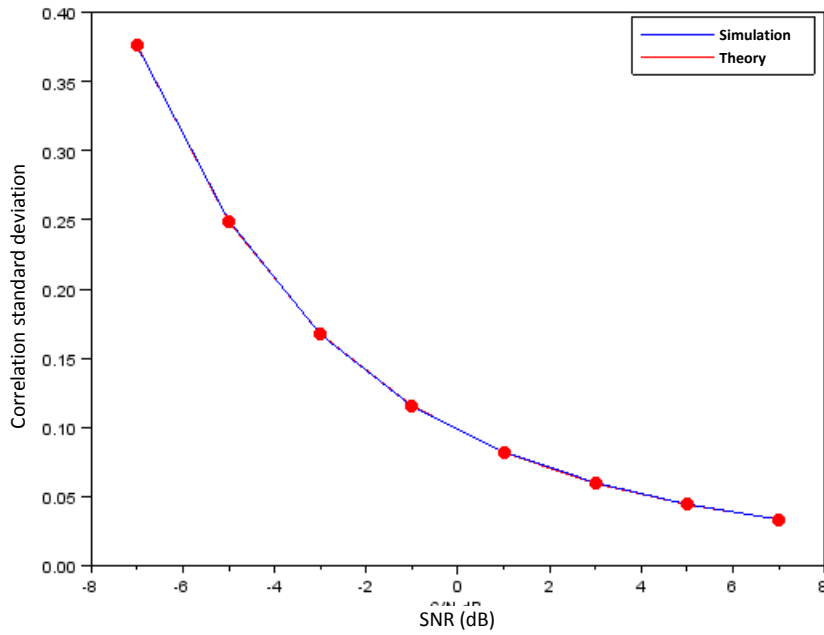


Figure 82: Standard deviation of the sum of the correlations of the pilot symbols.

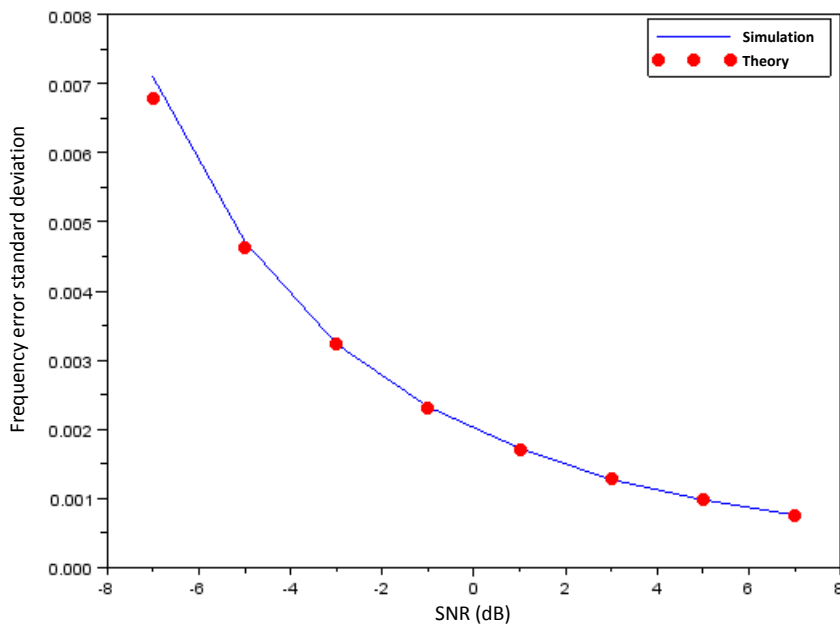
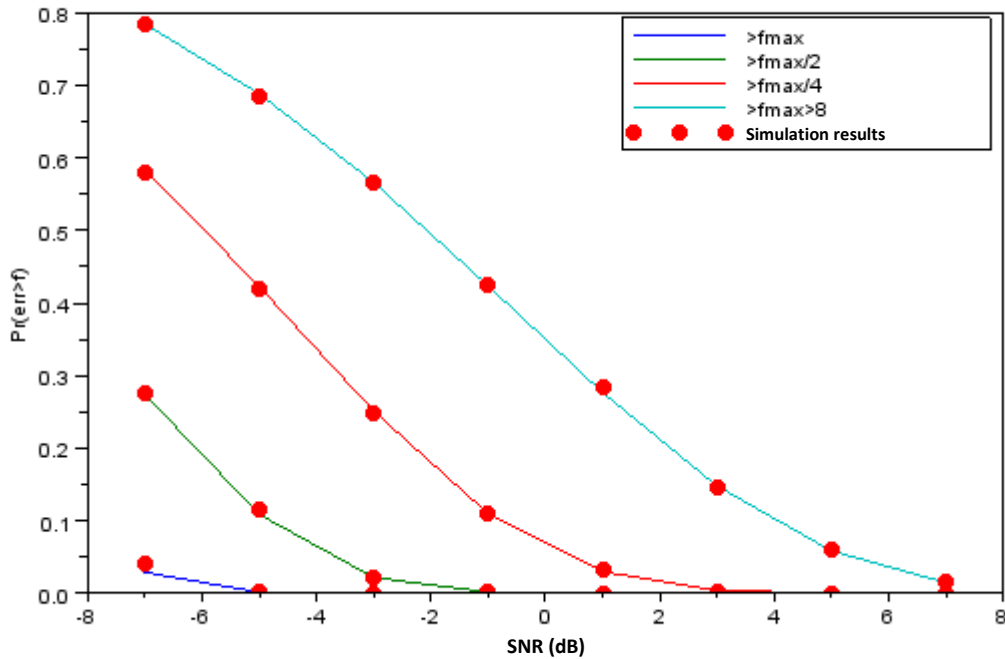


Figure 83: Standard deviation of the residual frequency error that has been estimated.

**Table 35: Probability of the error FFS to be greater than various values in function of the SNR.**

SNR(dB)	Pr(df>dfmax)	Pr(df>dfmax/2)	Pr(df>dfmax/4)	Pr(df>dfmax/8)
-7	0,0286988	0,274043	0,58	0,78
-5	0,0013288	0,1085272	0,42	0,69
-3	0,0000044	0,0216426	0,25	0,57
-1	1,53E-10	0,0013684	0,11	0,42
1	3,19E-18	0,0000135	0,03	0,28
3	5,04E-31	6,98E-09	0,00	0,15


**Figure 84: Error rate of the algorithm FFS for various SNR.**

## 6.7 Conclusion

The previous sections have addressed three synchronization algorithms based on the P1 symbol that have an influence on the demodulation of the rest of the frame:

1. P1 detection + coarse estimation of time synchronization (CTS) + fractional frequency error estimation
2. Integer part of the frequency error estimation (IFS)
3. Fine time estimation of the start of the P1 symbol (FTS)

From the previous studies, it is shown that the following conditions need to be satisfied to achieve good performances:

1. P1 detection:  $\text{SNR} > -8\text{dB}$
2. IFS :  $\text{SNR} > -8\text{dB} + \text{CTS} < 1200$  samples
3. FTS :  $\text{SNR} > -20\text{dB} + \text{frequency error} < 0.5$

If the P1 detection is successful, the probability to see the following two algorithms (IFS and FTS) fail is very low. Moreover, in the rare cases where IFS and/or FTS fail, either because of low SNR or bad coarse time synchronization, the threshold on the correlation peak FTS allows the detection of such failure and the LLRs can be forced to zero.

However, it is observed that for very low SNR where P1 detection works, but with a fractional frequency error slightly greater than the authorized maximum value of FFS:

$$f_{\text{error}} \geq f_{\text{FFS max}} = \frac{1}{2T_{\text{hybrid}} \left(1 + \frac{1}{GI}\right)} = \frac{1}{2 \times 6 \left(1 + \frac{1}{8}\right)} \approx 0,074. \quad (67)$$

This frequency error is high enough to make the FFS fails, but it is too low to make FTS fails: it is consequently not possible to detect it using the X128 correlation peak threshold.

If SNR remains low on the frame, the LLRs calculated in function of the SNR will be quasi zero and the false information caused by FFS failure will not be considered.

However if the SNR increases during the frame, the LLRs increase (in absolute value) but will be wrong: their values will not correspond to the confidence of symbols having a frequency error too high.

Some cases have been observed on LMS ITS channel: it can happen that even for a higher SNR BER can increase if during P1 synchronization SNR is low and then increases during the frame reception. The frame is detected but with a high residual frequency error. The LLR being high because of the SNR being high on the rest of the frame, the decoder will cause packets of errors.

In order to solve this problem, several solutions can be envisaged:

- Add a more robust estimator of the residual frequency error before processing data and pilots: a possible estimator is described in Section 6.2.5.
- Reduce the confidence of the symbols given by the synchronization: a threshold on the LLRs at the input of the decoder is fixed as a function of the maximal LLR values sufficient in order to have a proper decoding on AWGN channel.
- Add a fractional error detector: if fractional error is too high, the LLRs are set to zero.



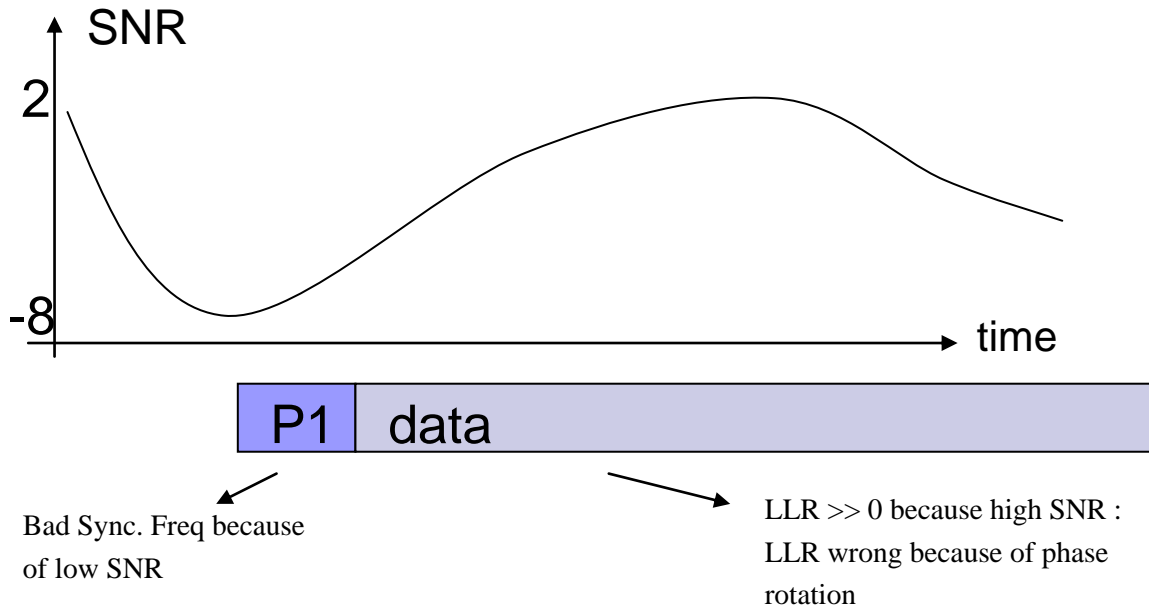


**Figure 85: Illustration of the LLR issue due to SNR varying between P1 detection and data.**

### 6.7.1.1 LLRs saturation

The saturation of the LLRs is useful in the case where synchronization can lead to an actual P1 detection but to a residual frequency error too high compared to the temporal filter used for channel estimation.

If frequency error is too high, the demodulated data will be wrong but the LLRs can be high if the SNR increases during time.

It is possible to limit the confidence of the decoder for the demodulated data without penalizing the rest of the link. The principle is to define a maximal value for the LLRs. This value is defined in function of the used modulation and the SNR for an AWGN channel for which there is no error.

For example, for a QPSK 1/3 the BER is nearly zero when SNR is greater than -1dB on AWGN channel, and for a QPSK 1/2 for SNR greater than 1dB. The LLRs distributions are depicted on Figure 86. The LLRs will be limited to 6 for the QPSK 1/3 and to 8 for the QPSK 1/2.

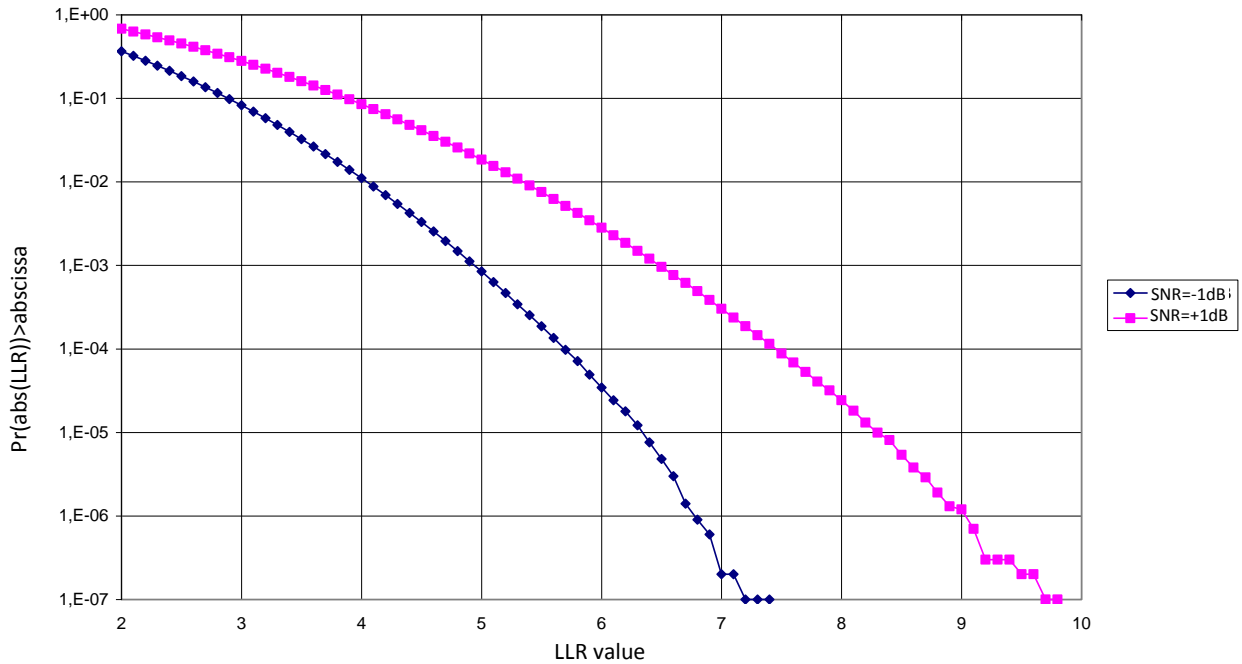


Figure 86: Statistics on maximal absolute value of LLRs for a QPSK at SNR = -1dB and 1dB.

## 6.8 Overall performances evaluation

This section evaluates by means of simulations the impact of the synchronization algorithms on the overall performance of the SC-OFDM receiver.

### 6.8.1 Simulator description

#### 6.8.1.1 Functional block diagram

The simulator that has been used implements the SC-OFDM signal generation, the propagation channel emulation and the signal reception. The functional block diagram of the transmitter and the receiver is depicted respectively on Figure 87 and Figure 88.



Figure 87: SC-OFDM transmitter.

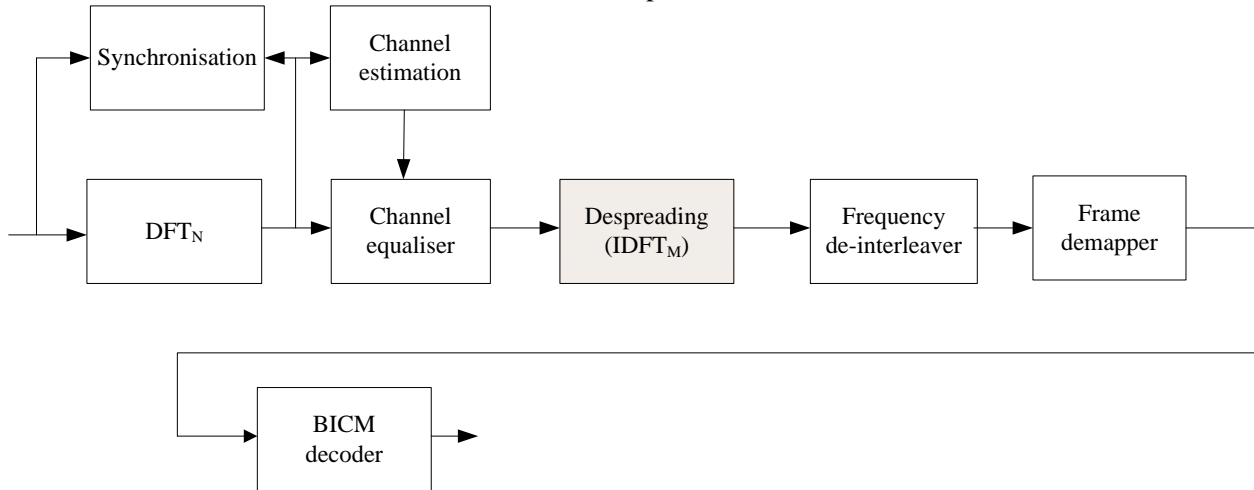


**Figure 88: SC-OFDM receiver.**

### 6.8.1.2 Synchronization blocks

All the synchronization algorithms presented in the previous sections have been implemented in the simulator. The architecture of the P1 synchronization block is shown on Figure 89.

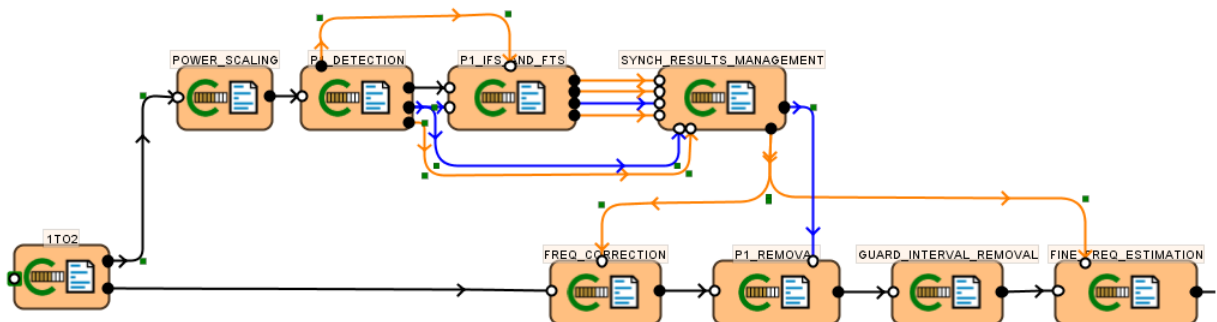


**Figure 89: Synchronization blocs before OFDM demodulation.**

The receiver can be configured in order to operate according to the following modes:

- PCE :Perfect channel estimation and perfect synchronization
- RCE PS: Real channel estimation, perfect synchronization. In this case the receiver uses a channel estimation algorithm
- RCE RS: Real channel estimation, real synchronization. In addition of channel estimation, the synchronization blocks are activated

### 6.8.1.3 Channel estimation

The channel estimation is performed using the hybrid symbols. Their repartition for SC-OFDM is recalled on Figure 90.

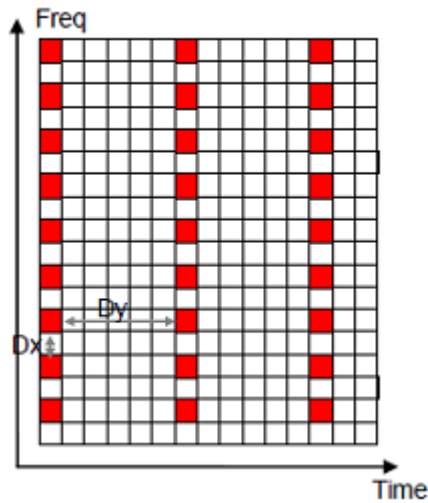


**Figure 90: SC-OFDM hybrid symbols.**

The channel estimation algorithm implements the following steps:

- Step1 : filtering in the frequency domain
  - The channel is observed at pilots' sub-carrier level (1 sub-carrier over 2) for each hybrid symbol.
  - A frequency filter is applied on these pilot sub-carriers. It is constructed based on the guard interval method:
    - This method consists in defining a filter bank that has a cut off frequency in inverse proportion to the guard interval.
    - The filter is selected based on the length of the guard interval. It is usually chosen to be large enough so as to contain a certain amount of channel correlation.
  - Linear interpolation in the frequency domain over all the subcarriers of the data based on the filtered estimated values.
- Step 2: filtering in the time domain
  - The number of coefficients of the filter is chosen as a function of the maximum residual Doppler frequency accepted by the system:
    - TF0: order zero corresponds to no filtering
    - TF1: order 1 is a filtering over 3 consecutive symbols
    - TF2: order 2 is a filtering over 5 consecutive symbols
    - TF3: order 3 is a filtering over 7 consecutive symbols
  - The user decides which time domain filter to use depending on the external Doppler and the precision of the synchronization algorithms.
  - The filter is applied for each subcarrier of the hybrid symbols

- A linear interpolation is applied on all the subcarriers of the data inserted between two consecutive hybrid symbols.

### 6.8.2 Simulation results

Simulations have been carried out using 5 different propagation channel models:

1. AWGN channel,
2. TU6 channel with a mobile speed of 60 km/h,
3. A Rice channel with  $K=5$  and a mobile speed of 60 km/h,
4. LMS open channel,
5. LMS ITS channel.

The simulations have been performed for the following receiver models:

- PCE : Perfect channel estimation and perfect synchronization
- RCE PS : Real channel estimation, perfect synchronization
- RCE RS :Real channel estimation, real synchronization

For real channel estimation, several temporal filters are used: TF0 to TF3.

#### 6.8.2.1 AWGN channel

Figure 91 depicts the BER performance obtained through the simulation of 1000 P1 symbol and a time interleaving of 0.19 seconds.

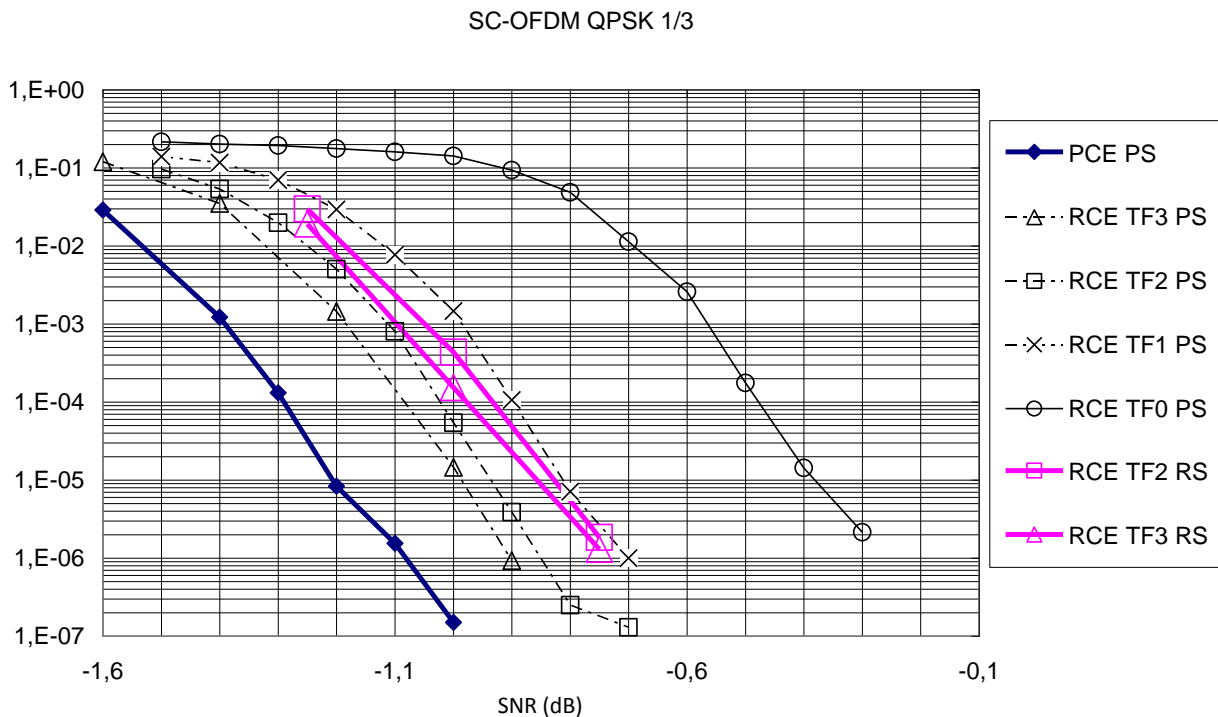
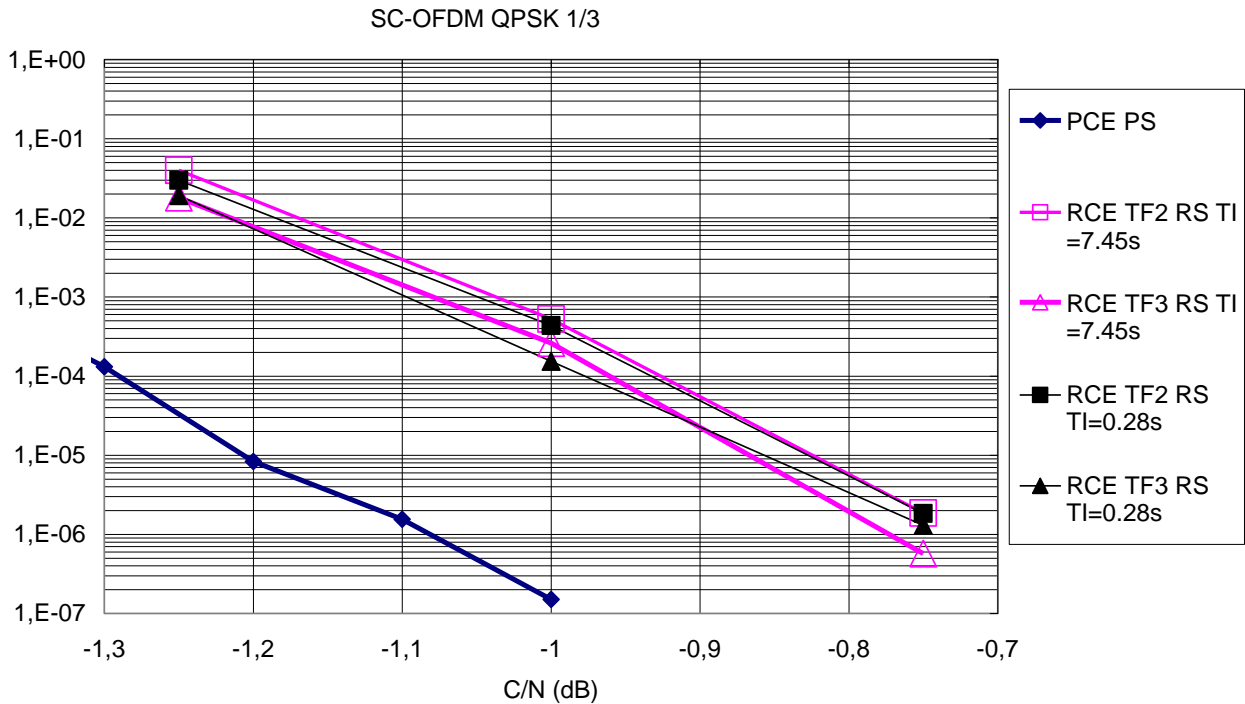


Figure 91: BER for an AWGN channel for a QPSK 1/3.

Compared to the receiver with perfect channel estimation and synchronization:

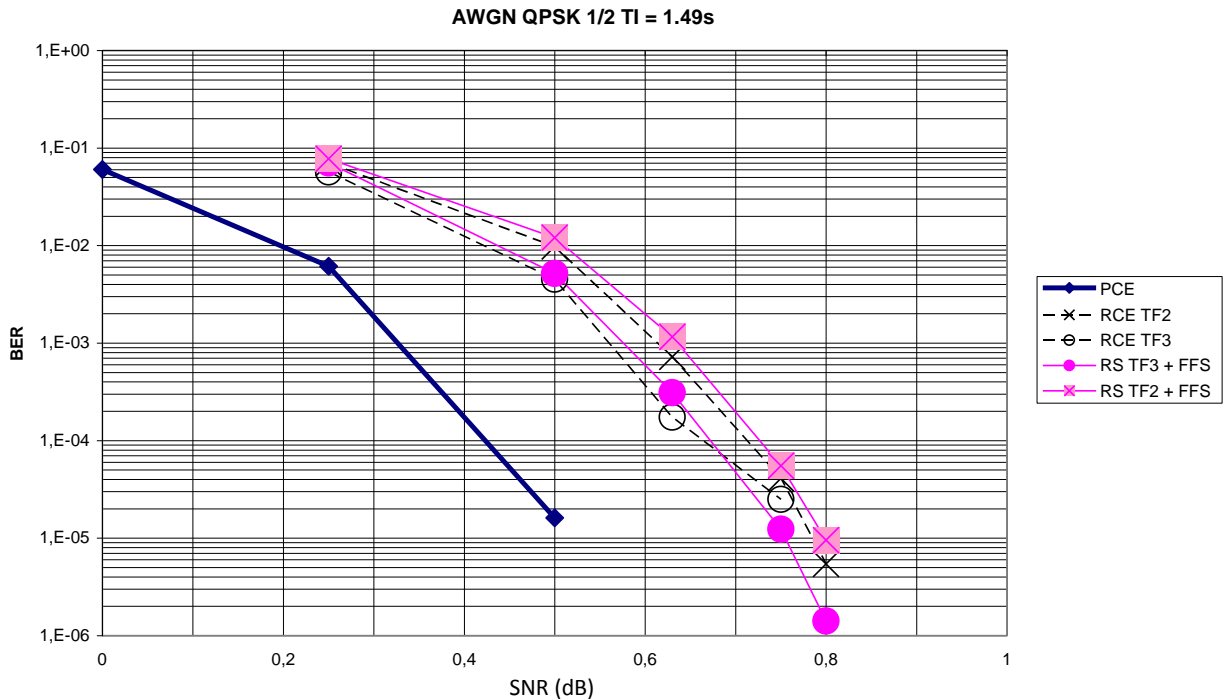
- The total loss due to synchronization and channel estimation is less than 0.5dB
- The loss due to synchronization is about 0.1dB

Figure 92 shows the performances obtained with real channel estimation and real synchronization for 2 interleaving duration: 7.45s and 0.28s.



**Figure 92: BER for an AWGN channel for a QPSK 1/3 with various interleaving time.**

The interleaving depth has no effect on the performances. This is not surprising as the channel is constant over time and the synchronization algorithms always work at these SNR values (as shown in the previous chapters). Figure 93 shows the performances for a QPSK 1/2. It can be seen there is an incidence on the synchronization.



**Figure 93: for an AWGN channel for a QPSK 1/2.**

### 6.8.2.2 TU6 channel at 60km/h with SNR-based P1 detection threshold

The simulations have been performed with the following parameters:

- QPSK 1/2 modulation
- Interleaving time  $T_i$  of 0.28s or 1.49s
- The P1 detection threshold is computed using the method depending of SNR and the values:
  - $K_n = 5$
  - $K_s = 55$

Figure 94 and Figure 95 displays the BER performance respectively for a time interleaving of 0.28 and 1.49s. From these two figures it can be noticed that:

- The loss due to the synchronization process is low (at most 0.1dB), as expected at these SNR values.
- The loss increases if the size of the time domain filter for channel estimation increases. For example 0.3dB for TF3 composed of  $3 \times 2 + 1 = 7$  hybrid symbols, instead of  $2 \times 2 + 1 = 5$  hybrid symbol for TF2.
- The performances are better (0.25dB) when the interleaving time increases from 0.28 to 1.49 sec, all the curves are translated according to this value.

TU6 QPSK 1/2 TI=0.28s

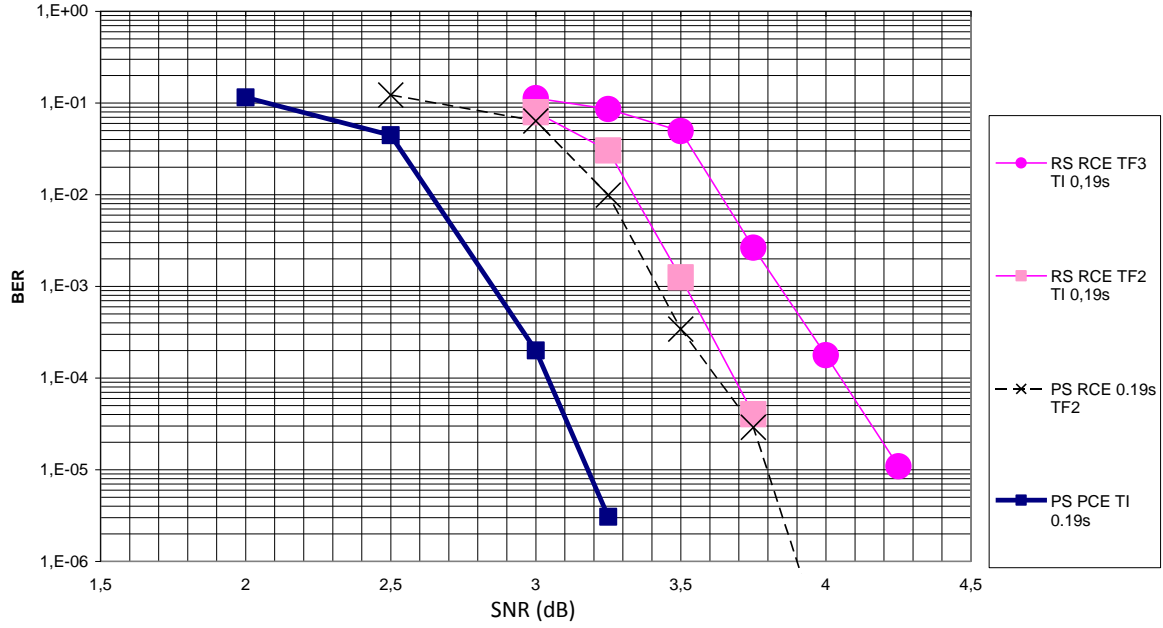


Figure 94: BER on TU6 channel with QPSK 1/2 and Ti=0.28s.

TU6 QPSK 1/2 TI=1.49s

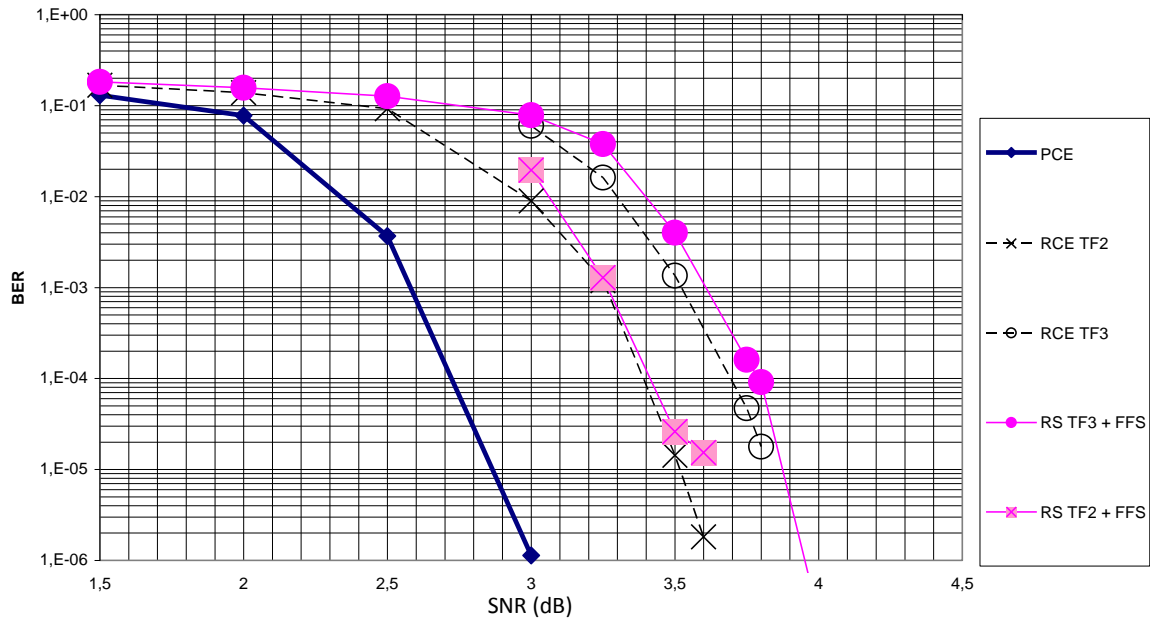


Figure 95: BER on TU6 channel with QPSK 1/2 and Ti=1.49s.



### 6.8.2.3 TU6 channel at 60km/h with fixed P1 detection threshold

The previous results were obtained using a threshold computation mechanism depending on the SNR. This section considers the fixed threshold computation. In this case, the single parameter  $K$  has been chosen in order to go from 25 to 55 with a step of 3 (25, 28 ... 55), and a value of 110 has been tested as well.

The values 25, 55 and 110 give good results on the LMS and RICE channels. With TU6 the same results are expected but with an interleaving time of 0.19s it is not the case. Depending on the chosen value of  $K$  the performance of the P1 detection algorithm varies:

- If  $K=25$  to  $36$ , some false alarms imply that the following P1 will not be detected and the BER is degraded
- If  $K= 39$  or  $42$  no error is encountered and the performances are optimal
- If  $K=45$  to  $55$  or  $110$  some non-detection occur and the BER is degraded

Figure 96 depicts the performance figures obtained in the case of a fixed threshold. It appears that the use of the fixed threshold computation method can provide good results if the coefficients are chosen appropriately.

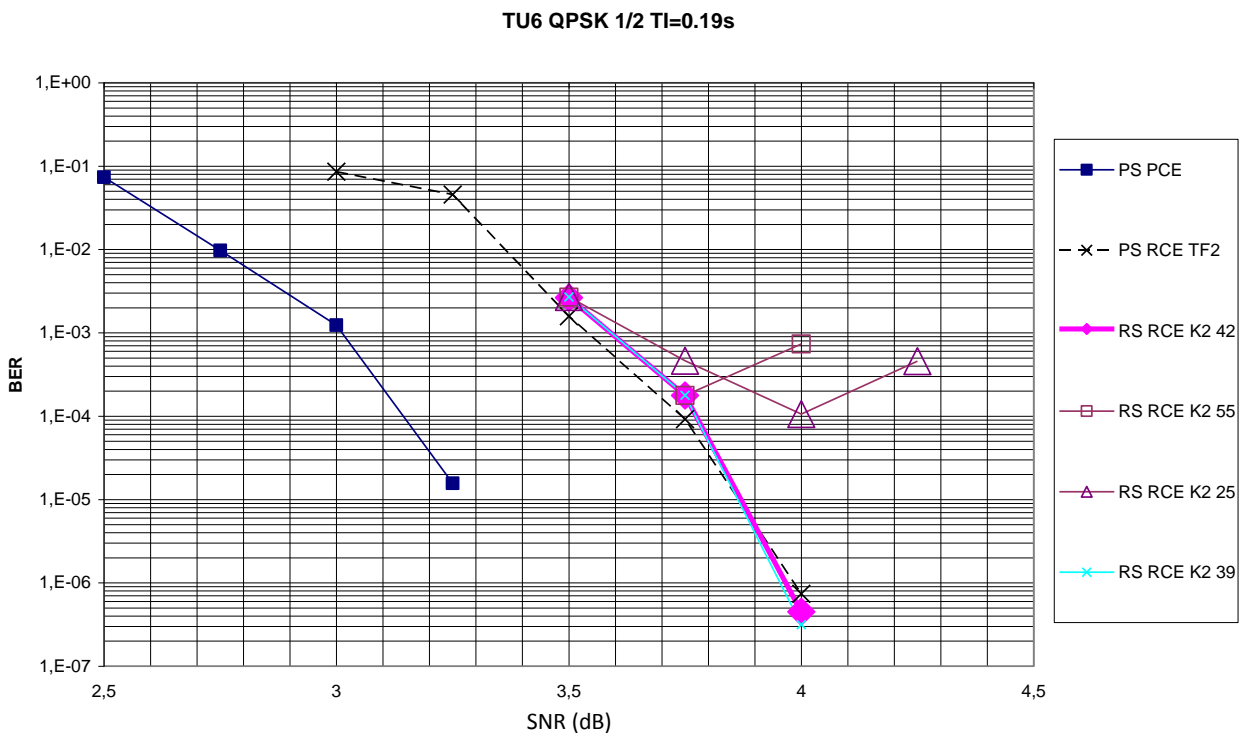


**Figure 96: Performances on TU6 channel QPSK 1/2 TI=0.19s fixed P1 detection threshold, various parameter settings.**

### 6.8.2.4 LMS open channel

The simulations have been performed with the following parameters:

- QPSK 1/2 modulation
- Interleaving time  $T_i$  of 0.28s or 1.49s
- Speed of 60 km/h

As shown on Figure 97 and Figure 98, the results are similar to those obtained with the AWGN channel: there is nearly no loss due to the synchronization mechanisms, and the interleaving time has nearly no effect on the performances (0.1dB).

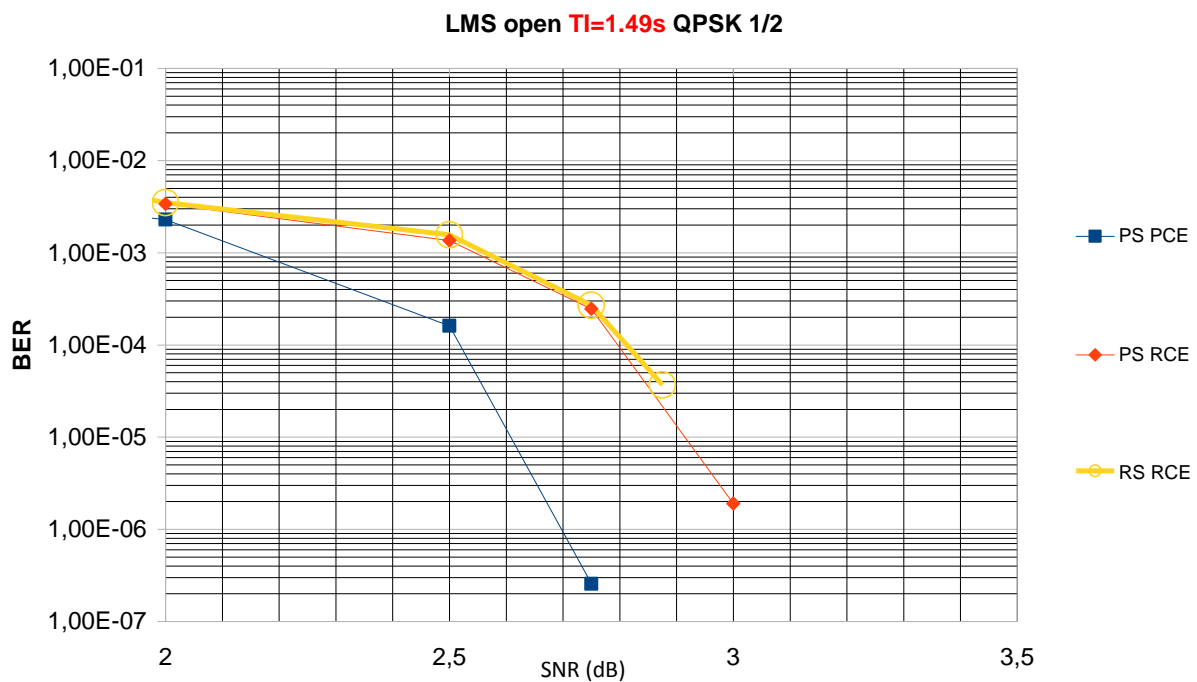


**Figure 97: BER on LMS open channel with QPSK 1/2 and TI=1.49s.**

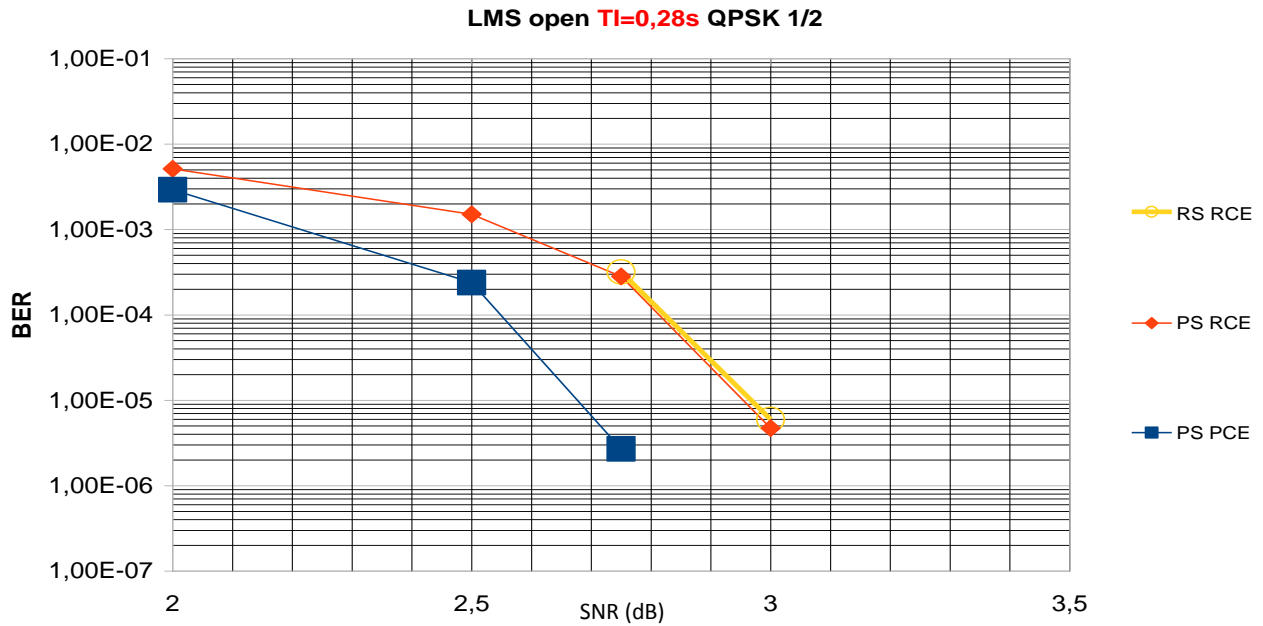


**Figure 98: BER on LMS open channel with QPSK 1/2 and TI=0.28 s.**

### 6.8.2.5 RICE channel with K=5 at 60 km/h

The AWGN, LMS open and TU6 channels do not contain deep fading. The attenuations that are encountered do not decrease the SNR to the values at which the synchronization algorithms fails. Consequently no performance losses have been observed on these channels when the P1 detection threshold is chosen correctly.

However for the RICE channel with  $K=5$  and the LMS ITS channel at 60km/h, deep attenuations are observed. Those fading make the SNR drop below the admissible SNR required by the synchronization algorithms and in some cases some P1 symbols may not be detected.

If a P1 symbol is not detected, the LLRs are set to zero, and if the time interleaving is too short losses will be observed. The performances will also decrease when too many P1 are not detected.

Figure 99 below shows that the losses can reach 1.5dB with a QPSK 1/3 and an interleaving time of 1.49 seconds.

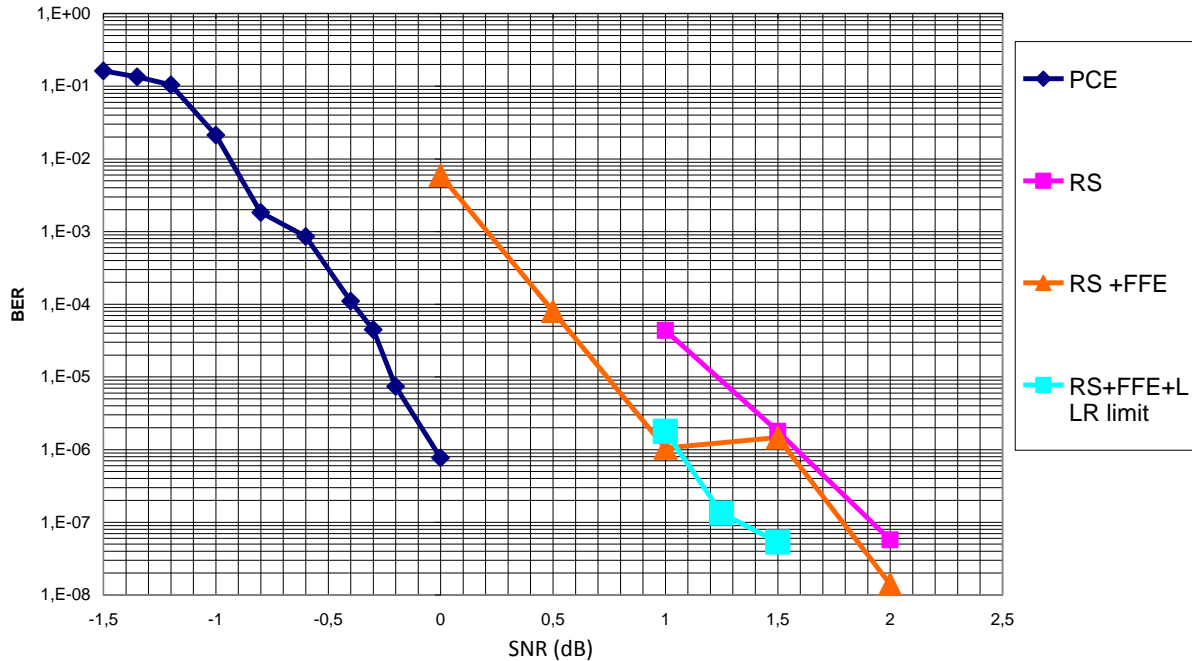


**Figure 99: BER on RICE channel with K=5 for a QPSL 1/3 and 3 methods of synchronization.**

Figure 99 shows the results for 3 synchronization methods:

- Blue curve: the reference curve with perfect synchronization and channel estimation.
- Magenta curve: the standard P1 detection using an adaptable threshold ( $K_n = 5$  and  $K_s = 55$ ). The loss is about 1.5dB.
- Orange curve: the fine frequency correction is activated; it allows improving the BER for low SNRs.
- Light blue curve: the fine frequency correction is activated and the LLRs limitation as well. It improves the BER for high SNRs.

The simulations are made with  $10^9$  bits of data corresponding to 10.000 P1 and 191.132 code words, representing 271 packets of 1.49 seconds.

The errors occur in packets when there are too many non-detected P1 symbol over 1.49 seconds (about 40 P1). In this case, the decoder is not able to correct the missing data.

For  $10^9$  simulated bits with a BER=  $10^{-5}$  with synchronization, only 1, 2 or 3 packets of errors are observed: it is too small to obtain a good statistics and performance curves are to be taken carefully.

The phenomenon described in Section 6.7 is observed for the FFE only: in certain cases, even at high SNRs the BER curve increases due to detected P1 with a high residual error frequency. In these simulations, the LLRs are not set to zero and the decoder cannot correct the errors on data.

### 6.8.2.6 LMS ITS channel at 60 km/h

Like for the RICE channel, the LMS ITS channel shows strong fading that may cause non detections of P1 symbols. For example a fading of 1second will impact about 40 P1 symbols. The modulation is QPSK 1/3 and interleaving time is 1.49 second. For each point  $10^9$  bits were transmitted. Curves shown on Figure 100 are obtained using a P1 detection threshold depending on SNR (method 1) with:

- $K_n = 5$  and  $K_s = 55$
- $K_n = 15$  and  $K_s = 55$

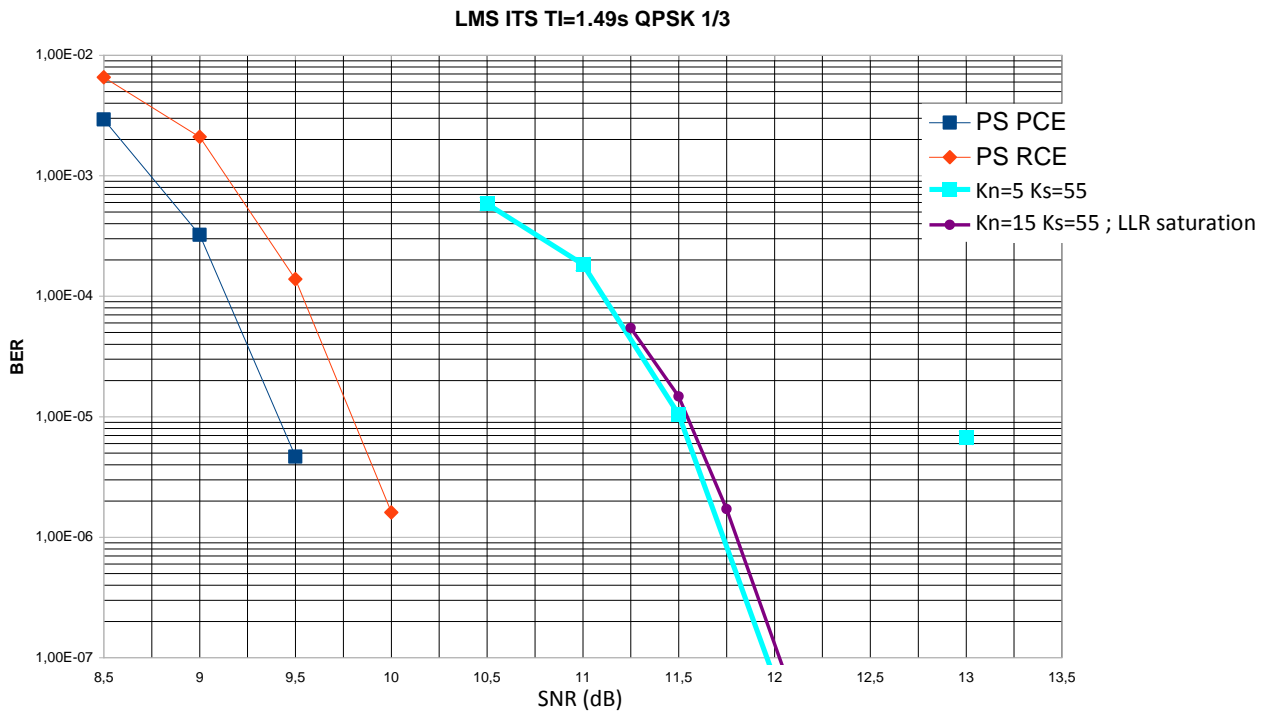


**Figure 100: BER on LMS ITS channel.**

The curves represent:

- In blue, the reference curve with perfect channel estimation and perfect synchronization
- In red, real channel estimation and perfect synchronization
- In light blue, basic synchronization
- In purple, synchronization with LLRs saturation activated

For the basic synchronization (RS RCE), there is an error appearing at SNR=13dB whereas it was error free at SNR= 12.5dB. This is due to a P1 detected during a fading for which the frequency estimation was wrong, as described in chapter 6.7. By activating the LLRs limitation, this phenomenon disappears.

### 6.8.3 Conclusion

As presented in the first sections, the synchronization algorithms are quite robust for SNR values higher than -3dB. For the propagation channels for which no deep fading are observed, the synchronization algorithms



## Technical Report TR4.2

do not degrade the BER, as the synchronization algorithms work correctly at the considered SNR values. For AWGN, TU6 and LMS OPEN cases, the degradation brought by synchronization compared to the perfect synchronization case (with real channel estimation) is about 0.1dB.

However over the RICE channel with  $K=5$  and the LMS ITS channel both showing deep fading, several consecutive P1 symbols may not be detected causing packet errors. In the presented simulations the interleaving time was chosen to be short (less than 1.5 seconds) and in this condition, the wrong P1 detections cause BER degradations. The losses for these channels spread from 1 to 2 dB. Taking into account that the DVB-NGH traffic is made of bursts (by opposition to continuous transmission in DVB-SH), these amount of losses appear quite reasonable in comparison to erasure channels.

## 7 CONCLUSION

This technical report entitled “Second Interim report on Hybrid Access Technologies” deals with the combination of the satellite and terrestrial components to extend the capacity of the DVB Next Generation Handheld (NGH) broadcasting system. It updates and complements the results presented in the second interim report TR4.2 issued in June 2012. The whole set of technologies studied as part of the TF4 activities will be described in Deliverable D4.2 – “Novel Access Technologies” to be published in November 2012. This document addresses the four following topics:

- *The satellite role in the DVB-NGH hybrid profile architecture and satellite link characterization.* This topic starts with an overview on the state-of-art of mobile services over satellite, specifying the current issues and the DVB technologies used for satellite broadcasting. After this, a characterization of the different DVB-NGH satellite scenarios is presented and the main distribution requirements are established. A final study is focused on the satellite link characterization where some examples of DVB-NGH link budgets are presented according to the latest information available from DVB. The link budget examples consider medium and high power satellites and a channelization of 1.7MHz in OFDM mode.
- *The SC-OFDM for the implementation of the satellite transmissions in the DVB-NGH Hybrid Profile.* It is shown that the SC-OFDM modulation is intrinsically robust to the Power Amplifier non-linear degradations with the ability to operate with a reduced OBO in comparison to OFDM and a total degradation improved by 1.6 dB. It is thus possible to improve the power efficiency of the PA while improving the coverage. It must be pointed out that this result still holds when considering the PAPR reduction solutions for OFDM such as the Tone Reservation approach used in DVB-T2. This kind of solution actually performs well for large IBOs but not for the small IBOs (a few dBs) commonly used in satellite transmissions. In a third wing, the section shows that the SC-OFDM behaves similarly to OFDM when it comes to compensate for the degradation due to the channel and mobility, either in SISO or MIMO.
- *The Convolutional interleaving scheme selected for the Long TI Feature of DVB-NGH.* It is shown that the best performance is achieved by single FEC with a uniform CI profile. The performance of single FEC with the CI uniform-late profile is reduced about 2 dB compared to the CI uniform profile. CI with TI length of 10s achieves gains between 6-8 dBs.
- *The robustness of L1 signaling schemes provisioned in the DVB-NGH standard for the satellite segment.* In a first study, it is shown that the mechanisms devised in the Terrestrial profile to improve L1 signaling robustness satisfy the requirements of the Satellite path. However, with some configuration of Additional Parity (AP2), L1-dyn repetition is needed. In addition, with AP3 configuration, the robustness of L1 signaling is enough to get better performance than data. Globally, it appears that the mechanisms assumed for the Terrestrial profile (4k, AP/IR and Fabric decoding) when used in conjunction with L1-dyn repetition meet the requirements of the Satellite path. In a

second study, it is shown that the Additional Parity mechanism is getting more efficient when associated with spreading. Nevertheless, despite of hard receiving conditions in satellite mobile environment, it has been seen that reduced spreading could be introduced providing more robust modulation (BPSK), very low coding rate ( $\sim 1/6$ ) and reduced size code (LDPC 4K), as it is approved now in the NGH standard. The selected scheme is well suited for the scenario with a 600ms spreading duration between satellite frames. Nevertheless, for satellite transmission, only satellite NGH frames are emitted (Stand-alone mode) with 250 ms spreading duration that might be a weak point. Fortunately, NGH standard implements another mechanism, Incremental redundancy (not studied here) enabling using another previous frame to carry other bit redundancy.

- *Time and frequency synchronization algorithms in the context of satellite transmissions with application to the SC-OFDM waveform.* This part of the report describes a set of algorithms designed for improving the performance of time and frequency synchronization over the satellite channel. Most of these algorithms rely on the DVB-T2/NGH P1 symbol that also serves to detect DVB-T2/NGH transmission. The whole range of synchronization needs is covered starting with the coarse time synchronization (CTS), the estimation of the fractional frequency offset (Fractional Frequency error Synchronization - FFS), the estimation of the integer frequency offset (Integer Frequency Synchronization - IFS) and Fine Time synchronization (FTS). It is shown that the P1 detection is very robust (for SNR down to -8dB). If the P1 detection is successful, the probability to see IFS and FTS fail is very low. Moreover, in the rare cases where IFS and/or FTS fail, either because of low SNR or bad coarse time synchronization, the computation of an appropriate threshold on the correlation peaks allows the detection of such failure. Interestingly, it is shown that with the LMS ITS channel, it may happen that if the SNR increases over the frame, LLRs values and thus the detected bits might be erroneous even for high SNRs due to an a high residual frequency error during P1 synchronization. Solutions to overcome this issue are proposed.

The overall performances of an SC-OFDM system have been evaluated when applying the proposed algorithms. It is shown that synchronization algorithms are quite robust for SNR values higher than -3dB. For the propagation channels for which no deep fading are observed, the synchronization algorithms do not degrade the BER, as the synchronization algorithms work correctly at the considered SNR values. For AWGN, TU6 and LMS OPEN cases, the degradation brought by synchronization compared to the perfect synchronization case (with real channel estimation) is about 0.1dB. However over the RICE channel with  $K=5$  and the LMS ITS channel both showing deep fading, several consecutive P1 symbols may not be detected causing packet errors. In the presented simulations the interleaving time was chosen to be short (less than 1.5 seconds) and in this condition, the wrong P1 detections cause BER degradations. The losses for these channels spread from 1 to 2 dB. Taking into account that the DVB-NGH traffic is made of bursts (by opposition to continuous transmission in DVB-SH), these amount of losses appear quite reasonable in comparison to erasure channels.

All these results have been submitted to the DVB-NGH standardization group and have significantly influenced the definition of the standard, meeting the original expectations of the ENGINES project.





Technical Report TR4.2

## 8 REFERENCES

- [1] Draft ETSI EN 303 105 v1.1.1: “*Digital Video Broadcasting (DVB); Next Generation broadcasting system to Handheld, physical layer specification (DVB-NGH)*,” Sept. 2012.
- [2] Technical Report TR4.1, “*Interim Report on Hybrid Access Technologies*”, September 2011.
- [3] Technical Report TR4.2, “*Interim Report 2 on Hybrid Access Technologies*”, June 2012.
- [4] ETSI EN 300 421 V1.1.2, “*Digital video broadcasting; Framing structure, channel coding and modulation for 11/12 GHz satellite services (DVB-S2)*”, August 1997.
- [5] ETSI EN 302 307, V1.2.1, “*Digital video broadcasting; Second generation framing structure, channel coding and modulation systems for Broadcasting, Interactive Services, News Gathering and other broadband satellite applications (DVB-S2)*”, August 2009.
- [6] ETSI EN 302 583: “*Digital Video Broadcasting (DVB); Framing Structure, channel coding and modulation for Satellite Services to Handheld devices (SH) below 3 GHz*”, January 2008.
- [7] ETSI TS 102 584 v1.2.1, “*Guidelines for the Implementation for Satellite Services to Handheld devices (SH) below 3GHz*,” 2011.
- [8] F. Pérez-Fontán, et al., “Statistical Modeling of the LMS Channel,” *IEEE Trans. on Vehicular Technology*, vol.50, no. 6, pp. 1549-1567, 2001.
- [9] G. Faria, J. A. Henriksson, E. Stare, and P. Talmola, “*DVB-H: Digital Broadcast Services to Handheld Devices*,” *Proc. of the IEEE*, vol. 94, no. 1, pp. 194-209, 2006.
- [10] ETSI EN 302 755 v1.3.1, “*Digital Video Broadcasting (DVB); Frame Structure Channel Coding and Modulation for a Second Generation Digital Terrestrial Television Broadcasting System (DVB-T2)*,” Oct. 2011.
- [11] ETSI TS 102 831 v1.2.1q: “*Digital Video Broadcasting (DVB); Implementation guidelines for a second generation digital terrestrial television broadcasting system (DVB-T2)*,” February 2012.
- [12] 3GPP TS 36.211 V10.4.0: “*3rd Generation Partnership Project; Technical Specification Group Radio Access Network; Evolved Universal Terrestrial Radio Access (E-UTRA); Physical Channels and Modulation (Release 10)*,” December 2011.
- [13] D. C. Chu, “*Polyphase Codes With Good Periodic Correlation Properties*”, *IEEE Trans. on Information Theory*, vol. 18, no. 4, pp. 531-532, July 1972.
- [14] J. Tellado, “*Peak to Average Power Reduction for Multicarrier Modulation*,” Ph.D. thesis, Stanford University, 2000.
- [15] C. Ciochină, “*Physical [layer design for the uplink of mobile cellular radiocommunication systems](#)*,” PhD Thesis n° 2009PA112300, Université de Paris-Sud, Faculté des Sciences d'Orsay (Essonne), France, 2009.
- [16] C. Rapp, “*Effects of the HPA-nonlinearity on a 4-DPSK/OFDM signal for a digital sound broadcasting system*,” *European Conference on Sattelite Communications ECSC'91*, Liège, Belgium, Oct. 1991.
- [17] C. Ciochina, F. Buda and H. Sari, “*An Analysis of OFDM Peak Power Reduction Techniques for WiMAX Systems*,” *IEEE International Conference on Communications, ICC'06*, Istanbul, Turkey, June 2006.
- [18] D. Wulich, N. Dinur, and A. Gilinowiecki, “*Level Clipped High Order OFDM*,” *IEEE Trans. on Communications*, vol. 48, no. 6, pp. 928-930, June 2000.
- [19] DVB TM-NGH183, “*Land Mobile Satellite Propagation channel model*,” May 2010.



Technical Report TR4.2

- [20] P. Moss, T. Yeen Poon, and J. Boyer, “*A Simple Model of the UHF Cross-Polar Terrestrial Channel for DVB-NGH*,” *BBC White Paper WHP205*, Sept. 2011.
- [21] TM-NGH 1319, “*L1 signalling robustness in the SAT path*”, Hognsil Jeong.
- [22] TM-NGH 1158, “*Simulation Results of L1 signalling LMS channel*”, Hognsil Jeong.
- [23] TM-NGH 1159, “*PF72 4k codes for L1 signalling*”, Hognsil Jeong
- [24] TM-NGH 105, “*Proposal for improving the performance of L1 signalling in mobile channels*”, Samsung, Nokia, 23-24 March 2010.